Carlos Andrés Arce Campos The São Francisco portal in Almeida: modelling, analysis and conservation

Portugal | 2016

ADVANCED MASTERS IN STRUCTURAL ANALYSIS
OF MONUMENTS AND HISTORICAL CONSTRUCTIONS

Master's Thesis

Carlos Andrés Arce Campos

The São Francisco portal in Almeida: modelling, analysis and conservation

University of Minho

Czech university of Prague

Education and Culture

Erasmus Mundus

ADVANCED MASTERS IN STRUCTURAL ANALYSIS
OF MONUMENTS AND HISTORICAL CONSTRUCTIONS

Master's Thesis

Carlos Andrés Arce Campos

The São Francisco portal in Almeida: modelling, analysis and conservation

This Masters Course has been funded with support from the European Commission. This publication reflects the views only of the author, and the Commission cannot be held responsible for any use which may be made of the information contained therein.

Portugal | 2016

DECLARATION

Name: Carlos Andrés Arce Campos

Email: aarce.cr@gmail.com

Title of the MSc Dissertation: The São Francisco portal in Almeida: modelling, analysis and conservation

Supervisor(s): Francisco M. Fernandes

Year: 2016

I hereby declare that all information in this document has been obtained and presented in accordance with academic rules and ethical conduct. I also declare that, as required by these rules and conduct, I have fully cited and referenced all material and results that are not original to this work.

I hereby declare that the MSc Consortium responsible for the Advanced Masters in Structural Analysis of Monuments and Historical Constructions is allowed to store and make available electronically the present MSc Dissertation.

University: Universidade do MInho

Date: 15/07/2016

Signature: _____

Quiero dedicar esta tesis a mi madre Ana Campos Quesada.

AKNOWLEDGEMENTS

I would like to thank my professors Luis Ramos and Francisco Fernandes for giving me their time and guidance in this project. Their experienced advise always came in the most friendly tone giving me motivation to keep on working, specially with a “Bom trabalho”. I am indebted to you both.

I thank Carlos Miguel Alves Amorim de Barros and all the people that worked hard in the testing campaign to obtain the material properties that were used in these models.

I want to thank my classmates for sharing with me laughs and hard times. Especially my friend Kostas Katris who endured with me the hardest challenges in all the projects we worked in together.

Finally I thank again my family that supported me to start this journey.

ABSTRACT

Portugal possesses a long history that is often conserved in the form of historical constructions. The fortress of Almedia in Guarda is one of those. Erected in the 17th century, it has been the object of repairs and adaptations throughout the centuries. Despite this, very little information can be found relatively to the construction techniques used, materials, and past interventions. Today, this monument needs some attention due to the continuous deterioration of materials and the need to increase knowledge about this building for future interventions.

This works purpose is to study the structural stability of the San Francisco Gate with the purpose of determining its level of safety and level of interventions if necessary so it can continue keeping the history of the Portuguese nation. To do this a numerical finite element model was used. The model created was a 2D nonlinear model of the original structure followed by a nonlinear model including the damage in specific deteriorated sections by means of phase analysis.

The mechanical properties of the materials were obtained from a sonic testing campaign. The amount of damage was measured with the help of 3D laser scanning. For the model sensitivity to variation of mechanical properties of the two materials used (stone masonry and infill) were studied. Results show that the model is highly sensible to the variation of the compressive value in the stone-masonry material and the type of infill used.

Safety analysis was done for two locations of loading, a live load applied till failure in the top of the structure or only on its right side. This analysis was repeated for three different models that represent the gradually deterioration of the structure to the actual condition. Safety analysis demonstrated that for this type of macro model the structure is always safe.

Furthermore five scenarios of hypothetical additional damage were modeled to study the vulnerable areas in the structure, results from these scenarios show that the critical condition would be to have additional damage in the middle of the arch where actually most of the present damage is located. This analysis indicated that even for additional damage that would leave only 5cm of width of the barrel vault that composes the Gate the structure can still sustain its self-weight and even a load factor of 10 times 5 kN/m. Further studies are proposed based on the results obtained in this project.

RESUMEN

Portugal posee una larga historia que frecuentemente se conserva en forma de construcciones históricas. La Fortaleza de Almeida en Guarda es una de ellas. Levantada en el siglo 17, ha sido objeto de reparaciones y adaptaciones durante siglos. A pesar de esto, muy poca información se puede encontrar acerca de las técnicas de construcción usadas, materiales e intervenciones pasadas. Hoy, este monumento requiere atención debido al continuo deterioro de sus materiales y la necesidad de incrementar el conocimiento acerca de este edificio para futuras intervenciones.

El propósito de este trabajo es estudiar la estabilidad estructural de la Puerta de San Francisco con el objetivo de determinar el nivel de seguridad y el nivel de intervención requerido para que continúe guardando la historia de la nación Portuguesa. Para lograr esto un modelo númerico de elemento finito fue utilizado. El modelo creado ha sido un modelo 2D no lineal de la estructura original seguido por un modelo no lineal de la estructura incluyendo el deterioro actual todo a través de un análisis de fases.

Las propiedades mecánicas de los materiales fueron obtenidas mediante una campaña de ensayos sónicos. La cuantía del daño fue medida con la ayuda de escaneo laser 3D. La sensibilidad del modelo a las propiedades mecánicas de los dos materiales usados (mampostería de piedra y material de relleno) fue estudiada. Los resultados muestran que el modelo es altamente sensible a la variación de la capacidad en compresión en el material de mampostería de piedra y también es sensible a la variación del tipo de relleno.

El análisis de sensibilidad fue hecho para dos tipos de carga, una carga viva aplicada hasta el momento de falla sobre toda el techo de la estructura o solamente en su lado derecho. El análisis fue repetido para tres modelos diferentes que representan el deterioro gradual de la estructura hasta su condición actual. El análisis de seguridad demostró que para este tipo de macro modelo la estructura puede ser considerada segura en todos los casos.

Más allá del análisis de la estructura en su estado actual modelos para 5 escenarios de daño hipotético fueron creados para evaluar las áreas vulnerables de la estructura. Los resultados de estos escenarios muestran que la ubicación critica de daño adicional seria en el centro de la parte interior del arco derecho, donde la mayoría del daño existe actualmente. Este análisis indica que incluso para una condición de daño adicional que dejaría solamente un espesor de 5 cm en la bóveda la estructura aún sería capaz de sostener su propio peso e incluso una carga viva de 50 kN/m. Nuevos estudios fueron propuestos con base en estos análisis.

RESUMO

Portugal possui uma longa história, conservada muitas vezes, na forma de construções históricas. A fortaleza de Almeida, na Guarda, é um desses exemplos. Erguida no século 17, tem sido objeto de reparos e adaptações ao longo dos séculos. Apesar disso, a informação que pode ser encontrada relativamente às técnicas de construção utilizados, materiais e intervenções passadas é escassa. Hoje, este monumento precisa de alguma atenção devido à deterioração contínua dos materiais e da necessidade de aumentar o conhecimento sobre este edifício para futuras intervenções.

Este trabalho tem como objetivo estudar a estabilidade estrutural do Portão de São Francisco, com o propósito de determinar o seu grau de segurança e o nível de intervenções necessárias, para que este possa continuar a manter a história da nação Portuguesa. Para isso, utilizou-se um modelo numérico de elementos finitos. Foi criado um modelo não-linear 2D da estrutura original seguido por um modelo linear, incluindo o dano das secções específicas deterioradas por meio de análise de fases.

As propriedades mecânicas dos materiais foram obtidas a partir de um conjunto de ensaios sónicos. A quantidade de danos foi medida com a ajuda do varrimento a laser 3D. Para testar a sensibilidade do modelo à variação das propriedades mecânicas dos materiais utilizados, dois materiais (alvenaria de pedra e de enchimento) foram estudados. Os resultados mostram que o modelo é altamente sensível à variação do valor de compressão de ambos os materiais usados.

A análise de segurança foi feita em dois locais, aplicando uma carga viva nas falhas do topo ou apenas no lado direito da estrutura. Esta, foi repetida em três modelos diferentes, que representam a gradual deterioração da estrutura com o estado real. Esta análise demonstra que, para este tipo de modelo macro, a estrutura é sempre segura.

Além disso, cinco cenários de lesão hipotética adicionais foram modelados para estudar as áreas vulneráveis da estrutura. Os resultados, a partir destes cenários, mostram que o estado crítico seria quando houvessem danos adicionais no meio do arco, onde, na verdade, a maior parte do presente dano está localizado. Esta análise indicou que, mesmo com os danos adicionais, onde apenas restariam 5 centímetros de largura da abóbada de berço que compõe o portão da estrutura, esta ainda pode sustentar o seu próprio peso e até mesmo uma taxa de ocupação de 10 vezes 5 kN / m. Mais estudos são propostos com base nos resultados obtidos neste projeto.

TABLE OF CONTENTS

LIST OF FIGURES

LIST OF TABLES

1 INTRODUCTION

1.1 Motivation

The Almeida fortress is an icon of Portuguese military Heritage. Erected in the 17th century, it has been the object of repairs and adaptations throughout the centuries. Despite this, very little information can be found relatively to the construction techniques used, materials, and past interventions. Today, this monument needs some attention due to the continuous deterioration of materials and the need to increase knowledge about this building for future interventions.

The entrance into the fortress is through two, tunnel shaped, portals. One of those portals, São Francisco, which is a curved tunnel, exhibits a high degree of deterioration. Being one of the main entrances into the town, its structural safety is crucial. Therefore, the structural assessment of this building is essential to determine its safety and/or strengthening solutions to ensure its safety.

This structure is visited nowadays by countless tourist and is especially relevant for Portuguese, Spanish and French visitors, the reason for this is its history. Almeida fortress acts as a story teller of the disputes that once occurred in the past between nations as Spain and Portugal and tells incredible battle stories from the times when Napoleon seize the fortress. It is necessary to study this structure and keep it as conserving this monument means conserving the history and the past of so many nations, particularly the Gate of Sao Francisco plays a fundamental role in this history of war, it is so representative for this purpose that every year there is a role play remembering the scenes of ward from 1810.

This works purpose is to study the structural stability of the San Francisco Gate with the purpose of determining its level of safety and level of interventions if necessary so it can continue keeping the history of so many nations.

1.2 Objectives

In this thesis the main objective is to determine the level of safety of the Gate of San Francisco in order to achieve this a set of secondary objectives has been set as listed below:

1. Elaboration of a short state of the art regarding the investigation of the portal (history, construction materials, etc.).
2. Building numerical finite element models of a typical crosssection of this portal by taking into consideration its geometry and material characteristics obtained from documents and all testing carried out previously.
3. Assessing the real structural capacity to determine the level of safety of this structure after all damage and deterioration received during this almost 350 years after its construction.

1.3 Methodology

For the purpose of assessing the safety level of the structure a finite element model is developed, the intention is to model the geometry of the structure and use the results from previous inspection campaigns to obtain parameters for the model. A first 2D linear static model is developed to have a general idea of the structural behavior as new. Furthermore, this model is refined by the evolution to a 2D nonlinear model of the original structure followed by a nonlinear model including the damage in specific deteriorated sections of the arch by means of phase analysis.

2 STATE OF THE ART

2.1 The Almeida fortress

The Gate of San Francisco is one of the two main Gates that allowed the transit in and out the fortress of Almeida (Figure 1) in the past and nowadays, sharing this function with a third modern Gate that has been introduced in the fortress wall.

Figure 1. The Almeida fortress (Technical comission for the candidacy of Almeida, 2009)

The fortress is located in the Historic Centre of Almeida. This fortified village has a population of around 1491 habitants by 2001 with 335 of them living inside the fortress (Technical comission for the candidacy of Almeida, 2009). Almeida is located in the district of Guarda, close to the border with Spain in the northeast of Portugal (Figure 2) at an altitude of 760 m.

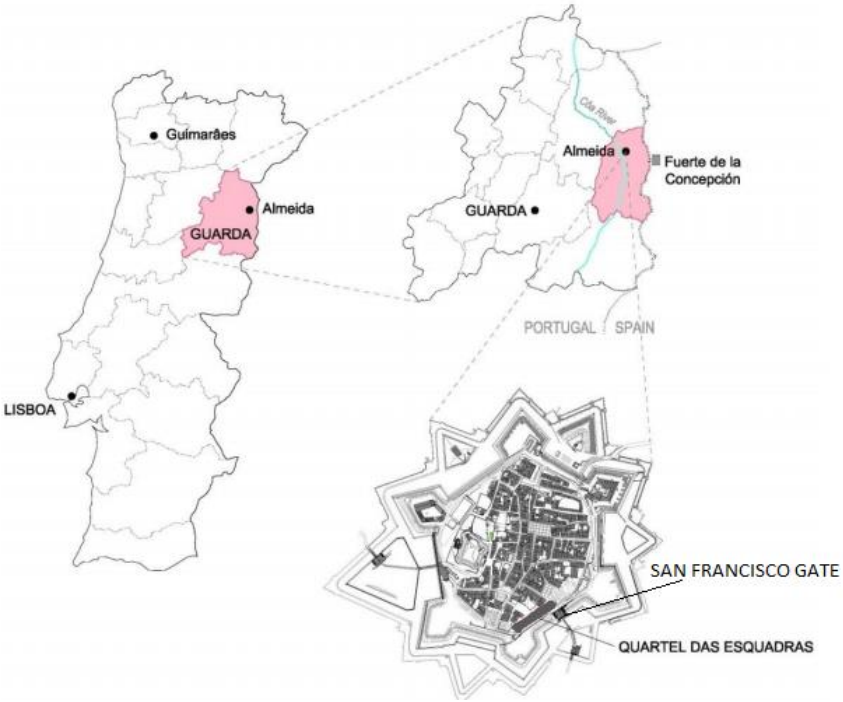

Figure 2. Location of Almeida Fortress (URB Atelier, 2013)

Since the beginning of the Iberian nation Almeida stood as a military place defending the borders through history. In the middle age and till 1297 it was a space for dispute between Christians and Muslims. After that date it was an essential defensive system for the kingdom acting as the first defensive line, its relevance as the first front for stopping invasions explains its dense and troubled military history. The village's defensive functionality was translated in constant investments by the central government to provide it with the most effective defensive devices. This was evident during the reign of King Dinis in the 14th century (Technical comission for the candidacy of Almeida, 2009).

Almeida is only one of the group of fortresses known as the complex of A Raia (Portuguese). This set of structures were located along the border Portugal-Spain and its purpose it's to defend the country from foreigners invasions. Almeida is set on the east side of the Côa River, and due to its strategic location the city was exposed to frequent attacks and sieges since the independence from the Castilian Kingdom of Leon during the 13th century (Campos, 2009).

The reason there are mirrored fortresses on each side of the border is the common and iterative conflicts between inhabitants of both countries, most of the times the conflicts were of a minor scale and it was related to stolen cattle or goods.

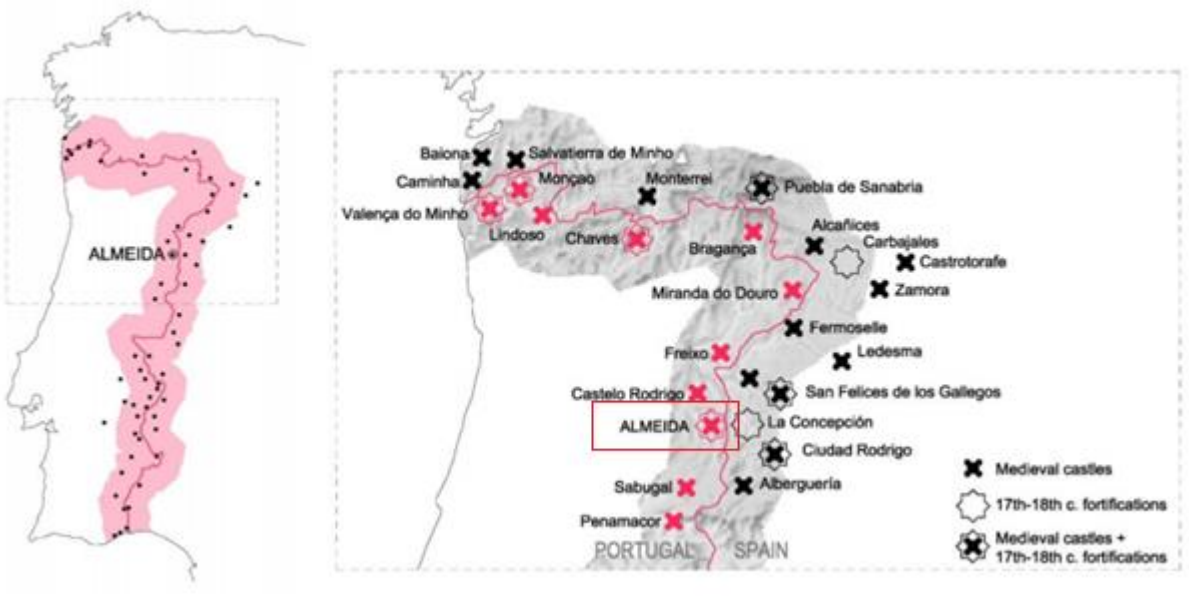

Figure 3. Main fortifications on both sides of the border Spain-Portugal (Cobos, 2013)

As it can be observed in Figure 3, the fortress was fortified in the 17-18th century. However, these were not the only occasions where interventions occurred in the fortress. The fortress of Almedia has lived a very long life acting as one of the most active fortifications of the Raia. Therefore it becomes relevant to describe its history in terms of construction, demolition and intervention phases that are shown in the next timeline depicted in blue, green and red color respectively. The orange letters refer to extensions in the structure. The timetable includes the history of construction since the first Muslim Castle that would later become the Castle of Almeida till the creation of the new Gate to allow modern traffic to town.

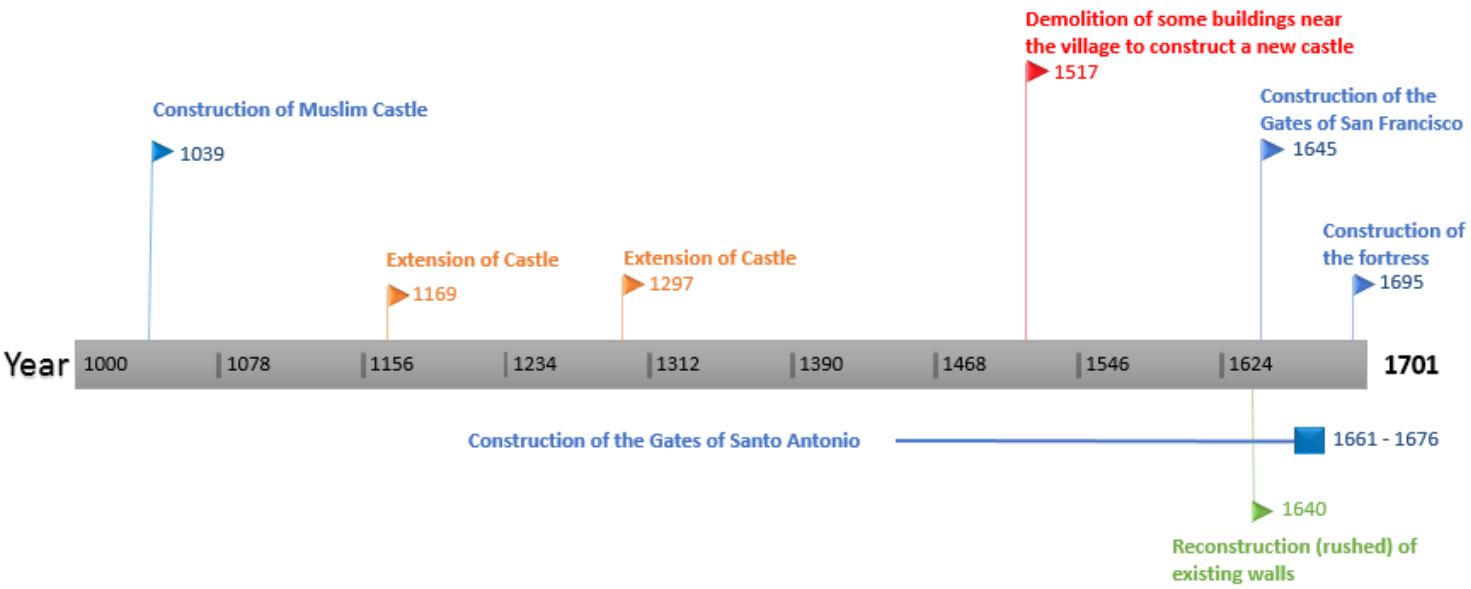

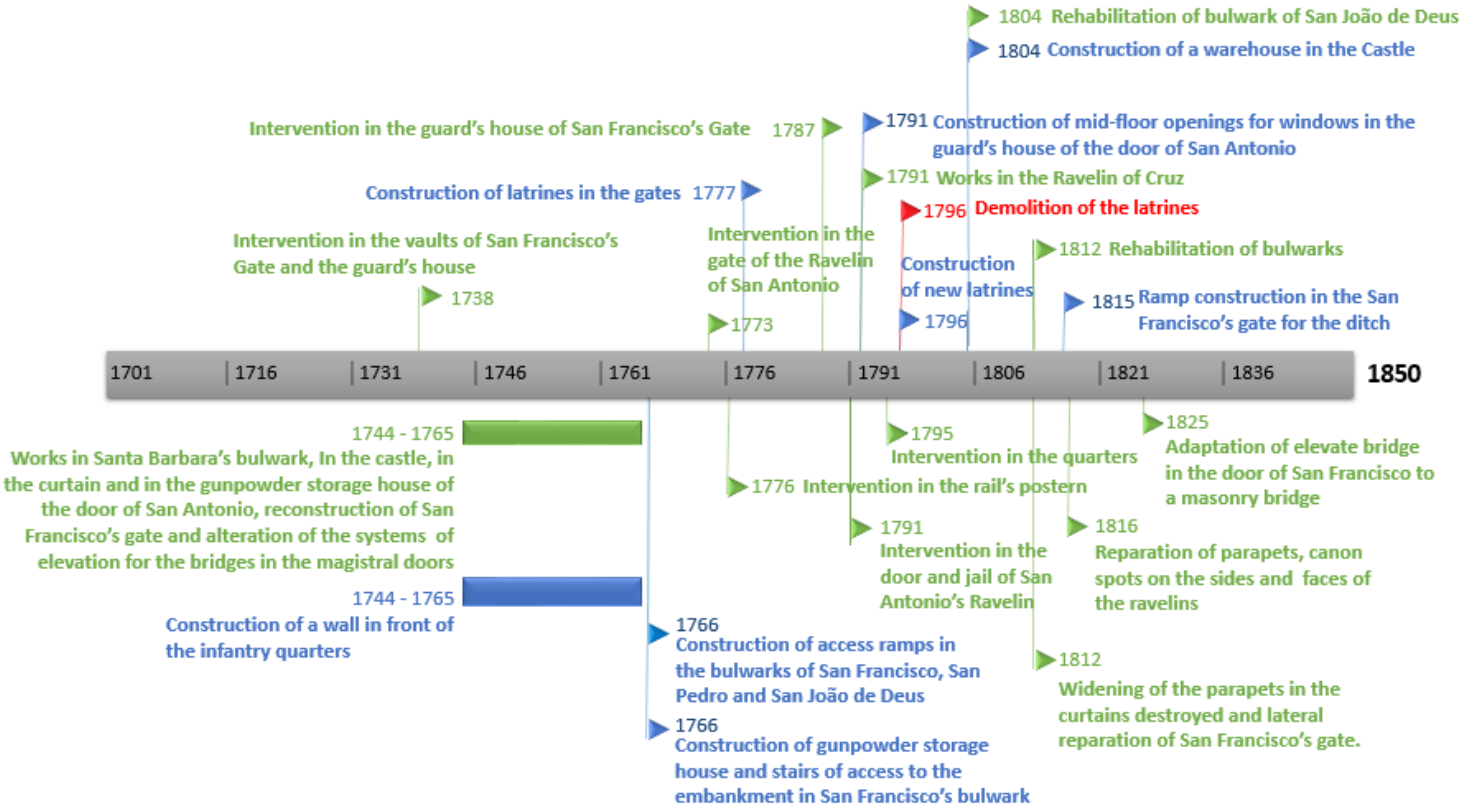
1804 Rehabilitation of bulwark of San João de Deus
1804 Construction of a warehouse in the Castle
Intervention in the guard's house of San Francisco's Gate 1787
1791 Construction of mid-floor openings for windows in the guard's house of the door of San Antonio
1791 Works in the Ravelin of Cruz
Construction of latrines in the gates 1777
1796 Demolition of the latrines
Intervention in the vaults of San Francisco's Gate and the guard's house
1738
Intervention in the gate of the Ravelin of San Antonio
1773
Construction of new latrines
1796
1812 Rehabilitation of bulwarks
1815 Ramp construction in the San Francisco's gate for the ditch
1701 1716 1731 1746 1761 1776 1791 1806 1821 1836 1850
1744 - 1765
Works in Santa Barbara's bulwark, In the castle, in the curtain and in the gunpowder storage house of the door of San Antonio, reconstruction of San Francisco's gate and alteration of the systems of elevation for the bridges in the magistral doors
1795
Intervention in the quarters
1825
Adaptation of elevate bridge in the door of San Francisco to a masonry bridge
1776 Intervention in the rail's postern
1791
Intervention in the door and jail of San Antonio's Ravelin
1816
Reparation of parapets, canon spots on the sides and faces of the ravelins
1744 - 1765
Construction of a wall in front of the infantry quarters
1766
Construction of access ramps in the bulwarks of San Francisco, San Pedro and San João de Deus
1812
Widening of the parapets in the curtains destroyed and lateral reparation of San Francisco's gate.
1766
Construction of gunpowder storage house and stairs of access to the embankment in San Francisco's bulwark

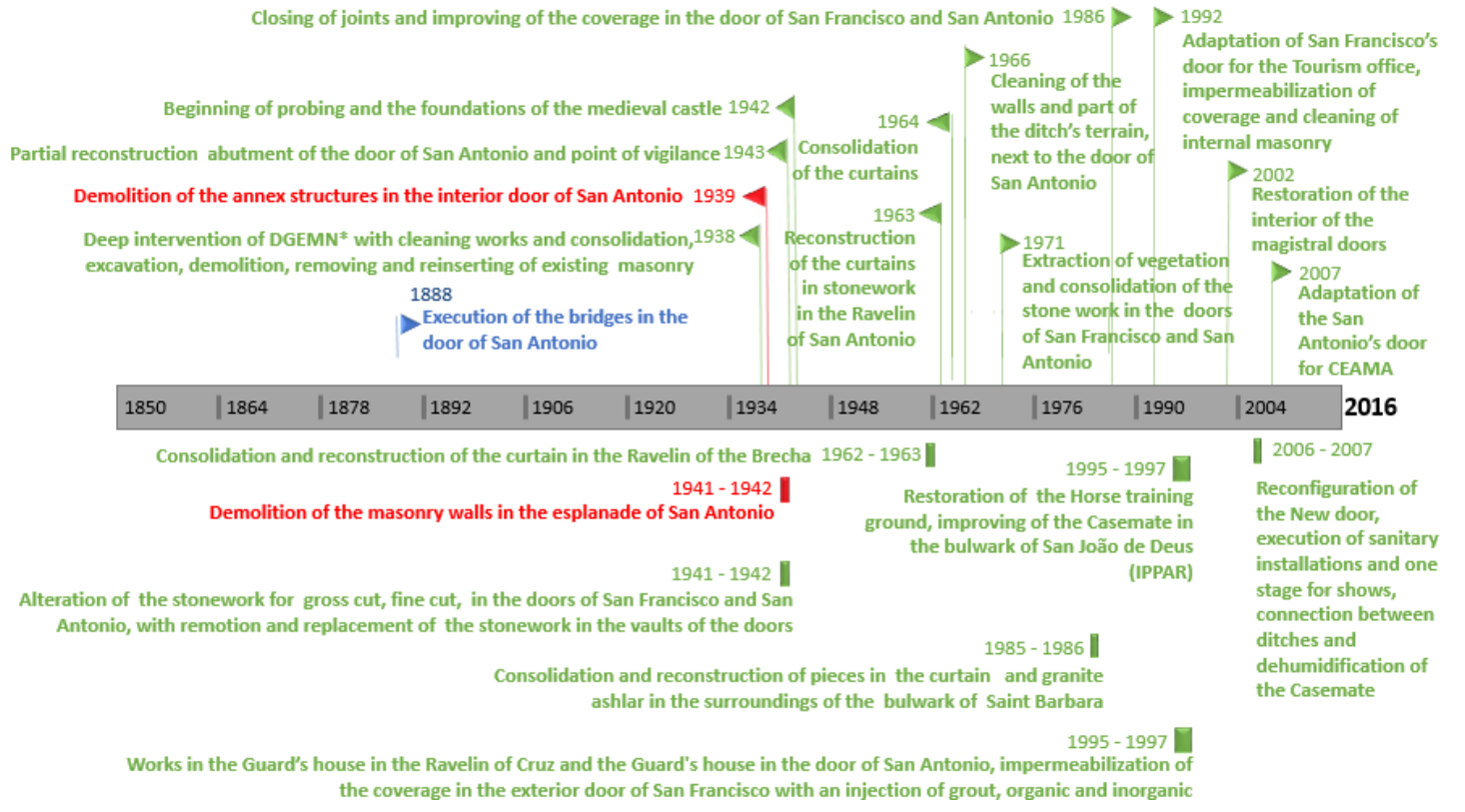
Closing of joints and improving of the coverage in the door of San Francisco and San Antonio 1986
1992
Adaptation of San Francisco's door for the Tourism office, impermeabilization of coverage and cleaning of internal masonry
1966
Cleaning of the walls and part of the ditch's terrain, next to the door of San Antonio
Beginning of probing and the foundations of the medieval castle 1942
1964
Consolidation of the curtains
Partial reconstruction abutment of the door of San Antonio and point of vigilance 1943
Demolition of the annex structures in the interior door of San Antonio 1939
2002
Restoration of the interior of the magistral doors
1963
Reconstruction of the curtains in stonework in the Ravelin of San Antonio
Deep intervention of DGEMN* with cleaning works and consolidation, excavation, demolition, removing and reinserting of existing masonry 1938
1971
Extraction of vegetation and consolidation of the stone work in the doors of San Francisco and San Antonio
2007
Adaptation of the San Antonio's door for CEAMA
1888
Execution of the bridges in the door of San Antonio
1850 1864 1878 1892 1906 1920 1934 1948 1962 1976 1990 2004 2016
Consolidation and reconstruction of the curtain in the Ravelin of the Brecha 1962 - 1963
2006 - 2007
1995 - 1997
1941 - 1942
Demolition of the masonry walls in the esplanade of San Antonio
Restoration of the Horse training ground, improving of the Casemate in the bulwark of San João de Deus (IPPAR)
Reconfiguration of the New door, execution of sanitary installations and one stage for shows, connection between ditches and dehumidification of the Casemate
1941 - 1942
Alteration of the stonework for gross cut, fine cut, in the doors of San Francisco and San Antonio, with remotion and replacement of the stonework in the vaults of the doors
1985 - 1986
Consolidation and reconstruction of pieces in the curtain and granite ashlar in the surroundings of the bulwark of Saint Barbara
1995 - 1997
Works in the Guard's house in the Ravelin of Cruz and the Guard's house in the door of San Antonio, impermeabilization of the coverage in the exterior door of San Francisco with an injection of grout, organic and inorganic

2.2 The interior Gate of San Francisco

The interior Gate of San Francisco was constructed between 1661 and 1667 under the supervision of a group of French technicians of who Pierre Garsin was part of and was the one directly in charge of the construction of this interior Gate (Technical comission for the candidacy of Almeida, 2009).

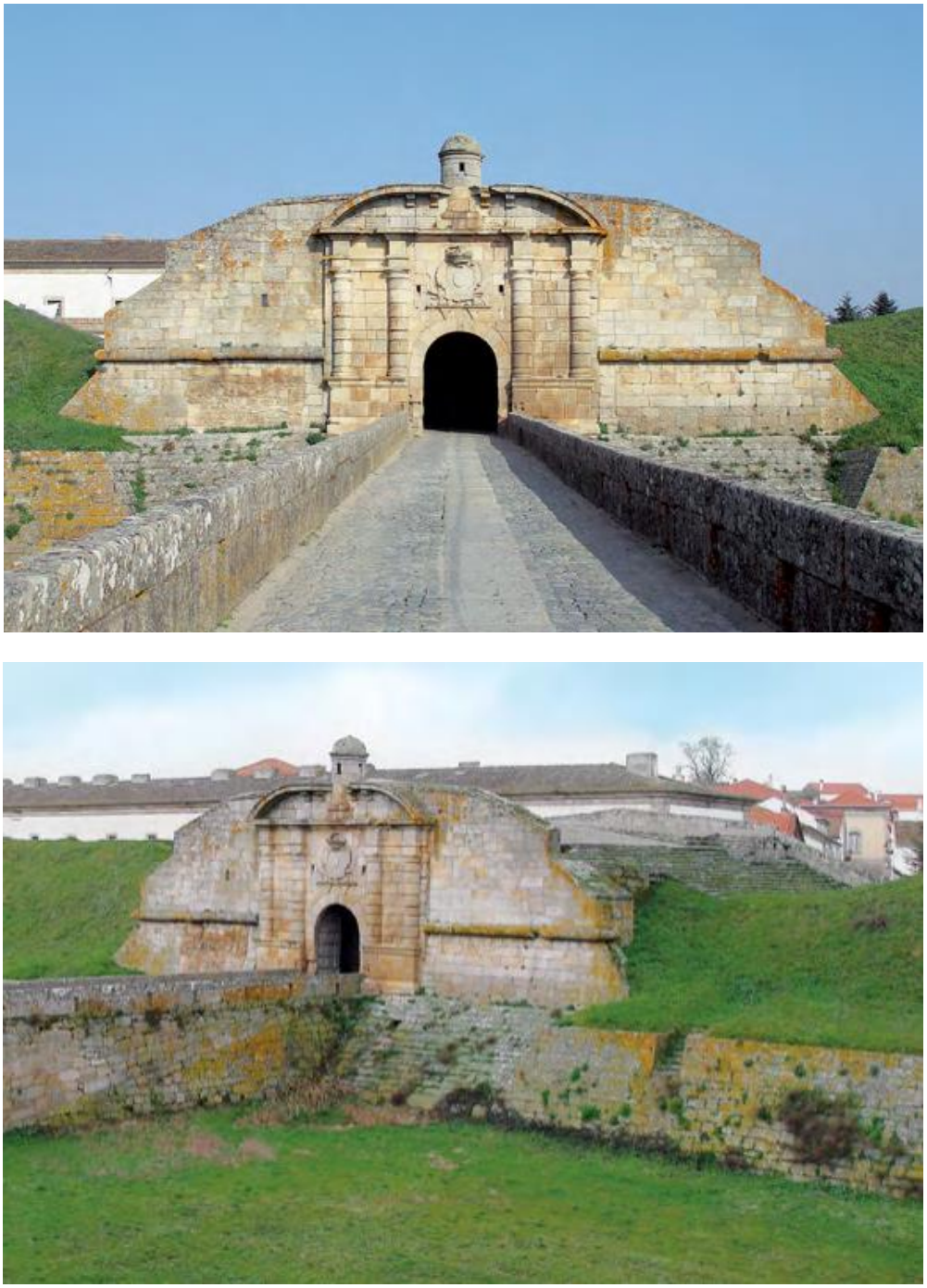

Figure 4. Frontal views of the Gate of San Francisco (Technical comission for the candidacy of Almeida, 2009)

The Gate is composed of a curved tunnel whose structure is a barrel vault made of ashlar stone masonry. The curvature of the tunnel has the purpose of allowing visibility from interior and exterior to a minimum degree, one possible reason for this curved shape is the prevention of cannon balls from crossing the Gate from the exterior.

Figure 5. View from the interior of the Gate of San Francisco (Technical comission for the candidacy of Almeida, 2009)

In the interior of the Gate two substructures can be differentiated: the tunnel that allows the transit out and into the city and the antique house of the guard whose purpose was to accommodate the guard of the Gate, today is used as a tourism office.

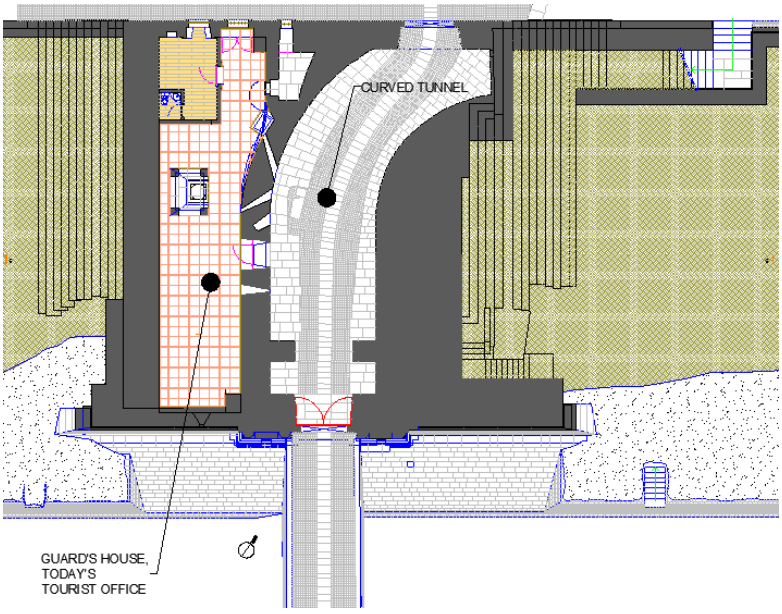

Figure 6. Plan view of San Francisco's Gate

2.2.1 Structure description

The Gate of San Francisco is a structure composed by four main types of elements: arches, vaults, walls and lintels, all of these elements are made of stone masonry.

Figure 7 shows the geometry arrangement of a cross section of the Gate of San Francisco. The main entrance consists of a curved barrel vault that has a diameter of 5.9 m at the entrance of the city and it diminishes to 4.9 m diameter at the side of the barrel vault that is connected to the village, the transition of this geometry is smooth and the height is kept constant. The stone dimensions are in the order of 40 to 100 cm.To the left side of this barrel there is another compartment constructed as the house of the guard, in this section another barrel vault acts as a roof and has the opposite geometrical evolution than the vault mentioned before, in this case the barrel starts with a diameter 4.5 m and opens to 5.9 m in the side of the interior of the fortress, in this case the height is also kept the same.

The house of the guard today is used as the tourism Centre, which main features are a small division made by two walls, which intention was to allocate the bedroom for the guard, there is a chimney and a small subdivision between the barrel and the other one that was used as a prison.

The columns that sustain the arch loads are respectively around 2.7 m high for the left arch and 3.7m high for the right one.

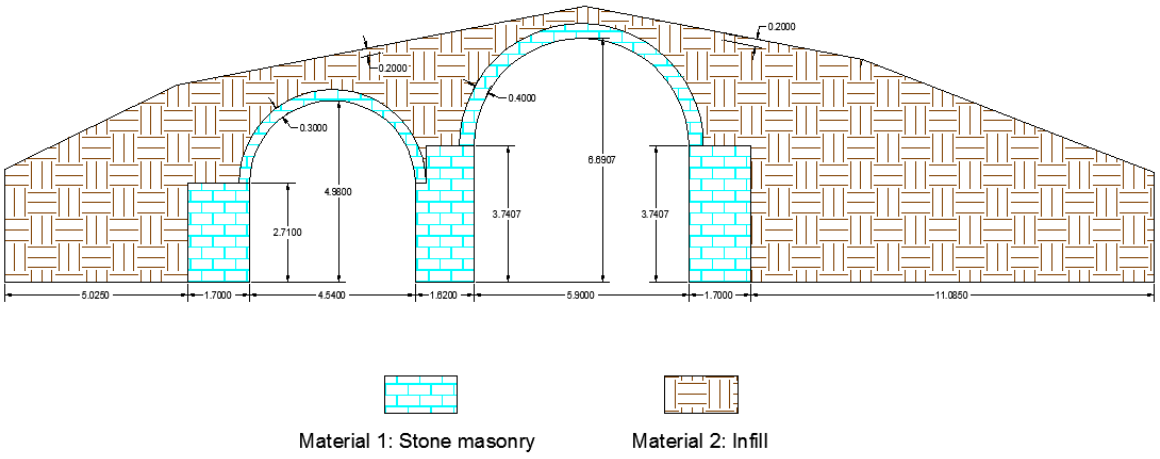

Figure 7. Structure's material composition

2.2.2 History of construction

The San Francisco's Gate was designed by the French architect Pierre Garsin. It's located in the middle of the Ravelin of San Francisco and forces the traffic to cross the ditch. The Gate's doors were designed as a system of double doors. The gate's structure consists of a large tunnel for traffic and laterally to this tunnel there is another structure whose function was to house the guard, it had a

fireplace for the official and openings faced to the esplanade of the interior of the village. The tunnel has a curve whose special feature is to act as an anti-bomb system having an angle to deflect projectiles and using the soil as an anti-impact system. The history of the San Francisco Gate, also called Gate of Cruz, is not brief and important events are related as follows.

1644-1668

It is said that the works of construction of the San Francisco Gate began around the year 1661 being concluded in the first phase of construction of the fortress 1644-1668 around 7 years.

1669-1735

In this period it is relevant to take into consideration the restoration war, this event resulted in damages to the San Francisco Gate, especially in the Gate shape that leads to the plaza that is believed was constructed originally rectangular but due to the damaged suffered was reconstructed as an arch as it was recommended by the rules of that period to improve defense.

1736-1763

The earthquake that stroke Lisbon in 1755 also stroke Almeida, generating some cracks on walls specifically in the parts with construction defects. However, no record indicates it damaged the San Francisco Gate. The war of 1762 also affected the edification as it is describe that the vault was full of dirt. The gaps between the front curtain of stones in the Gate and the guard's chamber structure are disconnected which seems to indicate that these structures were made in different times.

1744-1789

Comparison of documents from 1762-1764 indicate the creation of the actual tourism spot, originally the guard officer house. In 1764 a campaign to do repairs was undertaken in the internal Gate of San Francisco to replace damaged sections with new stones.

1810-1823

In 26 August 1810, the gunpowder storehouse next to the castle exploded generating great damage to Almeida fortress and to the castle. This explosion was not the only event causing damage, as the bombing due to the siege did a huge contribution as well.

The Magistral Gate of San Francisco was also heavily affected, having been destroyed its permanent bridge. Around September - October 1812 the reparation works on the San Francisco Gate began. War prisoners were used to work on the fortress reconstruction as there was a lack of workers.

In December 1812, the Gates of San Francisco were still not in operation due to the slow process of reconstruction. At this point, the Gate of Santo Antonio was the only one operational and also it was in this Gate where the gun powder was stored which was a dangerous combination and urged the reconstruction and habilitation of the San Francisco Gate.

In 1815 the order to start reconstruction works on the San Francisco Gate was issued but since the war was over in 1814 the urgency of reconstruction was not as high as before and the construction works were kept to a minimum. This was translated for example in the non-reconstruction of the bridge in the Gate of San Francisco but instead the access was replaced with a ramp as can be seen in a construction joint that is clear in the present photographs (Figure 8).

Figure 8. Ramp for access to the Gate of San Francisco (Technical comission for the candidacy of Almeida, 2009)

2.2.3 Recent past interventions

No major works were developed on the San Francisco Gate for a long period of time and it was not only till the fortress was classified as National monument in 1938 that it recovered the attention of the government entities which resulted in a wave of restoration works.

Decade of 30's in the XX century

This period of reconstruction is characterized by a more scientifically approach to the restoration of the fortress. The works in this period are influenced by the conclusion of the First International Congress of Architects and Technicians of Historic Monuments, in Athens in 1931 and the publication of the "Carta del Restauro". In 1938 a list of deep intervention works was developed to begin the reconstruction of the fortress.

Decade of 60's in the XX century

Restoration works in the San Francisco Gate began in this period: earth covering the longitudinal steps of the cover was removed.

Figure 9. State of damage in the Gate of San Francisco year 1962

Decade of 70's in the XX century

In 1973 a proposal for the repair of the bridge connecting to the San Francisco Gate was made, and works began in 1978. It was determined that the consolidation of this bridge would not be fitted as a solution to the heavy load traffic transiting to Almeida. Therefore, it was required the creation of a new access for heavy load traffic. So, a third Gate was proposed and developed.

Decade of 80's in the XX century

In 1986, works continued in the San Francisco Gate whose right side urgently needed consolidation and cleaning of the masonry. The mortar was then replaced for a hydrophobic mix with cement base, the mortar in this period had a proportion 1:2/3:6 cement, lime and sand.

Decade of 90's in the XX century

The information Centre was create in the Magistral Gate of San Francisco in 1992 after a few small adaptation works. External intervention was limited to vegetation cleaning.

2.3 Current research

Nondestructive techniques (NDT) were applied to reach an overall understanding of the structure, morphology and damage level. Even the material properties were obtained by the appropriate utilization of these techniques. In this case study, NDTs are of highest importance as some structural characteristics, for example the morphology, needed to be determined without causing severe damage to the structure.

Other techniques such as visual inspection and laser scanning were also carried out. Laser scanning, in particular, resulted in a great advantage to quantify damage in the tunneled structure by producing really valuable results that helped to measure the state of deterioration of the stone masonry.

Some parameters, such as material mechanical properties, are necessary in order to create a representative model. For that purpose, a nondestructive testing campaign was carried out in order to determine these values. Sonic testing and georadar are of outmost importance to obtain data without damaging the structure. Figure 10 shows the location of several tests done in the Gate of San Francisco, locations marked with a red-yellow circle represent indirect sonic testing which are the more relevant for this study as the material properties were direct or indirectly derived from them.

To measure the mechanical properties of the stone-masonry, sonic direct tests and impact echo indirect tests were carried out. The procedure required two persons, one member of the team would put the transducer in the stone while the other one would generate the impact in the desired location. Meanwhile, all data was being stored in a computer that was brought along. More details about the sonic testing procedure will be given in the next section.

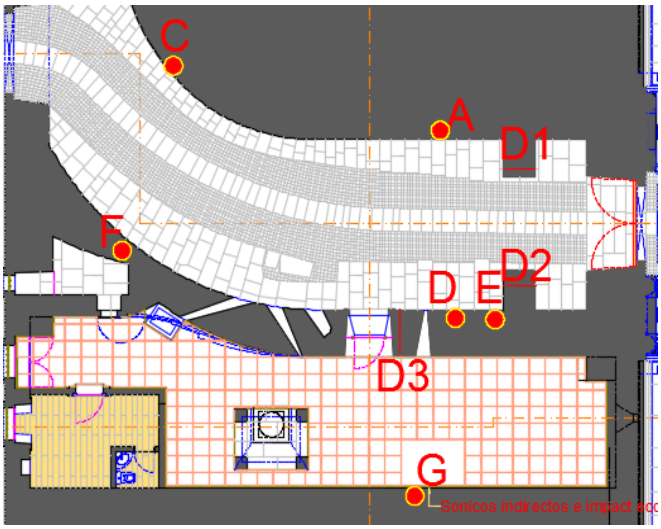

Figure 10. Positions of sonic testing

2.3.1 Sonic testing

Elastic wave methods allow the user to obtain information by means of measuring the wave propagation properties across a particular material. As the essential material properties like modulus of elasticity, density and Poisson ration are directly related to the velocity of the passing wave, the correct measurement of this property is fundamental. There are four types of waves that propagate in an elastic body:

- P waves: pressure or longitudinal waves
- S waves: shear or transversal waves
- L waves: superficial and transversal waves
- R waves: superficial and elliptical waves

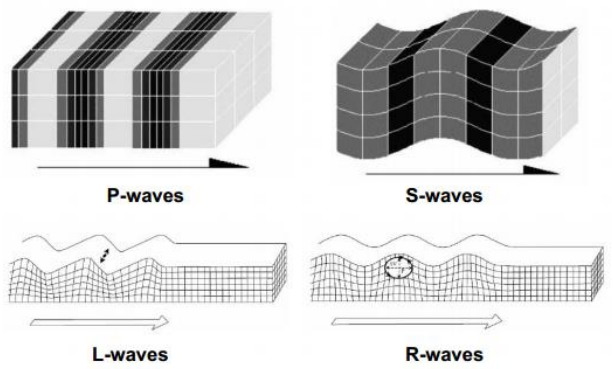

Figure 11. Types of waves that propagate in elastic bodies (Ramos & Lourenço, 2016)

For the type of sonic testing developed in this project and taking into account the available equipment, the P and R waves were measured in several locations.

During the execution of the sonic tests, the wave is created by means of an instrumented hammer connected to a computer that measures exactly when the wave is created and a transducer (accelerometer) that registers the resulted signal (see Figure 12). By measuring the distance between the impact point (hammer hit) and the location of the transducer the velocity of the wave can be calculated. According to the relative position of the hammer impact and the receiver transducer there are three types of testing that can be used: direct, indirect and semi direct. The selection of the type of test depends on the possibilities of mobility in the site and the objective of study (which wave to measure). Material properties for this case were determined by means of direct and indirect testing.

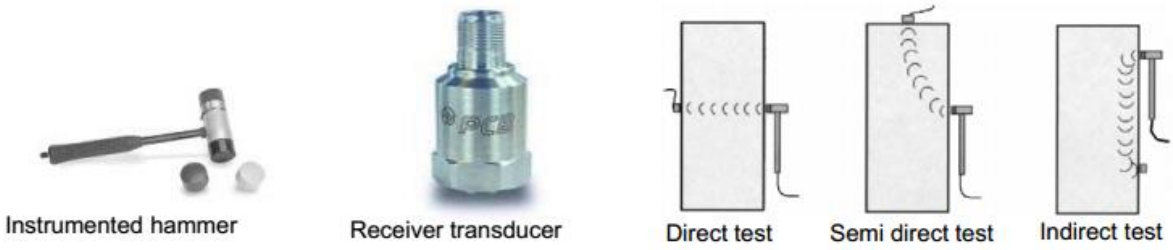

Figure 12. Sonic testing elements (Ramos & Lourenço, 2016)

Once the velocities of P and R waves were obtained, the following equations allow to determine the Poisson ratio and the modulus of elasticity:

$$\frac{V_p}{V_R} = \sqrt{\frac{2(1-v)}{(1-2v)}} \frac{(1+v)^2}{(0.87+1.12v)^2} \qquad \textbf{Equation 1}$$

$$\boldsymbol{V_P = \sqrt{\frac{E}{\rho}} \frac{1-v}{(1+v)(1-2v)}} \qquad \textbf{Equation 2}$$

As it can be seen from the formulas, the density is a property that must be known prior to the calculation of the mechanical properties. Because the influence of the density is relevant, the value to be used must be decided carefully. The results of velocity of both direct and indirect testing are shown in Table 1.

Table 1. Wave velocity for indirect sonic testing

Indirect tests	Distance (cm)	Speed P(m/s)	Speed R (m/s)
Point A (stone)	100.00	1985.72	987.15
Point C (stone)	70.00	1828.00	906.03
Point D (stone)	90.00	1818.96	854.17
Point E (stone)	130.00	1772.04	975.84
Point A (masonry)	70.00	1516.77	777.66
Point F (masonry)	100.00	1431.25	738.20

2.3.2 Laser scanning

Laser scanning is of great use to map and evaluate damage in stone masonry structures. This technique employs laser light taking advantage of the pure color and highly directional light beam to obtain and store 3D computer images of objects or sites. The technique works by employing a low power laser beam as the light source and then detecting the light that is reflected from the structure by means of very sensitive sensors (Pires & Borg, 2016). Employing this technique allows the recompilation of 3D information that vary from the size of a small handcraft to a huge site as the Gate of San Francisco.

The main advantages of the laser scanning method are its accuracy and the quality of the images or models that can be created by processing the information collected. The equipment is lightweight and allows easy operation even in places that are hard to access. It is a perfect approach for documenting monuments as the light doesn't damage the objects while it produces a lot of information.

In the specific case study of the Gate of San Francisco, the laser scanning method has been of great help mainly for two reasons: first documentation, thanks to implementation of this technique now it exists a 3D record of the San Francisco Gate that could be further used for study, documentation or even reproduction of parts of the original structure. Secondly the technique has allowed to quantify the deep and width of damage in the joints of the barrel vault. Measuring each joint manually would have required an immense amount of work while never being as precise as the results obtained from the laser scanning cloud of points. Figure 13 shows an example of the documentation of damage in the joints of the barrel vault by means of laser scanning.

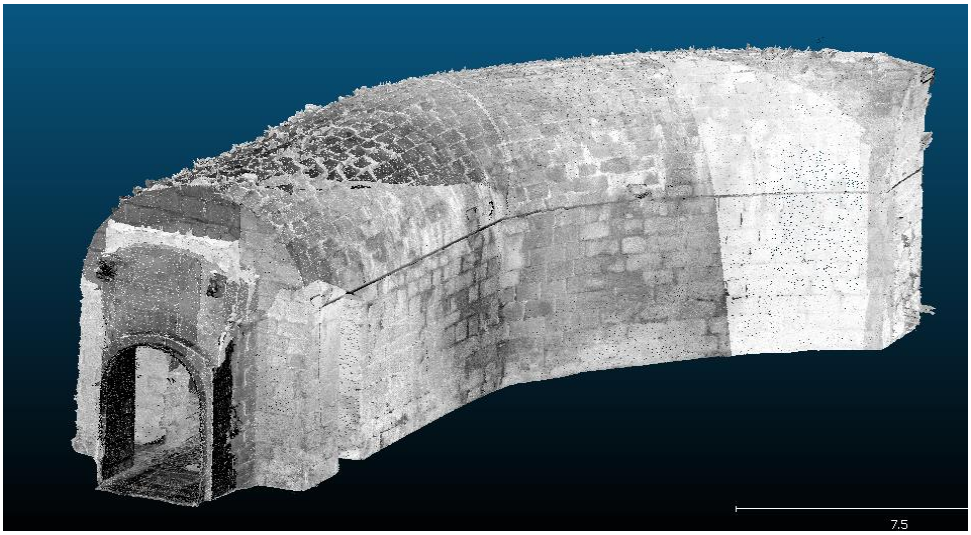

Figure 13. Laser scanning cloud of points of the tunnel in the Gate of San Francisco

2.4 Numerical modeling strategies for masonry

Several different approaches can be utilized to model masonry. These options will vary depending of the failure mechanism that is to be obtained and also to how much detail and effort the investigator is willing to invest in his model.

In general terms, there are three different types of approaches. Based on the level of accuracy and the amount of effort that wants to be invested in a model Lourenço (Lourenço P. B., 2013) proposes three types of models: a detailed micro model in which the units and the mortar in the joints are modelled by continuous elements while the interface between units and mortar is modelled as an interface; in a second approach where only the units are represented by continuous elements while the unit-mortar interface and the mortar itself are modelled by discontinuous elements; finally, a macro model approach is also available in which all materials are mixed into one homogeneous material.

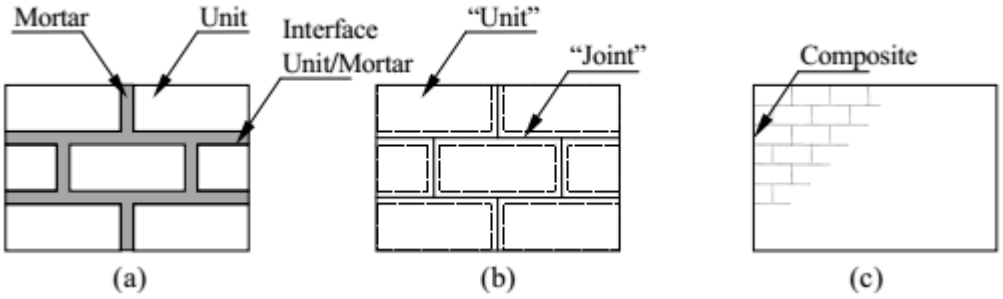

Figure 14. Types of models for masonry: (a) Detailed macro-modelling; (b) simplified micro-modelling; (c) macro modelling. Source: (Lourenço P. B., 2013)

Among all the methodologies available to model solid mechanics, the finite element method is the most popular and proof of this is that an extension to represent discrete joints was created for this method. This allows to create more precise modeling strategies as the micro modelling in which all possible failure mechanisms are included: cracking of joints, sliding over a head or bed joint, cracking of the units of crushing of the masonry either for monolithic or cyclic loads (Lourenço P. B., 2013).

2.4.1 Lourenço's proposal

Lourenço (Lourenço P. , 1996) proposed two models to describe the non-linearity of masonry. At this time, a micro model was developed that worked by concentrating the inelastic behavior in the joints. He concluded that, although this type of analysis shows results that represent reality as they are similar to the ones obtained in laboratory tests, the amount of computational effort and time required to make this type of modelling makes it more suitable for small structures or structural details.

He also proposed a macro model for larger structures that considers a Rankine failure in tension (cracking) and a Hill type criteria for compressive failure (crushing).

Nowadays investigation have gone much further and the initial models proposed by Lourenço evolved from two to three breaking the micro modelling category into two categories. These three models englobe the different approaches that, in the present, are available for modelling masonry.

2.4.2 Page's proposal

Page was one of the first investigators to propose a model to represent the non-linearity of masonry (Page, 1978). Pages model recreates masonry as the interaction of two materials: brick and masonry. Page's model uses plane stress quadrilateral finite elements with eight nodes and 4 degrees of freedom for each node to represent the bricks. Isotropic properties are assigned to each element and the mechanical properties are obtained from laboratory tests (Campbell Barraza, 2012).

He represented the mortar joints as link elements that could only be deformed in normal and shear directions. Material properties were also obtained from laboratory tests and, in general, they have low tensile capacity, high compressive strength and the shear resistance is associated to the state of compression. This method shows to be flexible and allows to be applied to a wide variety of geometries and material properties.

3 CONSTRUCTION OF THE FINITE ELEMENT MODELS

3.1 Basic principles for modelling of stone masonry constructions

The type of analysis chosen for this study is a 2D macro model, which means the joints and stone pieces will be homogenized in one unique material (see chapter 2.4). Since this method requires the assumption of the stone and joints to act as a sole and homogenous material it has the disadvantage that the material properties become harder to obtain in a precise way. Therefore a sensitivity analysis will be implemented to overcome this limitation. Additionally, due to the inherent nonlinearity of masonry and, globally, all materials used in old masonry structures, a nonlinear analysis will be used to consider the possible nonlinear physical behavior of structure. The numerical analysis will carried out using two software packages: DIANA 9.6 for processing and Midas Fx for pre and post processing.

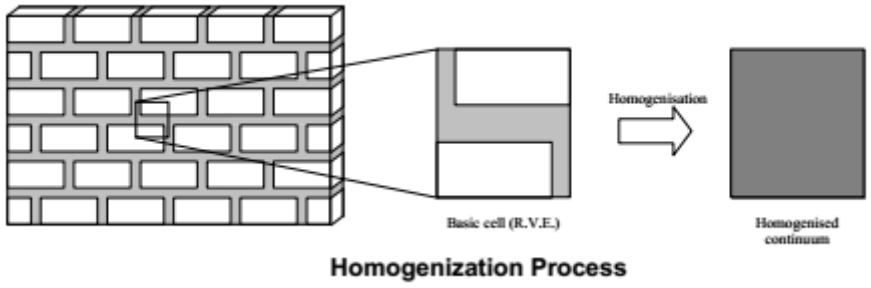

Figure 15. Homogenization explanation for macro modeling (Lourenço P. , 1996)

The 2D model created represents a cross-section of the entire structure that doesn't consider the holes made by the Gate or the windows that connect the main Gate path with the current tourism office, antique house of the guard, as illustrated in Figure 16. This cross section was chosen because it is representative of a large portion of the tunneled structure of the San Francisco portal.

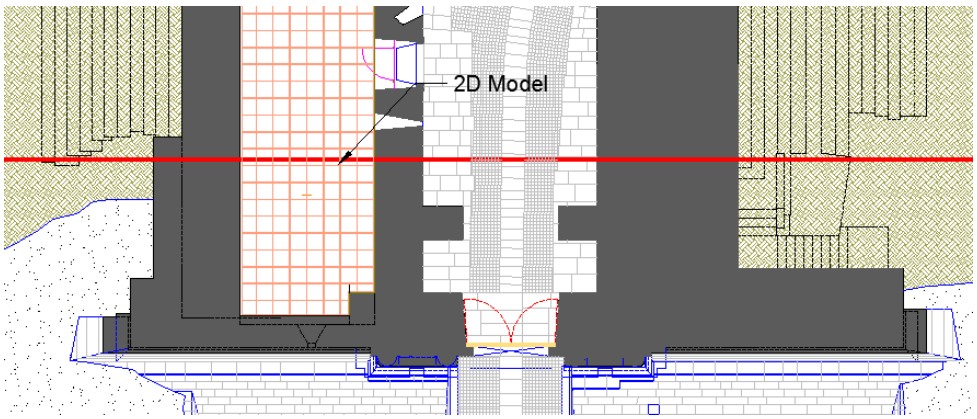

Figure 16. Cut section for the creation of the 2D model

The capacity of the structure will be assessed when subjected to its own weight and the regulated external live load (Eurocode 0). Two load types configurations will be used: self-weight only and self-weight and a live load of 5 kN/m, which will be applied as a distributed linear load on the roof of the structure that accounts for the possibility of having a dense group of people reunited and located on the top of the structure. Although this value might seem high for a live load it represents an unusual behavior that occurs every year in Almeida: a reconstitution of the battle between France and Portugal is carried out annually, which attracts lots of tourists. These people generally seat and watch from the top of the structure.

3.1.1 Constitutive material law

The constitutive model chosen is the Total Strain Crack Model that follows smeared approach for the fracture energy. The strain concept chosen for the model is the Coaxial, also known as Rotating Crack model in which the stress-strain relationships are evaluated in the principal directions of the strain vector, this kind of approach is commonly used in reinforced concrete as well (TNO DIANA BV, 2014).

Under this configuration the material can present cracking or crushing in the loading process. The material deterioration in cracking and crushing can be represented by the stress-strain curve illustrated in Figure 17 The shape of the compressive and tensile sections can be varied, for this model the tensile behavior will be represented by an exponential curve and the compression by a parabolic one. The material model for the soil was chosen as Drucker-Praguer, as recommended by the DIANA manual.

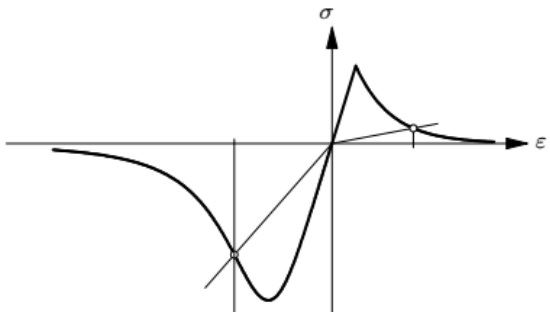

Figure 17. Constitutive law for material in Total Strain Crack model (TNO DIANA BV, 2014)

3.1.2 Element selection

For the 2D analysis, the section of the tunnel is assumed to be much larger in the out of plane direction restraining out of plane deformations, therefore plane strain elements are optimal to

represent this behavior. From the Diana manual (TNO DIANA BV, 2014) several options exist for plain strain elements but the one recommended for a nonlinear analysis are the group or regular plain strain elements:

"The regular elements may be applied in all kinds of structural analysis including nonlinear analysis with plasticity, cracking etc." (TNO DIANA BV, 2014)

These kind of elements are preferred when a nonlinear analysis is to be developed and they are specifically recommended for nonlinear cracking which is the constitutive law applied to the materials in this study. From the family of regular elements two are preferred: CT12E – triangle, 6 nodes, and CQ16E – quadrilateral, 8 nodes. Both elements use quadratic interpolation.

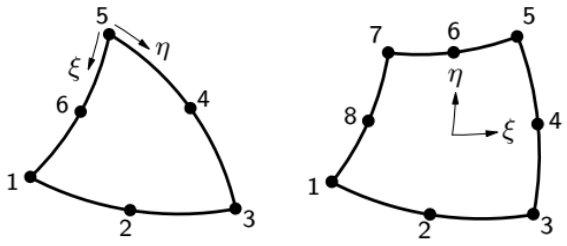

Figure 18. Element selection for non linear analysis (TNO DIANA BV, 2014)

3.2 Material properties

Two materials are considered in this model: a homogeneous material that characterizes the behavior of the stone masonry structure and an infill material that represents the soil that covers and surrounds this structure. For the selection of the material's parameters, a short comparison was made previously between values obtained from literature review and those extracted from the testing campaign. The values are shown in the Table 2 as follows.

Due to the high variability of the values for materials properties that can be found in an historic masonry structure, it is difficult to establish real effective values for these parameters. For that purpose, a sensitivity analysis was developed by changing the values of tension, compression and modulus of elasticity for the stone masonry material that composes the structure. The values utilized for this study can be found in Table 3.

Table 2. Parameters for stone masonry material according to literature review and testing campaign

Masonry	*	**	***	****	Testing campaign
E (GPa)	3	2.06	3	3	2.4
v	0.2	0.2	0.2	-	0.25
ρ (kg/m^3)	2300	2200	2000	2200	2100
f_c (MPa)	3 -6 -infinite	2	6	3 - 6- -9	2.4
G_c (N/m)	1.6*fc	3.2	9.6	1.6*fc	3840
f_t (MPa)	0	0.2	0.1	0	0.12
G_t(N/m)	0	120	50	0	120

* (P.B. Lourenco, K.J. Krakowiak, F.M. Fernandes, L.F. Ramos, 2007)

** (Núñez García, 2015)

*** (Garcia Roca, 2015)

**** (Pedro Lança, Paulo B. Lourenço, Bahman Ghiassi)

Table 3. Variation of parameters of the stone masonry material for the sensitivity analysis

Masonry	Referenc e	2 f_c & G_c	0.5 f_c & G_c	2 f_t & G_t	0.5 f_t & G_t	2 E	0.5 E
E (GPa)	2400	2400	2400	2400	2400	4800	1200
v	0.25	0.25	0.25	0.25	0.25	0.25	0.5
ρ (kg/m^3)	2100	2100	2100	2100	2100	2100	4200
f_c (MPa)	2.4	4.8	1.2	2.4	2.4	2.4	4.8
G_c (N/m)	3840	7680	1920	3840	3840	3840	7680
f_t (MPa)	0.12	0.12	0.12	0.24	0.06	0.12	0.24
G_t(N/m)	120	120	120	240	60	120	240

The properties of the infill material poses a high level of uncertainty. There is a written record of an intervention to the structure in 1997 in which is detailed that, with the purpose of impermeabilization, the structure was injected with organic grouts. The extent of these injections and the properties of this material are unknown. Therefore, for this project, the results will be projected for two types of infill material: a nonlinear infill material with characteristics similar to an infill studied in the Quartel das Esquadras (another military structure located right next to the San Francisco Gate) and a soil infill whose characteristics are also taken from a soil studied in a nearby area. No testing campaign has been made yet to analyze the properties of the infill, therefore, a sensitivity analysis was developed varying the soil characteristics to double of its values to study their influence on the model; the material properties of the soil that appear in Table 5 are based on a soil utilized in the bridge of Allariz.

Table 4. Parameters for the infill according to literature review and testing campaign

Infill	*	**	***	****	Chosen
E (GPa)	1	0.31	1	0.5	0.5
v	0.2	0.2	0.2	-	0.2
ρ (kg/m^3)	2300	1900	1400	1800	1900
f_c (MPa)	0.5 -1-2	1	1	1	0.5
G_c (N/m)	1.6*fc	1.6	1.6	1.6	900000000
f_t (MPa)	0	0.1	0.1	0	0.025
G_t(N/m)	0	0.012	0.012	0	900000000

Table 5. Parameters for soil model and variation for sensitivity analysis

Infill	Reference	Double cohesion	Double tension	Double angle of friction
E (GPa)	0.1	0.1	0.1	0.1
v	0.2	0.2	0.2	0.2
ρ (kg/m^3)	1700	1700	1700	1700
Cohesion (MPa)	2	4	2	2
Tensile strength (MPa)	2	2	4	2
Angle of friction (radians)	0.342	0.342	0.342	0.684

3.3 Description of the model for the original state of the structure

The geometry for this case is considered to represent the original state, right after the construction finished. Perfect semicircles were used to represent the barrel vaulted roof without any consideration of the degradation that exists in the present.

The structure is modeled as two arches resting on three columns while being all covered by an infill material as depicted in Figure 19. The gray color represents the stone masonry material and the golden one the infill material.

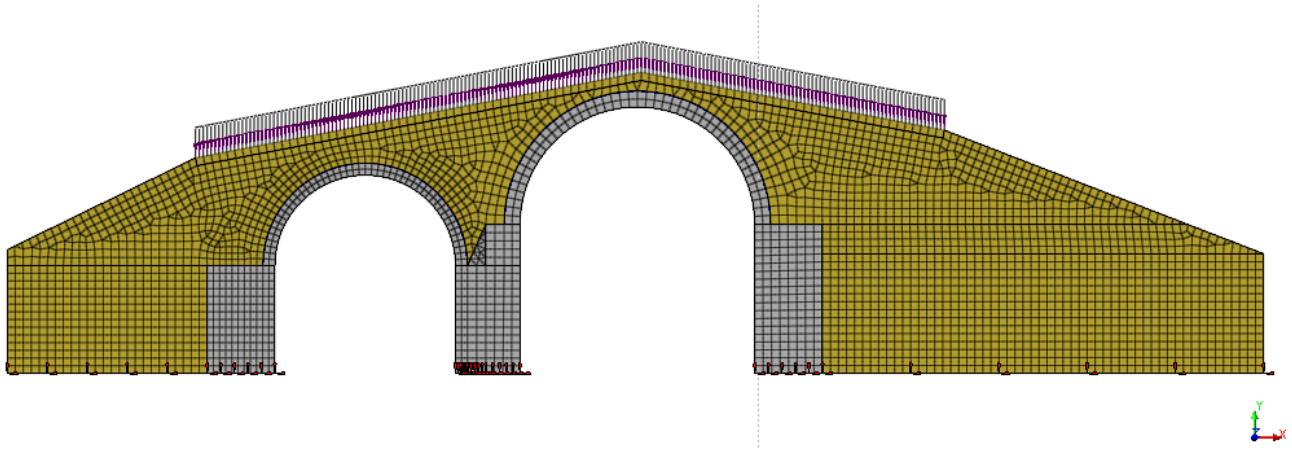

Figure 19. 2D model geometry, mesh and live load.

The boundary conditions for this structure consist in the fixation of displacement in both horizontal and vertical direction for all nodes at the bottom. This applies for both models damaged and undamaged.

There are two load cases: self-weight that is applied as gravity to all materials and a live load visible in purple color in the top of the structure with a value of 5kN/m. In this model, the mesh could be said to be coarse in the arch as only two elements per width exist. To improve the accuracy of the model, 8 nodes per element have been considered.

This model represent a 2D section of the real complex structure. This section was chosen as representative as it is a planar cut from the most damaged area of the tunnel. The amount of lateral infill considered in the model was chosen as to leave enough material to distribute stresses to the sides to a point where they would be low enough as to be negligible.

3.4 Description of model for the actual structure including deterioration

For the model to represent the damaged structure, it requires much more detail. This model was essentially generated from the previous original model by adapting the arch mesh and refining it to include four more elements per width as to have a total of eight elements per width, each one of them with 5cm and with a size ratio very close to one. This refinement can be seen in Figure 20.

For the refinement of the mesh, small alterations were made to the original model in its geometry, specifically in the columns. The original rectangular geometry was replaced for a rectangle and a transitional trapezoidal element to help keep the element size ratio as close as possible to 1 while keeping all nodes connected and maintain the original elements in other parts of the model.

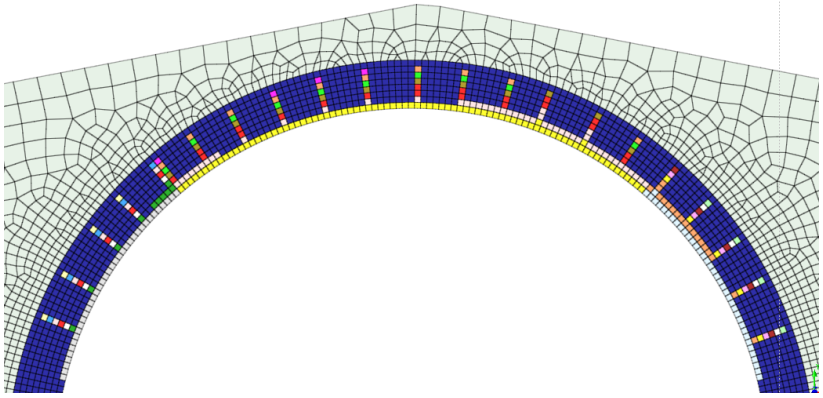

Figure 20. Mesh refinement for the deteriorated model

Notice in Figure 20 how the elements possess different colors as if they were assigned in groups. This is because actually 22 different groups of elements were created as to classify the elements according to their location: left, center or right. This classification was necessary in order to create a phase analysis that allows the study of the structure's response while gradually removing material from the arch.

The material properties remain the same although it would be logical to imagine that the material capacity has sustain a certain level of reduction with time. Nevertheless, there is no actual way to quantify what were the original properties of the stone. Therefore this model only considers the deterioration of the structure by the removal of elements without changing the material properties.

The elements removal for the representation of the actual state of damage will be done in three phases. In the first one a first layer the white yellow and light blue elements will be removed from the layer 1 in the intrados. In a second phase the green elements of the left, the white in the middle and the pink in the right will follow the same procedure of removal. Last the red elements from the middle section will be removed from the structure thus representing the actual state of damage.

4 SENSITIVITY ANALYSIS

4.1 Original properties

In this section, the analysis will focus on the structure's response to a continuous increment of a live load located in the top of the structure. The original live load had a value of 5 kN/m. To control the linear/nonlinear behavior of the structure due to the live load incremental, a single control point was chosen. The control point is located in the intrados of the biggest arch as seen in Figure 21 and is marked with a purple tag. The selected point corresponds to the area of highest deformation of the structure as a result of the applied load. It represents successfully the non linear behavior of the structure for all variation of material properties and loading conditions.

Figure 22 shows the displacement of the control point against the load factor. The direction of chosen displacement was the vertical one as it shows better the nonlinear behavior of the structure. When loaded, the arch not only displaces in the vertical direction but also its span widens. Damage by crushing and opening of cracks in the middle are testimony of the non-linearity of the material as a consequence of these combined effects. It can be noticed that the arch displaces the most in the middle, where the control point was placed.

For this analysis, the self-weight was totally applied in four steps before initiating the application of the live load. The steps for the self-weight were removed from the graphs for clarity purposes. The live load is incremented in steps of 25 % of the original 5kN/m, which means the structure receives a total of 1.25kN/m per step. As seen in Figure 22 the nonlinear behavior starts to be evident when the load factor reaches the value 30 (100% of the self-weight and a live load of 153kN/m). From this point, the structure shows a non-linear behavior until failure, at load factor 56 (100% of the self-weight and a live load of 280kN/m).

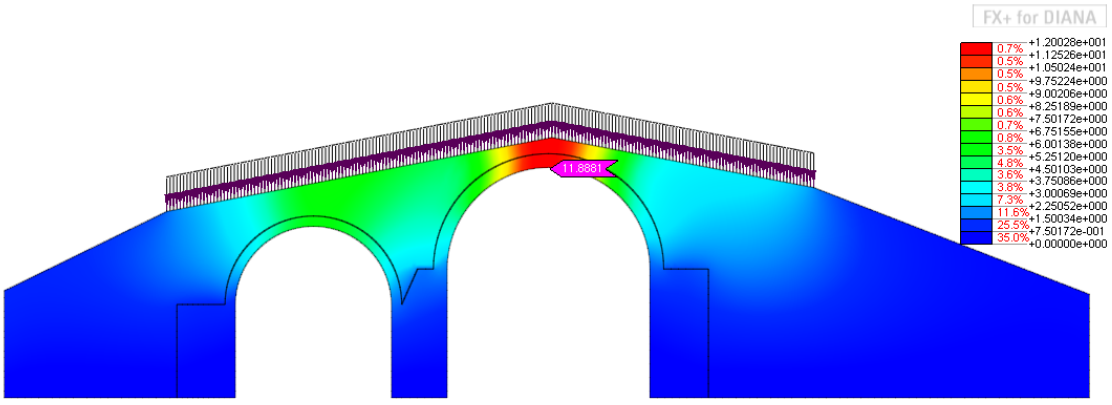

Figure 21. Deformed shape for live load

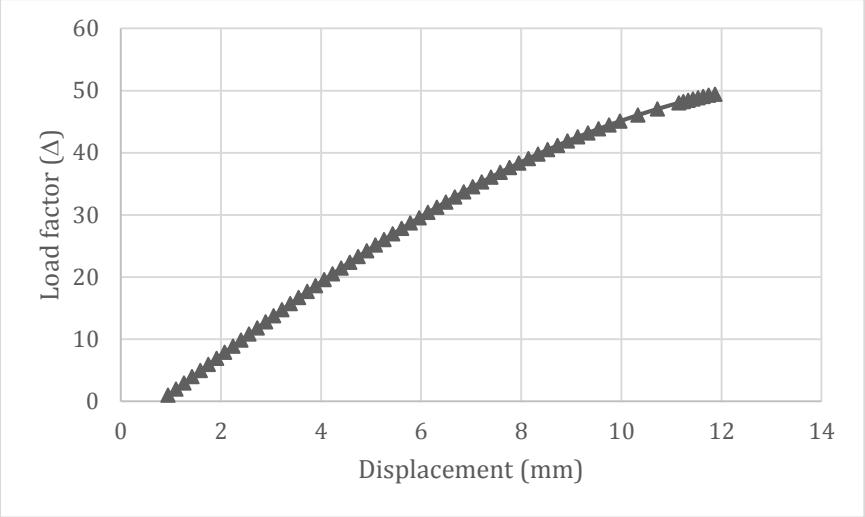

Figure 22. Load displacement diagram of the original structure for incremental of live load

Maximum vertical displacement occurs in the right arch and reaches a value of 12mm. The displacements are concentrated on the very top of the structure over the arches (Figure 23) concentrating damage on these elements of the structure.

Local failure occurs in the structure by the collapse of the barrel vault in which several hinges are formed before failure. The crack patter results clearly show severe damage in the middle of the intrados of the arch (Figure 23). This effect, combined with the crushing of the material by compression on the side's (as seen in the blue areas in Figure 24)results in excessive deformation in the arch and the generation of a local mechanism of failure.

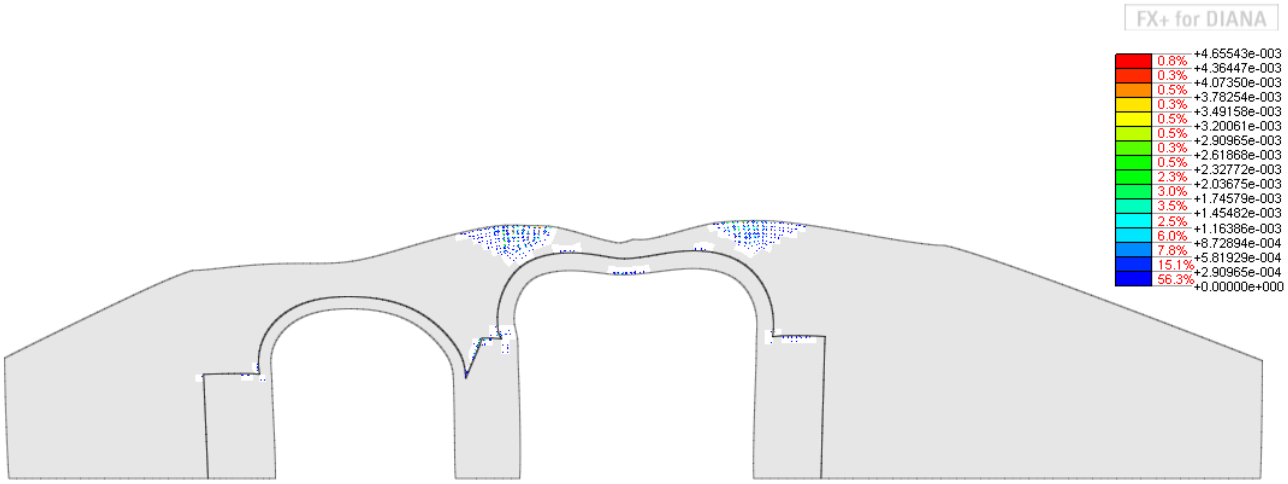

Figure 23. Crack pattern at failure by live load

At the failure, the compressive stresses have reached the maximum value of the material capacity, i.e., 2.4MPa. In the case of live load, the stone masonry material that composes the

supporting structure reaches the limit capacity in the right arch, specifically in the base of the arch as it is depicted by the blue colored zone in Figure 24. The failure mechanism is reached by crushing of the material in the base of the arches without producing important damage in the base of the columns.

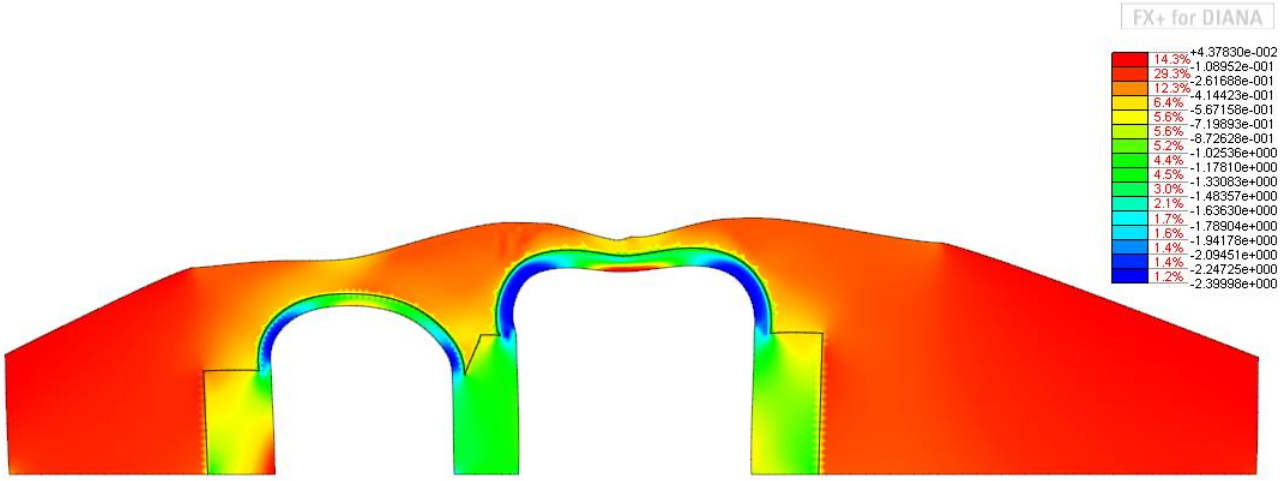

Figure 24. Principal stresses for incremental live load analysis

4.2 Variation of properties of the stone masonry

The compressive parameters are predominant in this analysis as it is this material property that defines the failure of the structure. Notice in Figure 25 how the response of the structure is almost directly proportional to the variation of the compressive strength limit of the stone masonry. Showing an increase in the load factor from 49 to 72 (≈+50%) when the compressive strength was doubled and a reduction from 49 to 27 (≈-50%) when the same property was halved.

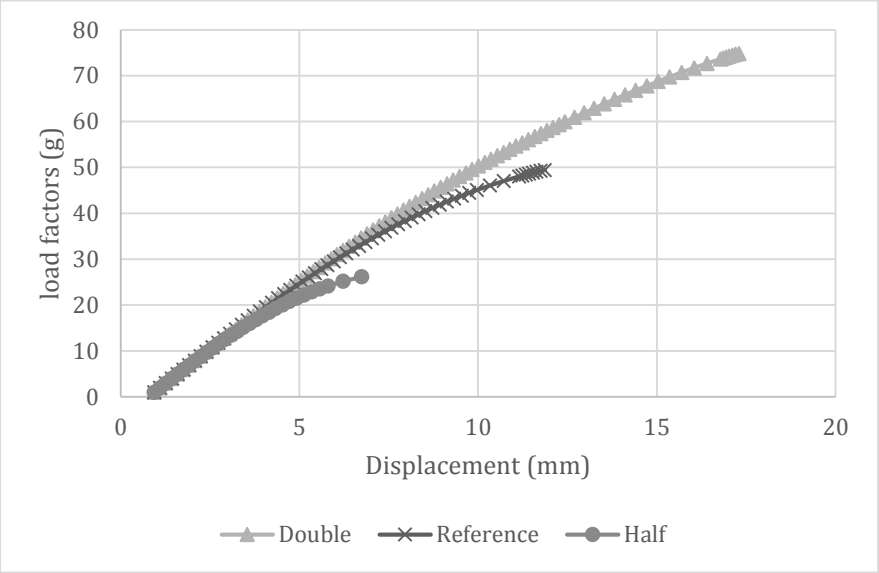

Figure 25. Sensitivity of results to variation of compressive characteristics for incremental of live load

Variation of the tensile strength of the material does not show any relevant effect in the failure history of the material as shown in Figure 26. For the reference properties the first crack appears at load factor of 11.8, while it develops much earlier at load factor 2.97 for half the tensile strength. When using twice the tensile strength value results in a later apparition of cracks, at load factor 29.6. Even though the comparison of history of crack apparition shows that the tensile strength does have a high influence in the formation of cracks, this effect is not reflected in the load history of the whole structure. This result can be interpreted as that the damage in tension is highly smaller than the one in compression. Therefore the structure failure is mainly governed by crushing of the material in compression.

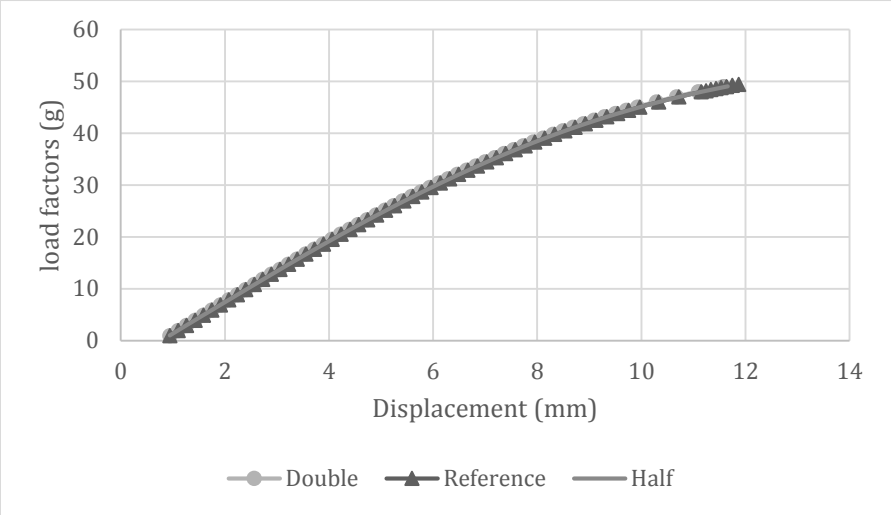

Figure 26.Sensitivity of results to variation of Tensile characteristics for incremental of live load

Variation of the modulus of elasticity shown in Figure 27 results in a direct change in the slope of the material curves in the load versus displacement diagrams. It is clear how a duplication of the modulus of elasticity results in a higher stiffness as the slope of the curve becomes higher. The structures rigidity is as well diminished after its modulus of elasticity its cut half. It must be noted that, while changing this parameter, the modulus of elasticity of the infill was not altered, which again point out the relevance of the material properties of the stone masonry structure compared to the infill material properties.

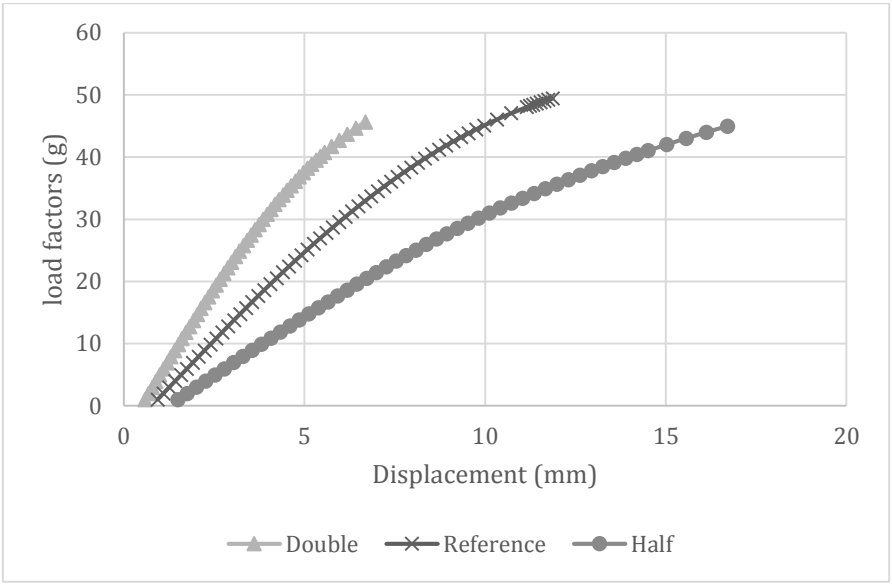

Figure 27. Sensitivity of results to variation of Modulus of Elasticity for incremental of live load

4.3 Variation of properties of the infill

4.3.1 Elastic infill

Variation of the infill from a nonlinear material to an elastic one does not have a great impact on the maximum load that the structure can take since the ultimate load factor varies from 49 to 56, which does not represent a large influence relatively to what can represent the variation of the properties of the stone masonry. The crack patter remains the same in the supporting structure while no cracks appear in the infill, as seen in Figure 28.

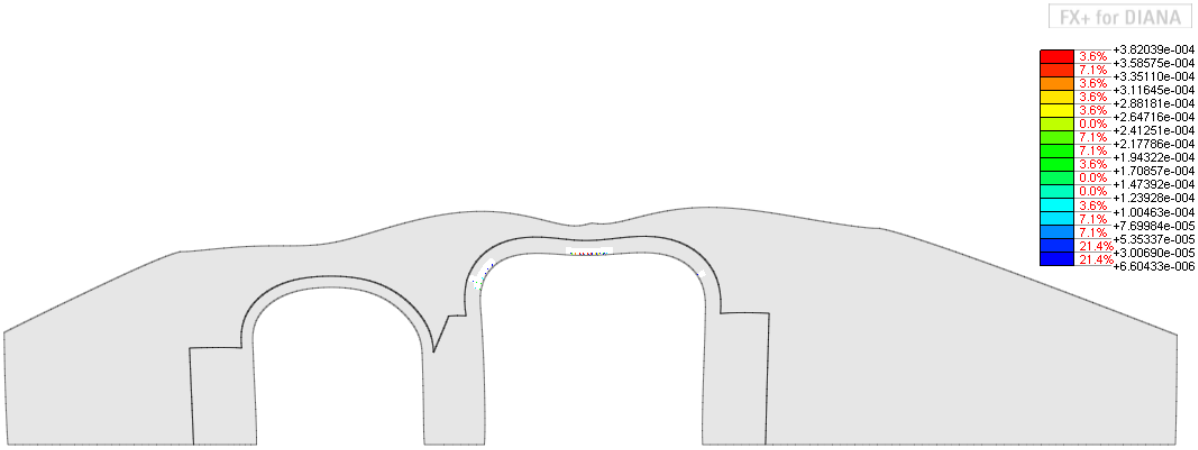

Figure 28. Crack patter for elastic infill

The principal stresses in tension and compression reach the material strength maximum capacity as well in the model with elastic infill. As it can be seen in the Figure 29, the zones of maximum compression remain the same. The principal stresses in tension, illustrated in Figure 30, varies strongly from the results with nonlinear infill as the tensile maximum stresses are obtained now in the infill, in contrast with the supporting structure in the nonlinear infill model.

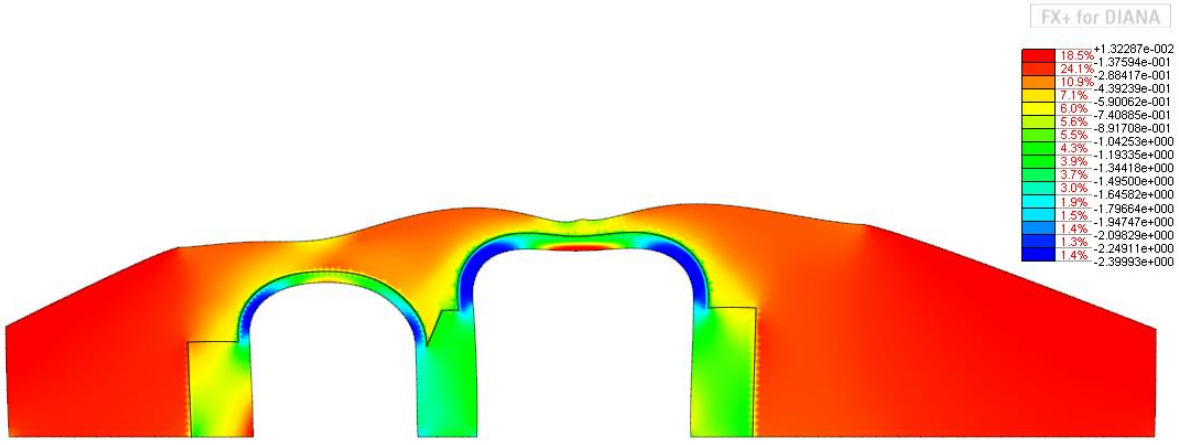

Figure 29. Principal stress for elastic infill

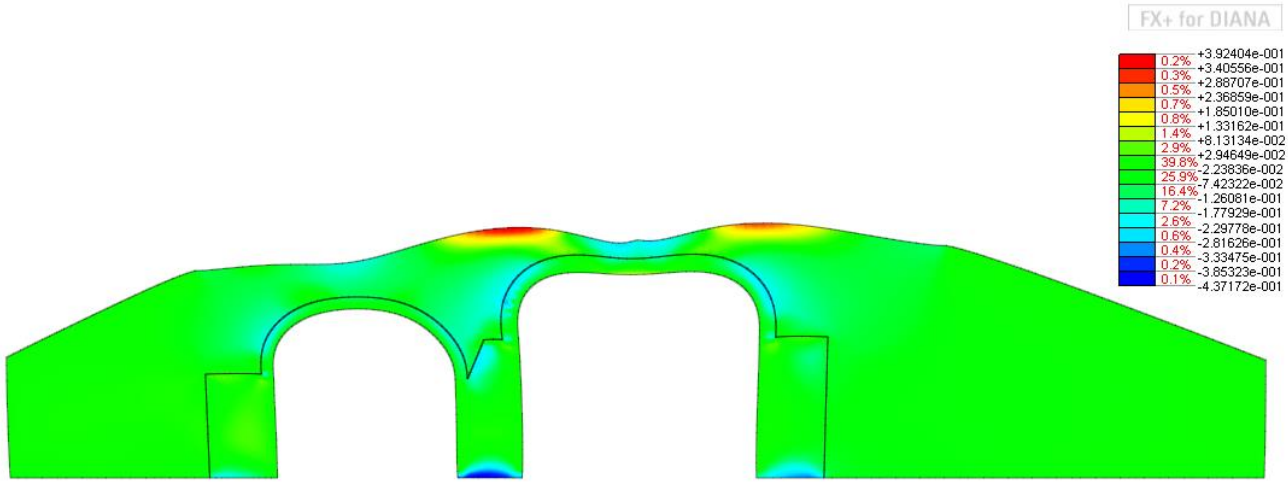

Figure 30. Principal stress for elastic infill

4.3.2 Soil infill

Another model was created with a soil material. For this model, the load factor varies greatly and the influence of the soil properties show a high importance. Figure 31 shows a comparison of the structure's behavior as a result of a change in the infill model. The nonlinear infill modeled with a total strain crack model results in a general higher stiffness for the structure and a higher load factor. A value of 49 compared to a value of 18.1.

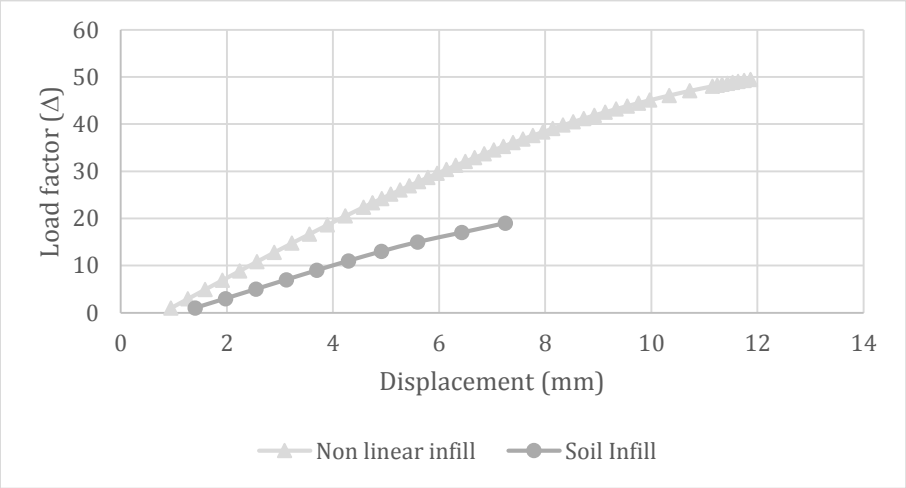

Figure 31. Comparison of load vs. displacement for a soil infill

Within the scope of using a soil material for the infill there are several others variables to take into consideration. Variation of the cohesion of the soil has a great impact on the structure as shown in Figure 32 where it can be seen that by doubling the cohesion of the soil the load factor increases significantly from 18.1 to 32. The tensile strength of the soil does not show a relevant influence in the

structure's response, while the variability of the angle of friction has a huge impact, making the model reach failure much faster, with a load factor of 8.2.

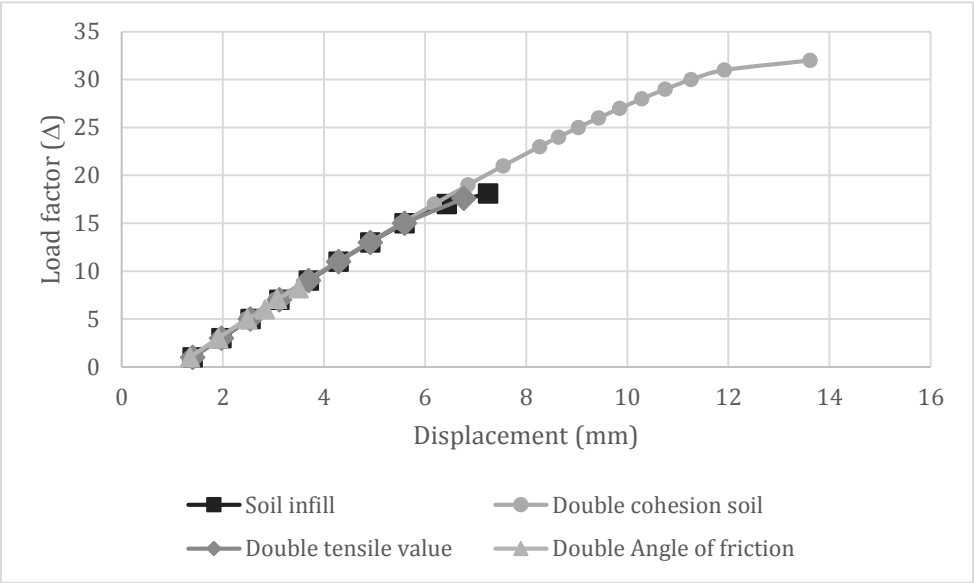

Figure 32. Sensitivity of properties for the soil infill

Despite lower capacity levels, the crack pattern for the soil model is much clearer and show several crack locations in the right arch that correspond to a failure mechanism due to symmetrical loading. The soil infill shows a more clear mechanism of failure which seems to make it a more adequate candidate to use for the study of the structural behavior of the Gate of San Francisco. But there is no certainty of what kind of material is in the infill as there are records that show there have been grout injections in the past.

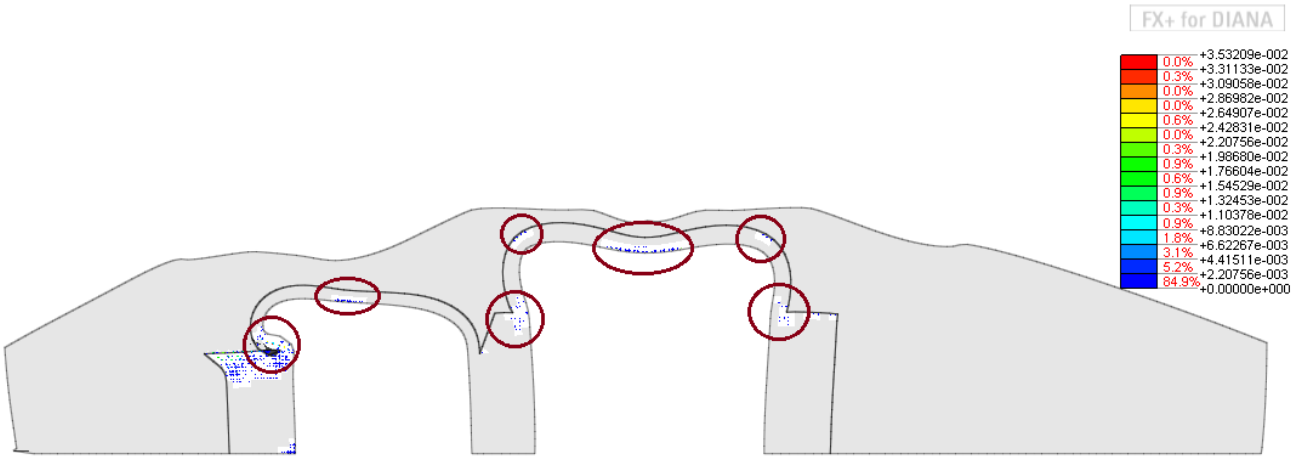

Figure 33. Crack pattern for a model with a soil infill

5 SAFETY ANALYSIS

The main purpose of this project is to determine whether or not the structure is still safe. For that purpose, a new model was created with a refinement of the mesh in the arch in such a way that the elements from the joints can be removed to represent the actual level of damage.

Thanks to the laser scanning several damaged profiles could be obtained. How this damage profiles were combined in order to obtain a model that would represent the reality is described in chapter 5.1.

For the safety analysis, a phase analysis was preferred. In this analysis, the elements that existed in the original structure will be removed until the geometry of the model corresponds to the present state of the structure. The removal of elements will be developed in three phases as to avoid abrupt changes in their stress state.

In a first phase, the structure will be loaded with its self-weight. Then, the elements will be removed without any extra loading as to represent the real evolution of stress due to deterioration in the building. A second phase will consider the structure to be loaded till failure by the live load. For this, the structure will be loaded till failure in three scenarios that represent the removal of the deteriorated part of the structure in three steps. Finally, the final step represents the structure actual state of damage.

5.1 Quantification of actual damage

Clouds of points were obtained in the zones that show more damage and thanks to this points that depth of the damage in the stone and the loss of material in the joints could be more easily quantified.

Three main damage zones were identified and studied (see Figure 34), the one that shows the worse state is the area closest to the exterior side of the fortress.

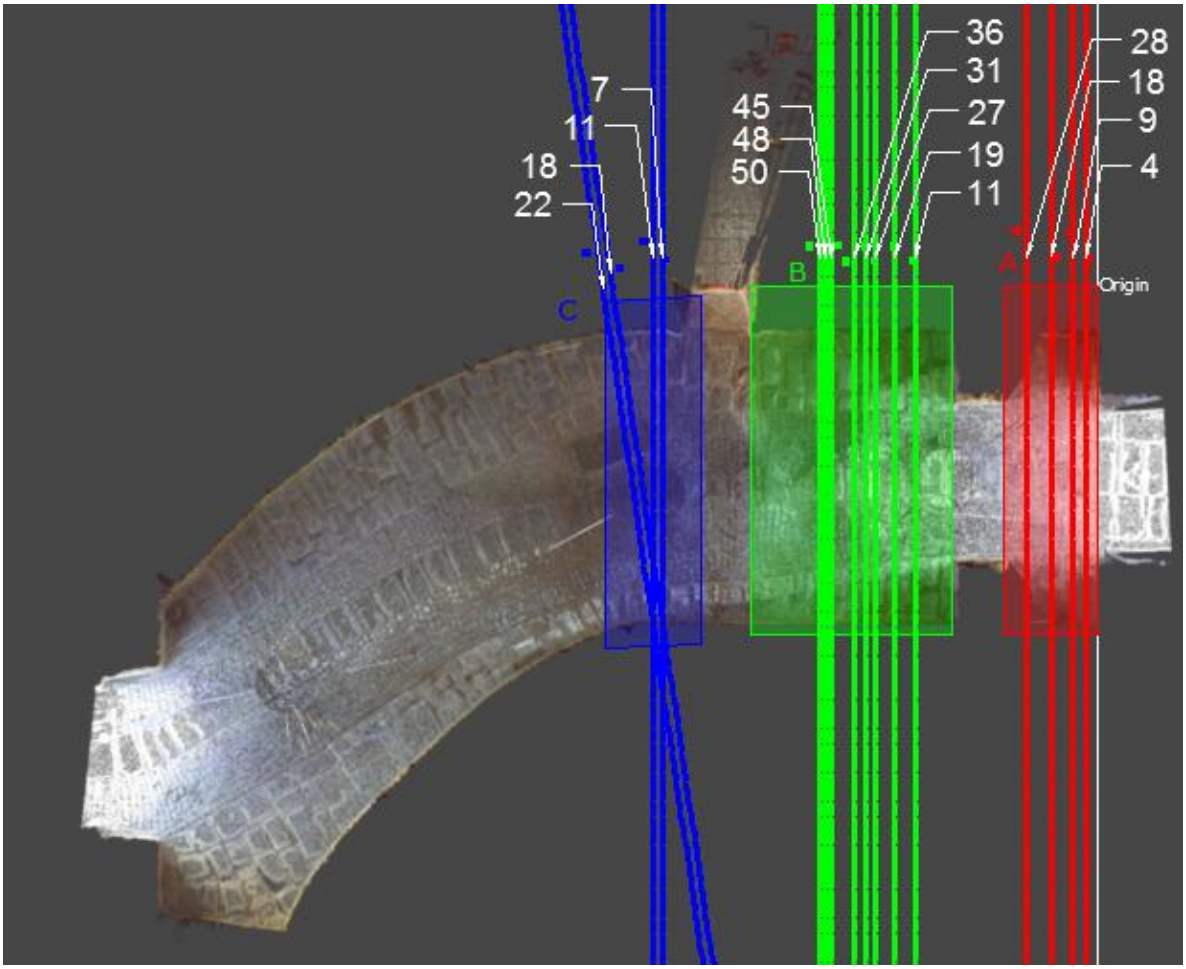

Figure 34. Laser scanning testing zones A (Red), B (Green), C (Blue)

By visual inspection it was clear that the highest level of damage occurred in the red zone (A). One of the hypothesis to explain the deterioration in the structure is the damage due to the wind entering the tune, if this cause were to be the mayor factor it would make sense to have the highest affectation in the entrance were the wind comes stronger.

An average from the clouds of points for zone A (Figure 35) was drawn as a line to represent better the deterioration and allow for comparison of the profiles. Profiles for Zones B and C are shown in Figure 36 and Figure 37. Note that the loss of material in the joints that resemble peaks are higher and more frequent in zone A than in zones B and C.

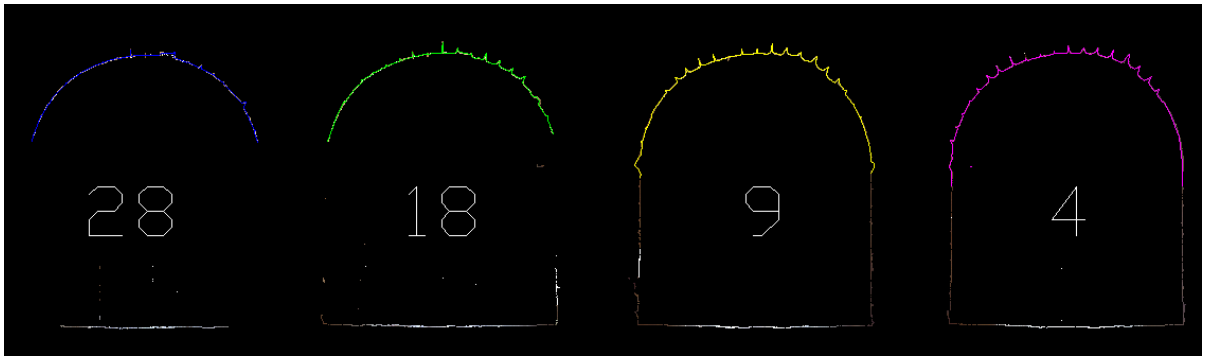

Figure 35. Damage profiles from clouds of points for Zone A

Figure 36. Damage profiles from clouds of points for Zone B

Figure 37. Damage profiles from clouds of points for Zone C

Figure 38 shows a superposition of the damage profiles in zone A, damage is not only deeper in this section of the tunnel but also the location of joints are approximately aligned which results in a higher risk of failure for the structure.

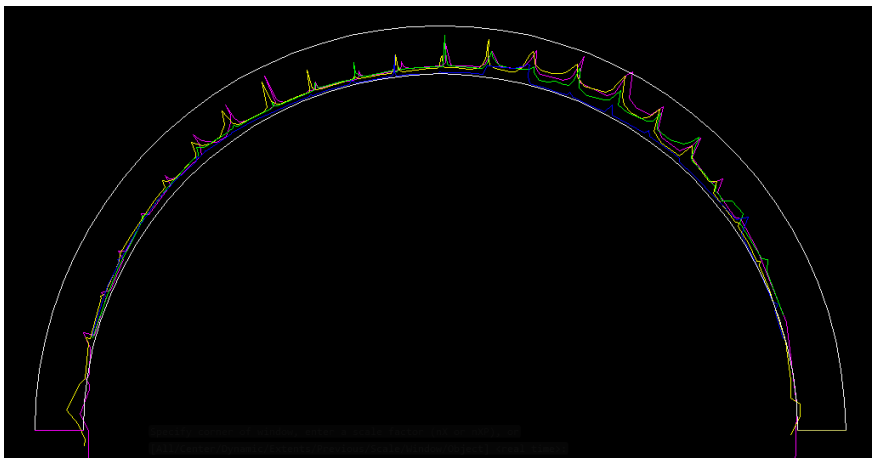

Figure 38. Superposition of damage profiles in Zone A

By using a graphical procedure to determine the mean values of all curves a new average curve can be created (Figure 39), this new curve purpose is to represent the state of deterioration of the whole section in zone A and will then also be used to create the model for the deteriorated state of the structure, see Figure 40 for a full detail of the final average damage profile.

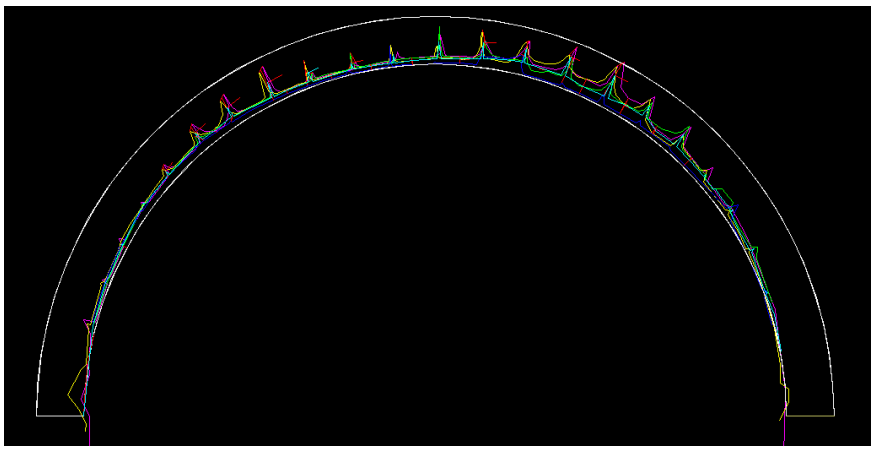

Figure 39. Average damage profile for Zone A

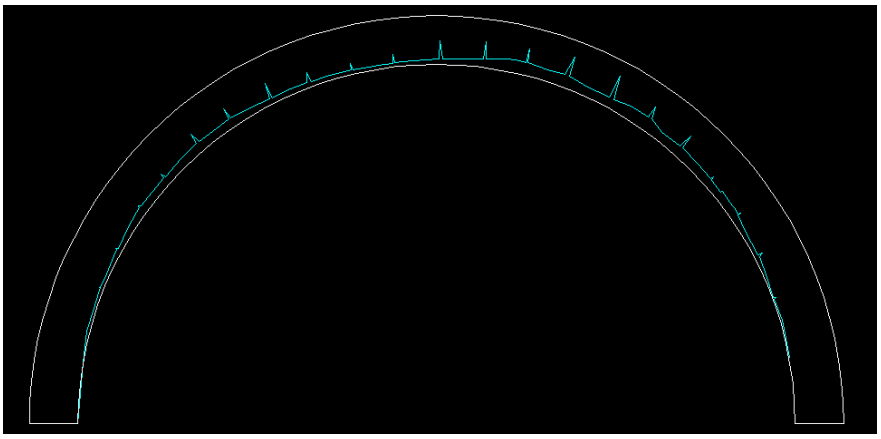

Figure 40. Detail of average damage profile for modelling

In order to verify that the profile obtained in zone A does represent the worst scenario of deterioration for the whole tunnel the average profile was compared to the damaged profiles in zones B and C (Figure 41). All cross sections of the tunnel in Zones B and C are contained by the average of zone A. In order to study the structural capacity of the deteriorated structure it is reliable to create a model based on the damage profile attained in from Zone A as it represents a higher level of damage than all the rest of the profiles and would most likely be the first section to fail.

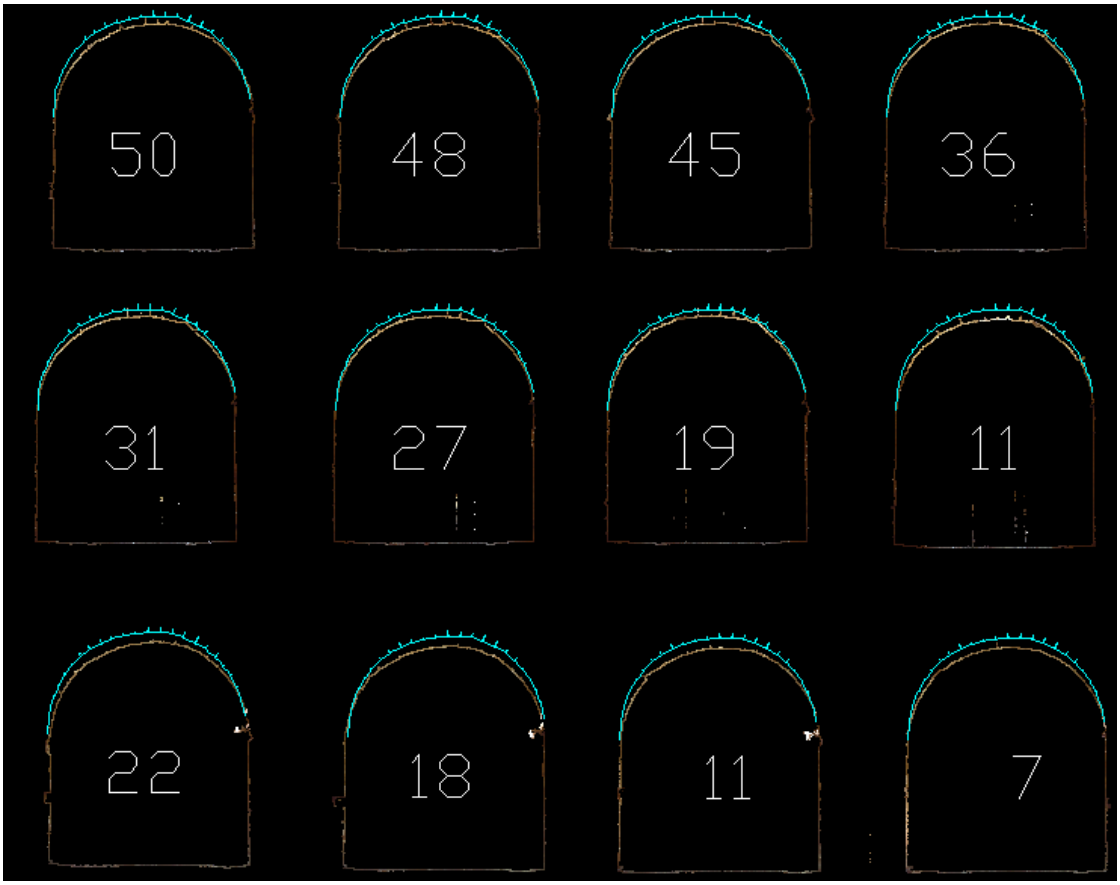

Figure 41. Comparison of damage from Zone A to the other damage profiles

5.2 Phase analysis only for self weight

This section will study the evolution of damage in the structure from the original state when the structure was just built to the present condition. Initially the structural properties of the Gate will be shown for the original condition without damage and subsequently the actual state of deterioration will be added in three steps described as: Phase 1, Phase 2 and Phase 3. It is to be noted that for this analysis, only the self-weight will be taken into consideration. An initial phase called Phase 0 considers the structure's state before any damage. In further phases the stresses will increase only because of the redistribution of forces as no new loads are added to the model in this scenario.

5.2.1 Phase 0: Original structure, zero damage

In order the study the evolution of stresses and cracking of the structure, the analysis begins with a view of the original geometry only loaded with gravity. Displacement for this condition reaches a value of 0.79mm, which is small when compared to the maximum displacement obtained at failure. Cracks do not appear on the structure at this level of loading (Figure 42).

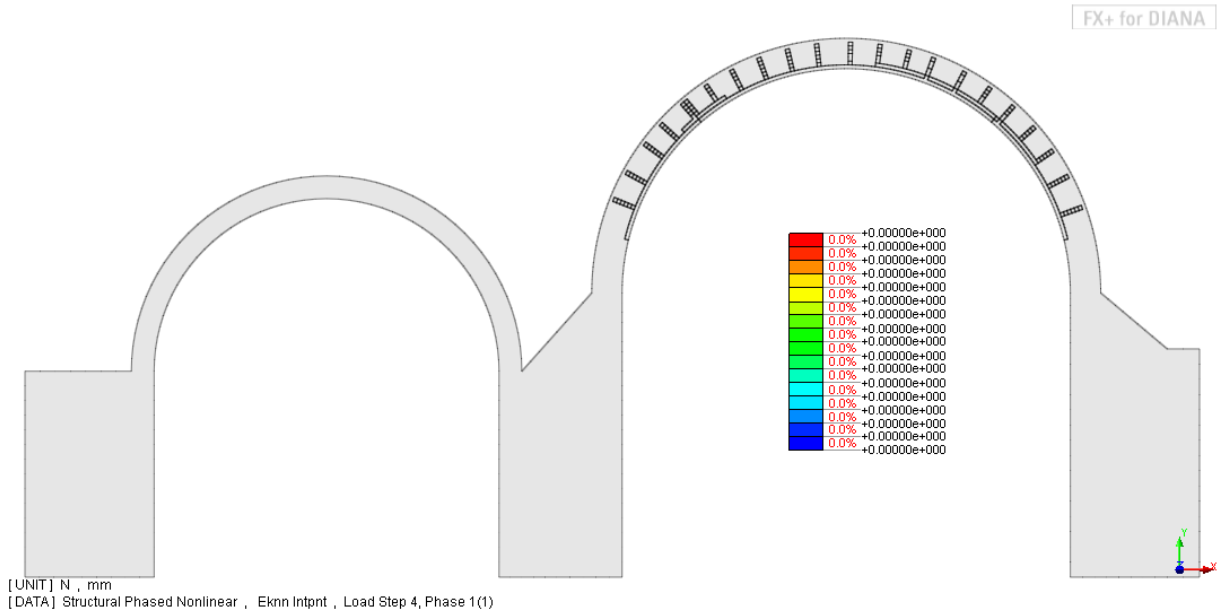

Figure 42. Crack pattern in original structure loaded only by self-weight

Compressive stresses reached a maximum value of 0.41MPa, around 17% of the material capacity, and it's concentrated on the base of the arch as shown in Figure 43. Therefore, if the structure would not present any damage and would not be overloaded, the safety factor for the compressive capacity would be higher than 5. The maximum tensile stresses reach a value of 0.059MPa, which is almost negligible compared to the tensile capacity of 0.12MPa (not even 0.5% of

the materials capacity). The location when this stress is developed is the middle intrados of the right arch, as seen in Figure 44.

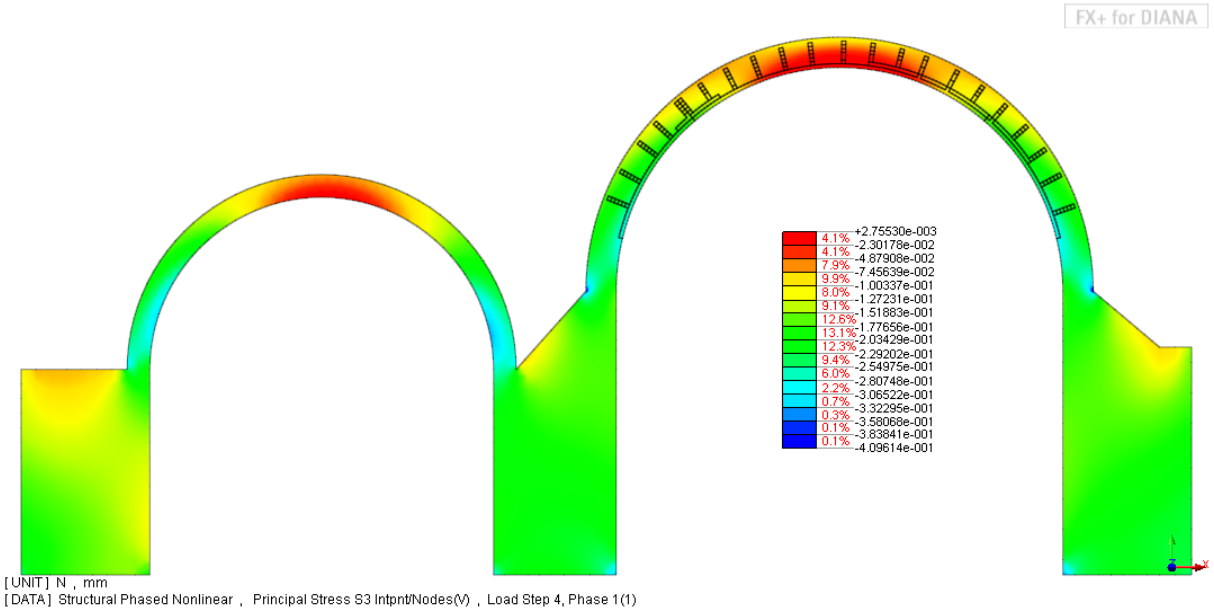

Figure 43. Principal compressive stress in original structure loaded only by self-weight

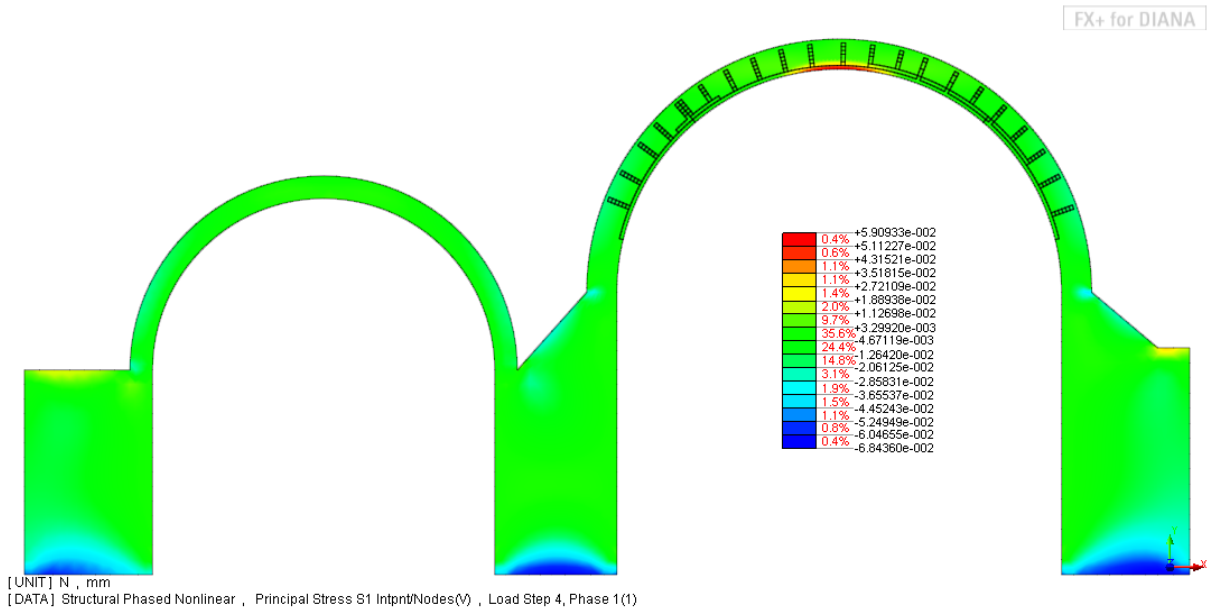

Figure 44. Principal tensile stress in original structure loaded only by self-weight

5.2.2 Phase 1: Removal of the initial portions of elements currently inexistent

So, after the analysis of the original condition with the whole structure functional, the next phase will be the removal of the most exterior layer from the intrados. The structure is not loaded

again but the stresses redistribute due to the absence of that part of the arch. In this case, the new maximum stress in compression (Figure 45) is 0.45MPa (19% of the material capacity) and the location is the same as in the previous case. Tensile stresses raised up to 0.06MPa and keeps the same location as in the structure with no damage (Figure 46). So, besides a very small increment in the state of stresses no other relevant changes appear and the location of maximum values for stresses remain the same. No cracks appear in the arch yet.

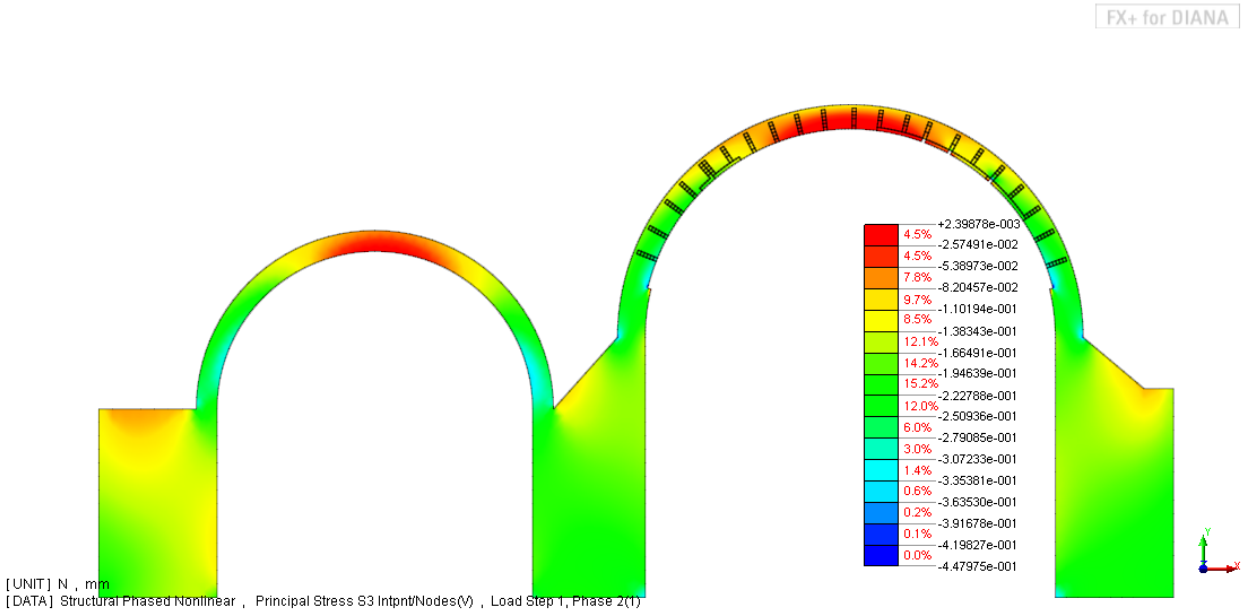

Figure 45. Principal compressive stress after redistribution of stresses in first step of the phase analysis

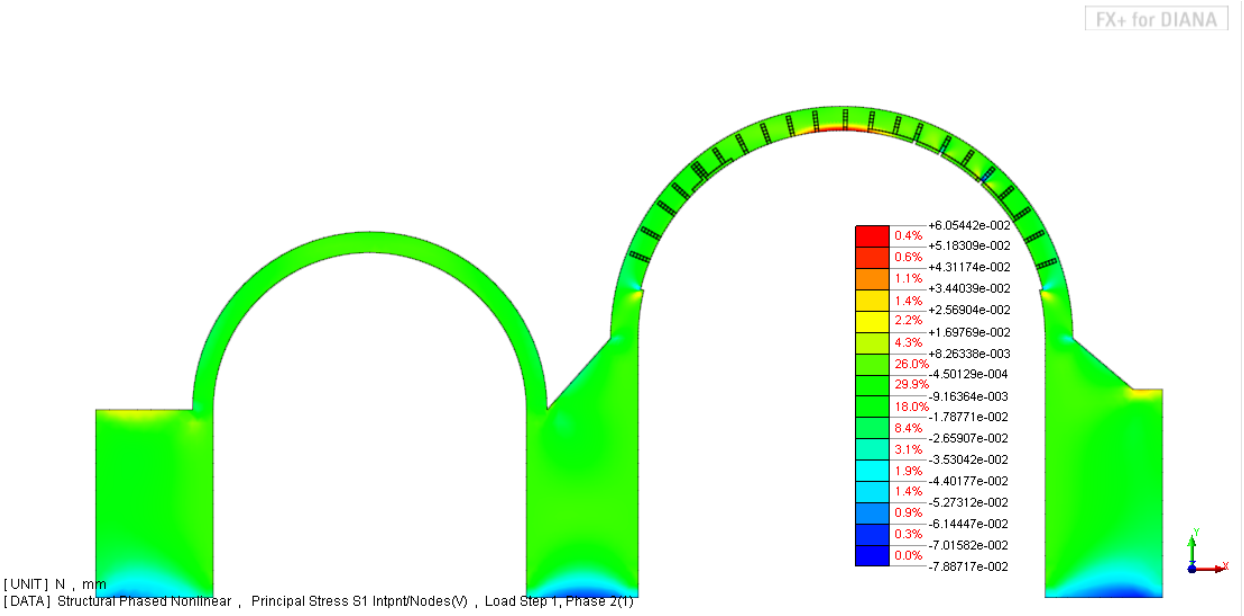

Figure 46. Principal tensile stress after redistribution of stresses in first step of the phase analysis

5.2.3 Phase 2: Removal of the second portion of elements currently inexistent

In the next step of the phase analysis the damage will be incremented by removing more elements and showing a pattern of damage more similar to the current state of deterioration. Concentration of damage in the joints also results in a concentration of stresses in these sections and a more relevant increment in the state of stress, when compared to the previous phases.

Compressive stresses show a jump to 0.59MPa (25% of the material capacity), which represents a higher increase than what was obtained in the previous phase transition. Zones of high stress concentration develop in the joints, especially in the ones situated closer to the base of the arch and in the joints where damage is deeper. This is illustrated in Figure 47.

Tensile stresses reach a value of 0.115MPa, equivalent to 96% of the tensile capacity, and are concentrated in the joints of the middle of the right arch as shown in Figure 48. Tensile strains confirmed in the same location (Figure 49) indicate the possibility of a crack opening in these joints. Crack status confirm the findings of the tensile strains analysis as the first cracks start to appear in the joints of the middle of the arch as seen in Figure 50.

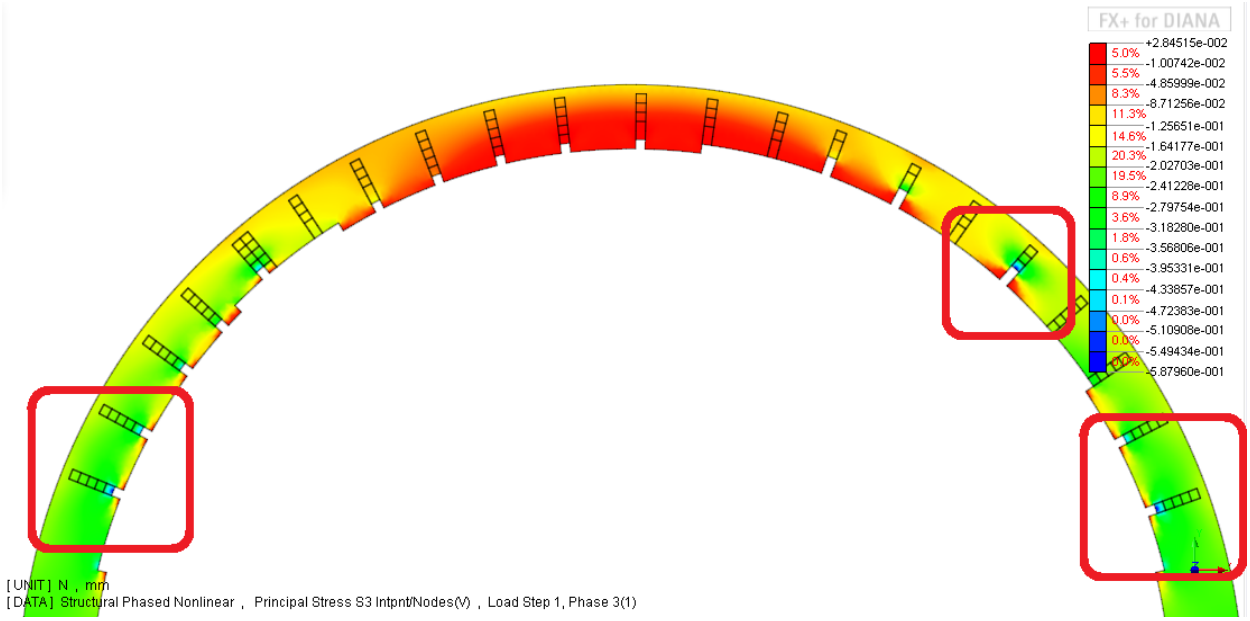

Figure 47. Principal compressive stress after redistribution of stresses in the second step of the phase analysis

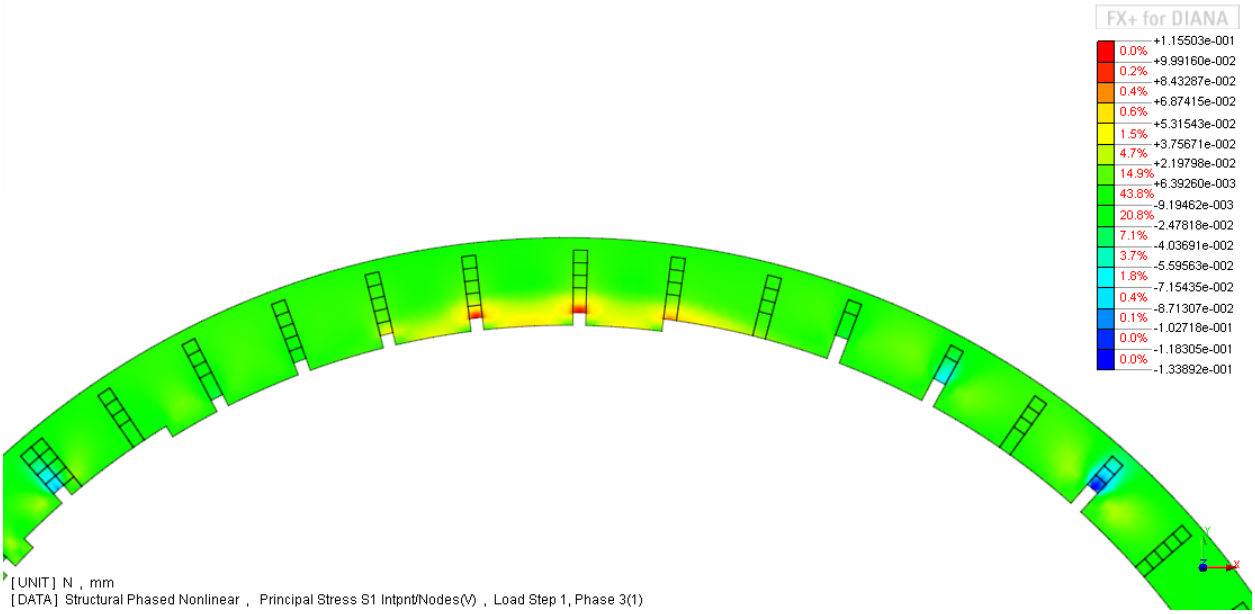

Figure 48. Principal tensile stress after redistribution of stresses in second step of the phase analysis

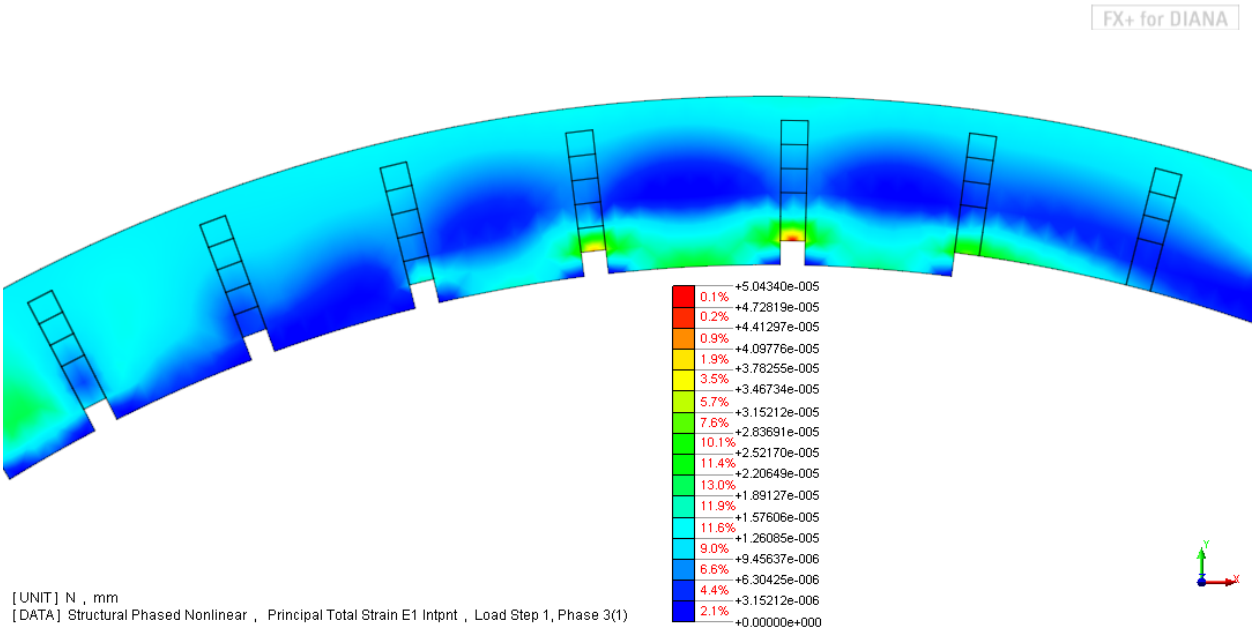

Figure 49. Principal tensile Strain after redistribution of stresses in the second step of the phase analysis

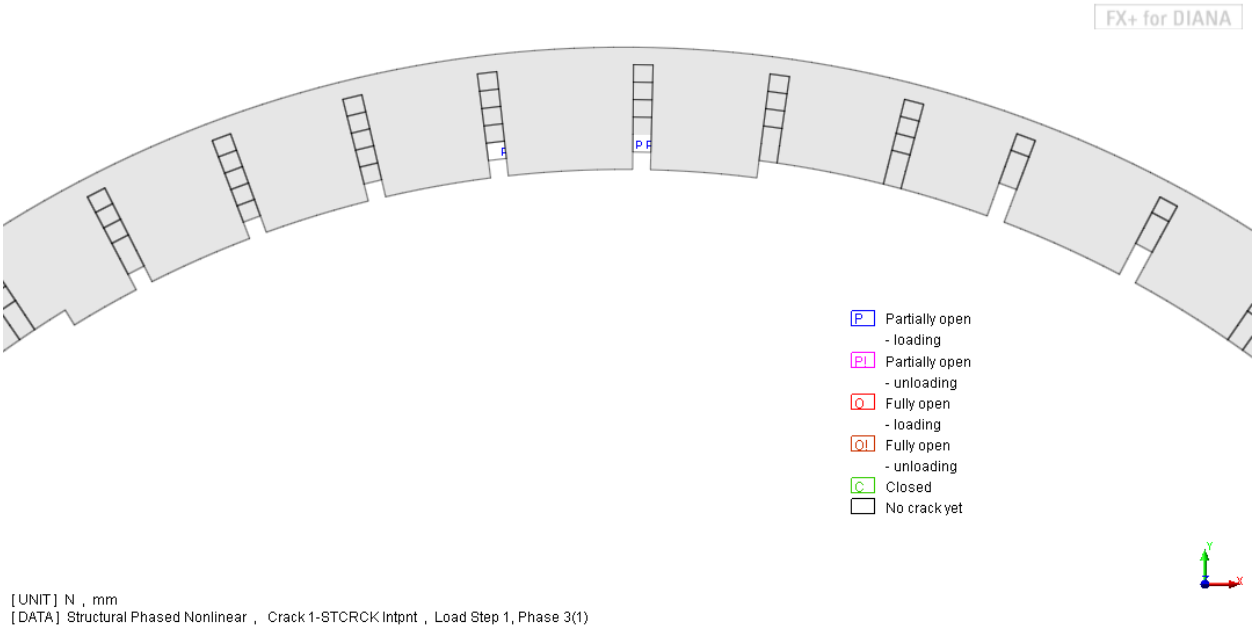

Figure 50. Crack development in the second step of the phase analysis

5.2.4 Phase 3: Full removal of elements currently inexistent

In the final step of this analysis, the rest of the elements associated to the material that no longer exists were removed. Zones of high stress concentration inside the joints are marked more clearly. This structure represents the actual level of damage of the structure for a condition of only self-weight. Notice that even without external loads the structure presents already damage in the form of cracking in the intrados middle part of the arch, these cracks are not easy to spot as they will most likely appear as an opening in the joint and not as a real crack appearing across the stones. Compressive and tensile stresses are slightly lower for this condition and the amount of joints that show a high concentration of stresses increase are shown in Figure 51 and Figure 52.

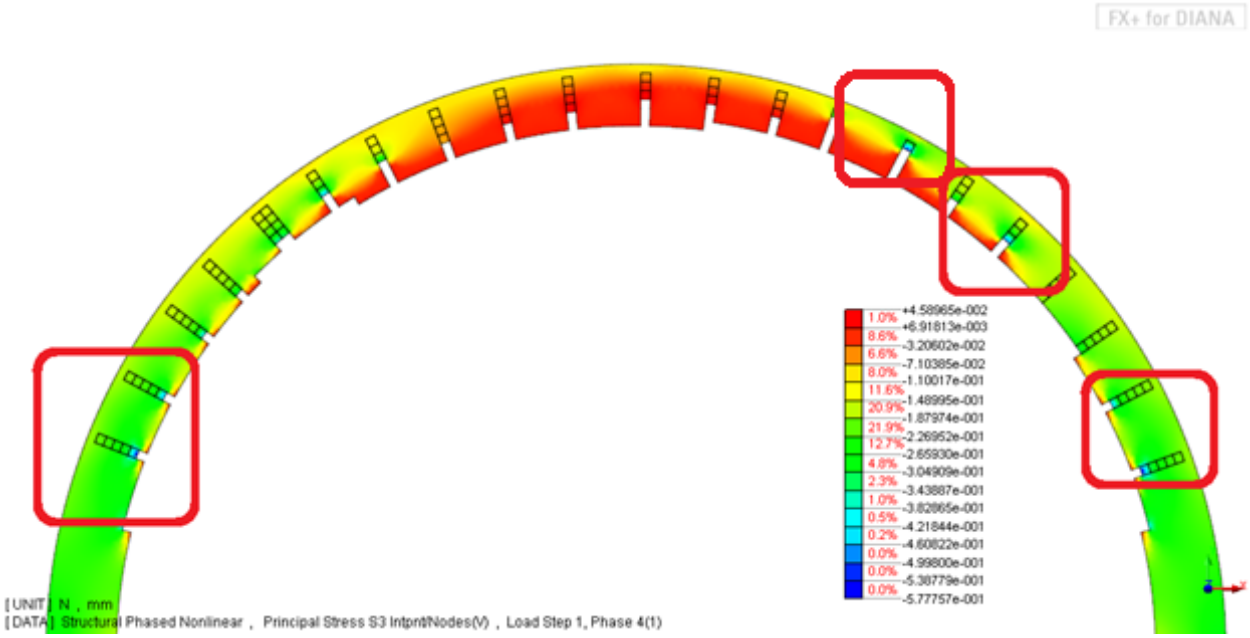

Figure 51. Principal compressive stress after redistribution of stresses in third step of the phase analysis

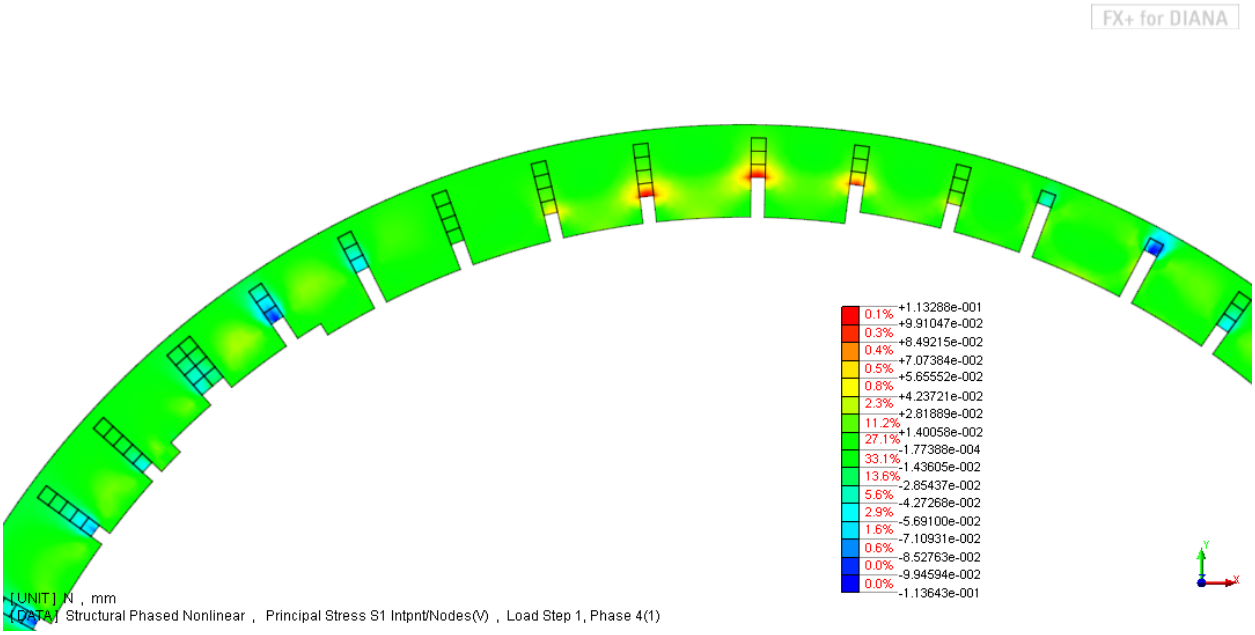

Figure 52. Principal tensile stress S1 after redistribution of stresses in third step of the phase analysis

Crack locations remain the same as in the previous step. A summary of the results for this phase analysis from the point where the structure sustains no damage at all to the current state of damage is shown in Table 6

.

Table 6. Summary of evolution of the structural properties from zero to the actual state of damage

Phase	Maximum displacement (mm)	Existence of cracks	Principal compressive stress (MPa)	Principal compressive strain (mm/mm)	Principal tensile stress (MPa)	Principal tensile strain (mm/mm)
Phase 0	0.789831	FALSE	0.41	1.56E-04	0.059	4.50E-05
Phase 1	0.836452	FALSE	0.448	1.69E-04	0.0605	4.88E-05
Phase 2	0.908196	TRUE	0.588	2.14E-04	0.115	5.04E-05
Phase 3	0.980722	TRUE	0.578	2.10E-04	0.113	5.72E-05

Figure 53 shows the relation between the maximum tensile stress and the maximum strain for the principal minimum stresses and strains. One can notice a linear behavior that contrasts with the results of the tensile stress vs. tensile strain diagram shown in Figure 54.

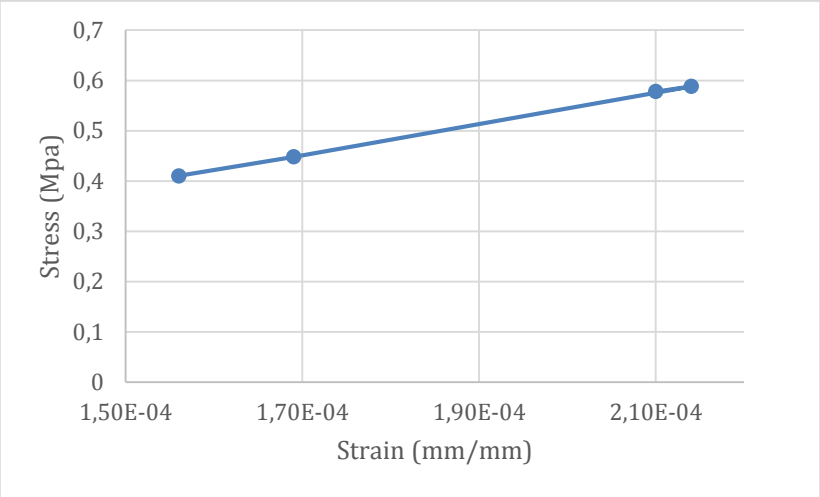

Figure 53. Stress/strain values for compression graphed for each step of the phase analysis for current damage

There is a jump in Figure 54 that appears between Steps 1 and 2. At the same time from the previous analysis it was detected the apparition of cracks between these two phases. The opening of a crack could have resulted in a higher concentration of tensile stresses.

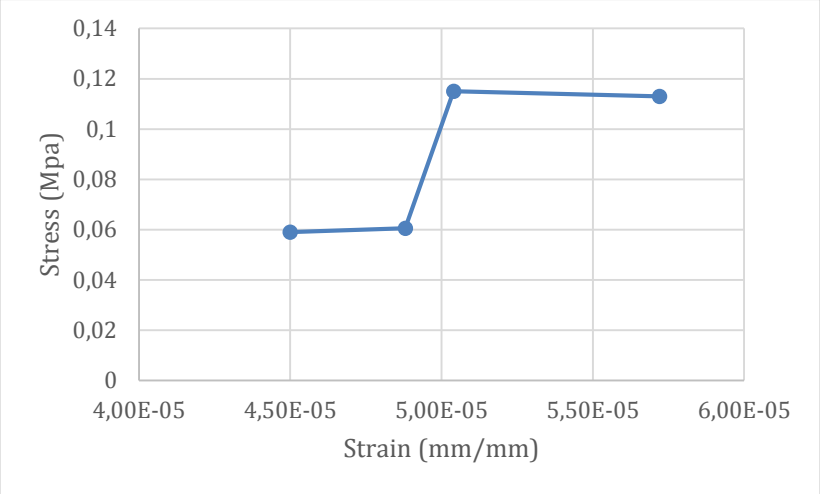

Figure 54. Stress strain values for tension graphed for each step of the phase analysis for actual damage

5.3 Phase analysis for ultimate live load

In this analysis, a live load will be applied till failure in each phase of deterioration. The aim is to determine the structure's loss of capacity step by step due to the phased removal of the elements. In contrast with the previous analysis, in this one, for each phase of deterioration, a new model was created and brought to failure by increasing the load factor that multiplies the live load on the top of the structure. Two scenarios are studied for the load: when it is applied symmetrically, like in the previous analysis, and when the load is applied asymmetrically, in the critical condition when load is on the right side.

5.3.1 Symmetrical live load

Figure 55 shows a comparison of the different levels of damage with respect to the original state of the structure. Notice how the increase of damage in the arch results in a loss of stiffness of the structure as the slope of the curve becomes lower each time a group of elements is removed. The load factor shows a great decrease as a result of the deterioration, original factor for failure due to the increment in the live load factor was 56.2 and for the phase 3 this value has been reduced to 23, less than half the structure's original capacity.

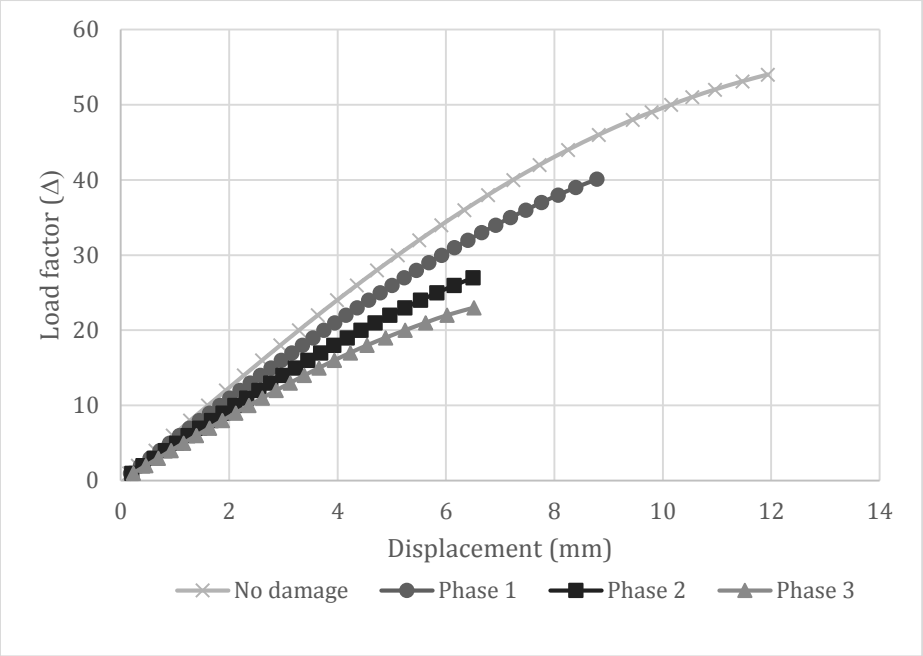

Figure 55. Safety analysis for symmetrical live load

Figure 56 shows the step by step reduction of the ultimate load factor. Notice how the change from the phase 2 and 3 is not as strong as from the original structure to the phase 1. This behavior can be related to the fact that phase 2 and 3 have a similar geometry and the damage is only increased but still concentrated in the same points while the change from the original structure to the phase 1 in which the first elements are removed represent a variation in the geometry of the arch that results in high stress concentration zones. This behavior will be further detailed in the following sections.

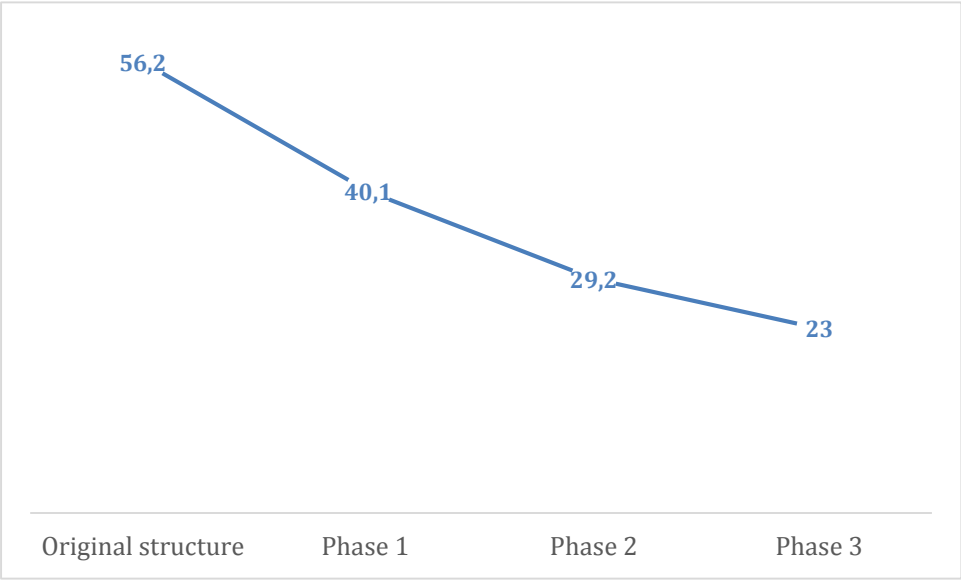

Figure 56. Reduction of ultimate live load factor symmetrical load

5.3.1.1 Phase 1: Removal of initial portions of elements currently inexistent

Phase 1 implies the removal of the most exterior layer of elements in the intrados of the arch. This results in a higher concentration of compressive stresses in the arch and a general reduction of the maximum load the structure can sustain. Load factor decreases from 56.1 to 40.1, which represents around 19% of loss in the structure's ultimate capacity due to a general loss of material of 5cm in the intrados of the arch. Figure 57 shows the compressive zones in the base of the arch where the crushing of the material occurs. Note that the compressed zones are not focalized but evenly distributed along the intrados base of the arch.

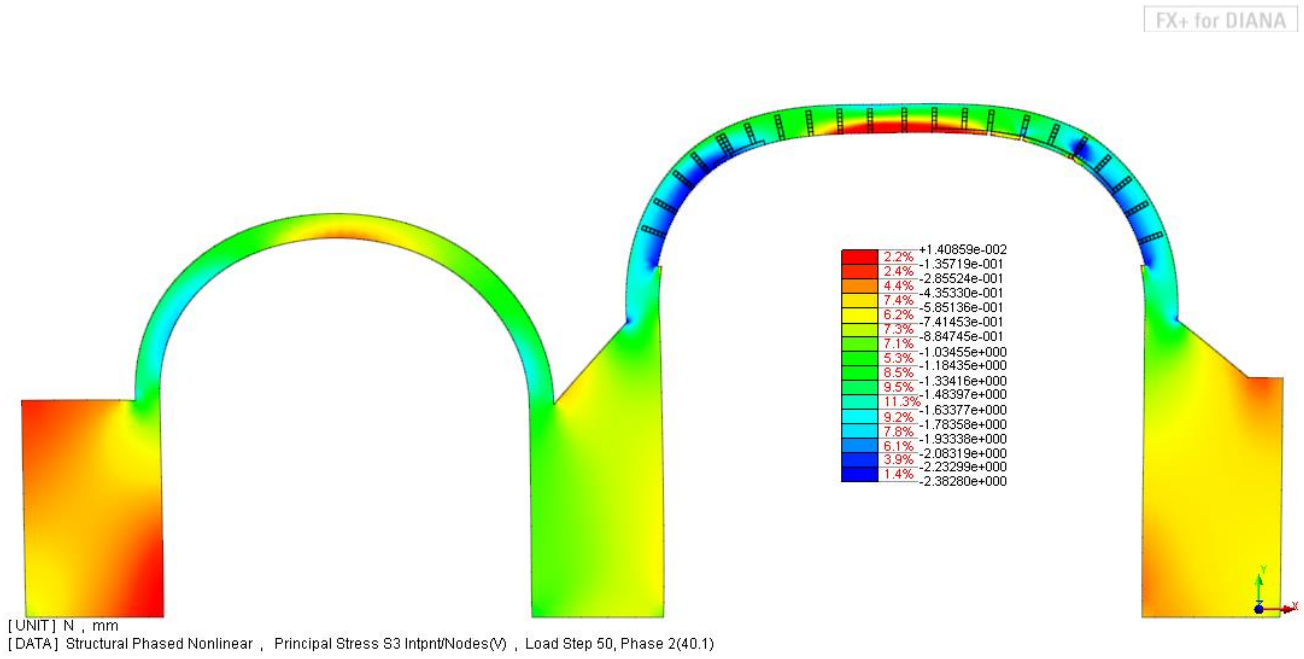

Figure 57. Principal stress S3 for symmetrical live load Phase 1

5.3.1.2 Phase 2: Removal of second portion of elements currently inexistent

By removing the second section of elements, the ultimate factor lowers a total of 48%. Almost half the capacity of the structure has been lost and this model does not even represent the actual damage. Anyway the load factor is 29.2 which is still extremely high, indicating that even though half the capacity has been lost the structure is still very safe. Figure 58 shows the principal compressive stresses. The biggest change in comparison with the previous step is the concentration of compressive stresses on much localized areas in both the left and right on the top of the arch.

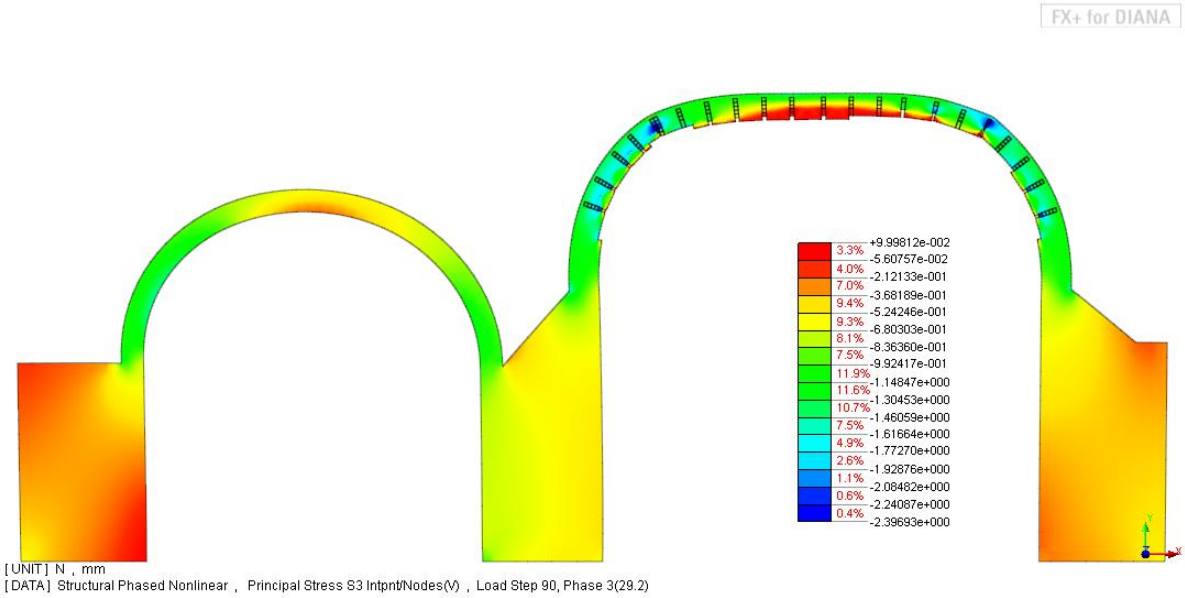

Figure 58. Principal stress S3 for symmetrical live load Phase 2

5.3.1.3 Phase 3: Full removal of elements currently inexistent

In the final step the elements removed leave a structure that resembles the most with the current state of deterioration. A high compressive hinge is clearly formed on the top right of the arch, where crushing of the material would most likely occur. The load factor has decreased from 56.1 to 23 resulting in a loss of capacity of 59%. Even in these conditions the structure can be considered safe, as the load factor of 23 represents a loading condition of 23 times 5kN/m, which equals to 115kN/m or 11.7tons per meter.

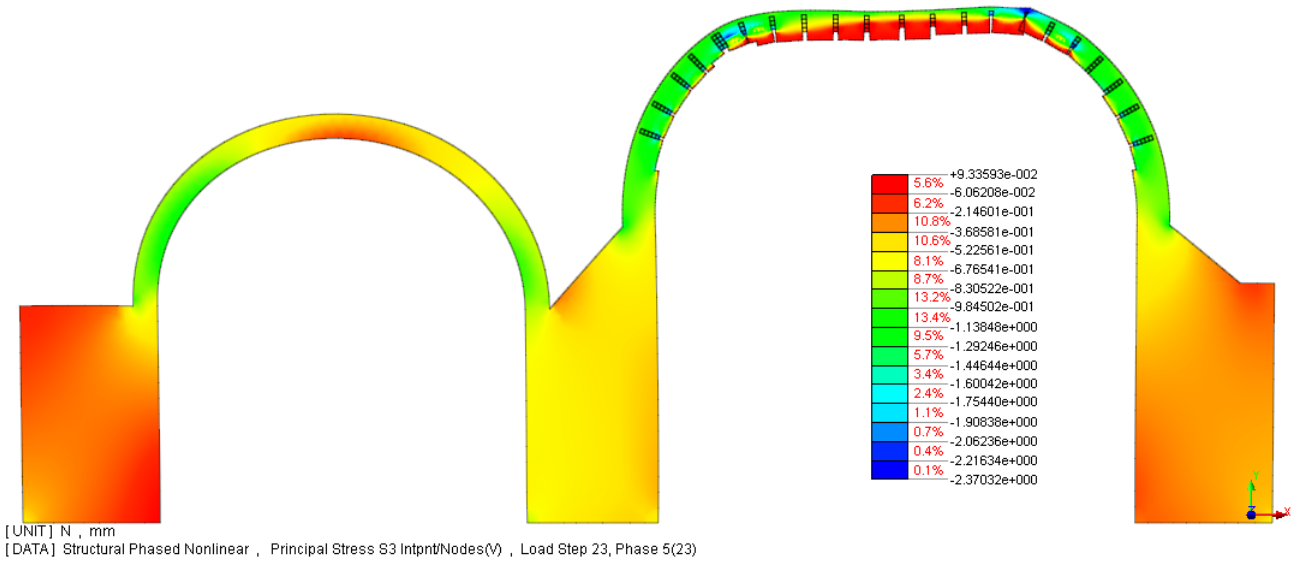

Figure 59. Principal stress S3 for symmetrical live load Phase 3

5.3.2 Asymmetrical live load

In order to better understand the level of safety of the structure, the phase analysis was also developed for an asymmetrical loading condition as shown in Figure 60. As a result, the structure's failure mechanism shows severe cracking in the middle of the arch and the whole arched system displaces to the left (Figure 61) resulting in the opening of cracks on the left arch as well.

Notice as well that the damage for this loading condition implies the opening of cracks in the base of the left and middle columns as a result of the horizontal pushing of the structure to the left. Even though the mechanism of failure for the structure varies greatly for this loading condition, the ultimate load factor remain fairly similar to the symmetrical loading case, showing a value of 54.

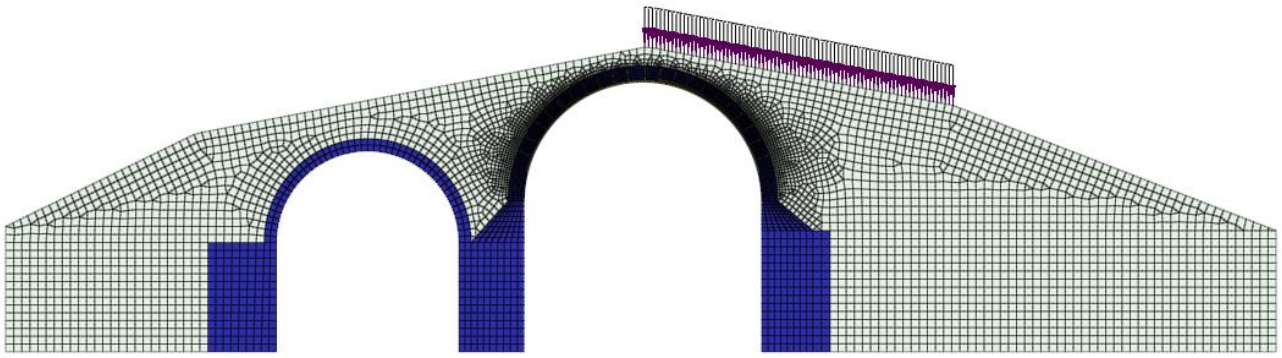

Figure 60. Location of asymmetrical live load

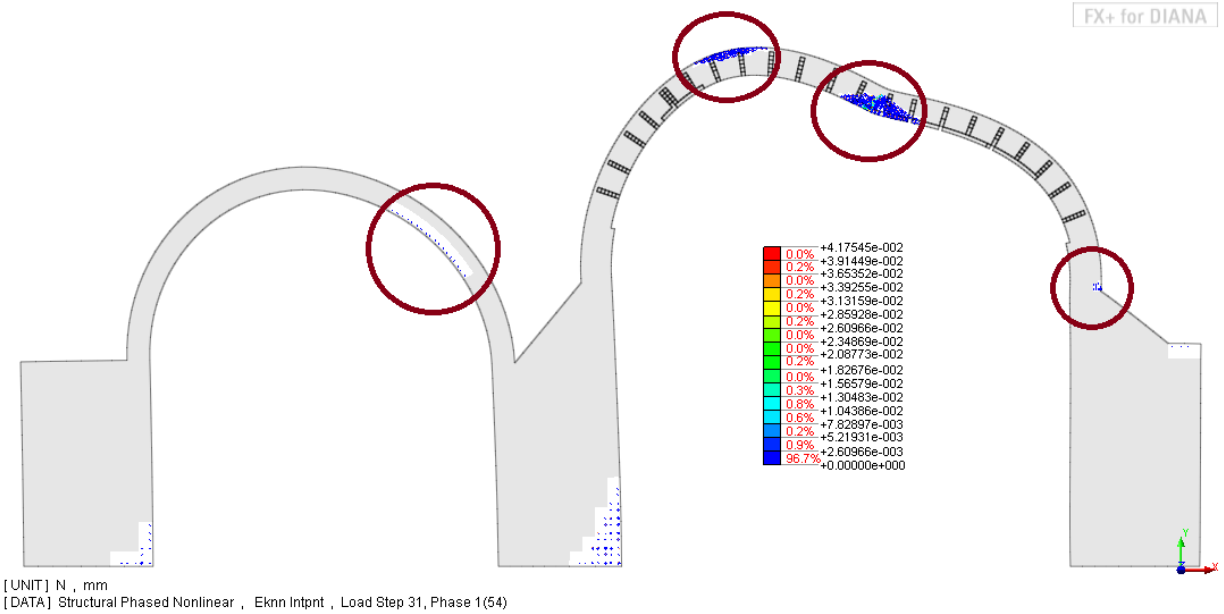

Figure 61. Crack pattern for asymmetrical live load

Figure 62 shows a comparison of the different levels of damage with respect to the original state of the structure. Notice how the increase of damage in the arch results in a loss of stiffness as the slope of the curve becomes lower each time a group of elements is removed, showing the exact same behavior as in the symmetrical load case. Again, the load factor is greatly reduced as a result of the removal of elements.

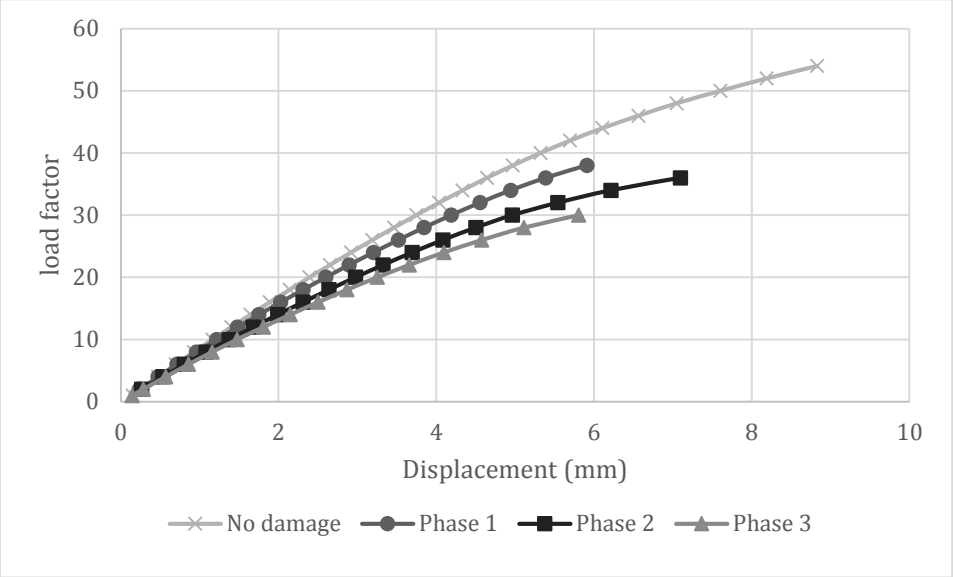

Figure 62. Safety analysis for asymmetrical live load

Figure 63 shows the step by step reduction of the ultimate load factor. As in the symmetrical case the apparition of damage in the phase 1 has a bigger impact in the first step in comparison to the other two as the arch changes from a perfect ring to a structure with concentrated stresses in the joints.

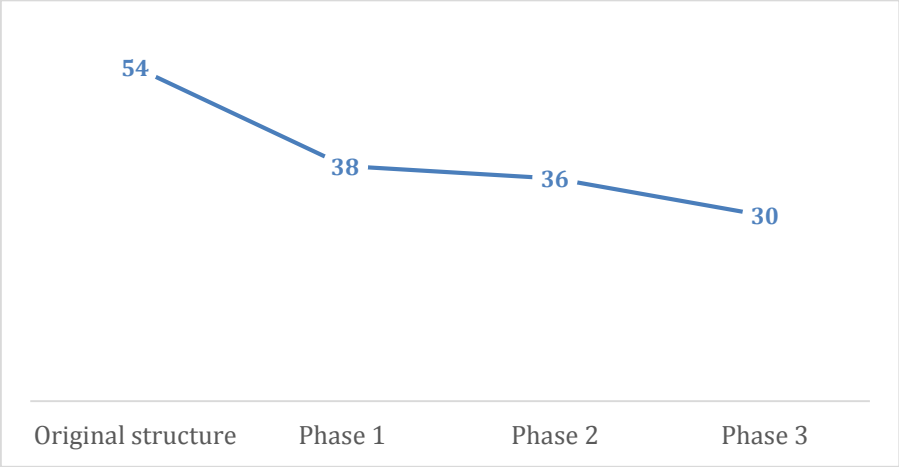

Figure 63. Reduction of ultimate live load factor asymmetrical load

5.3.2.1 Phase 1: Removal of initial portions of elements currently inexistent

For this step, the ultimate load factor is reduced from 54 to 43. This decrease represents around a 30% decrease in the structure's ultimate capacity. Figure 64 shows the formation of a compression zone on the right lower side of the arch and the top left corner where the material would be crushed. This crushed area act as hinge zone that composes the mechanism of failure of the arch in combination to the crack hinges shown in the previous Figure 61.

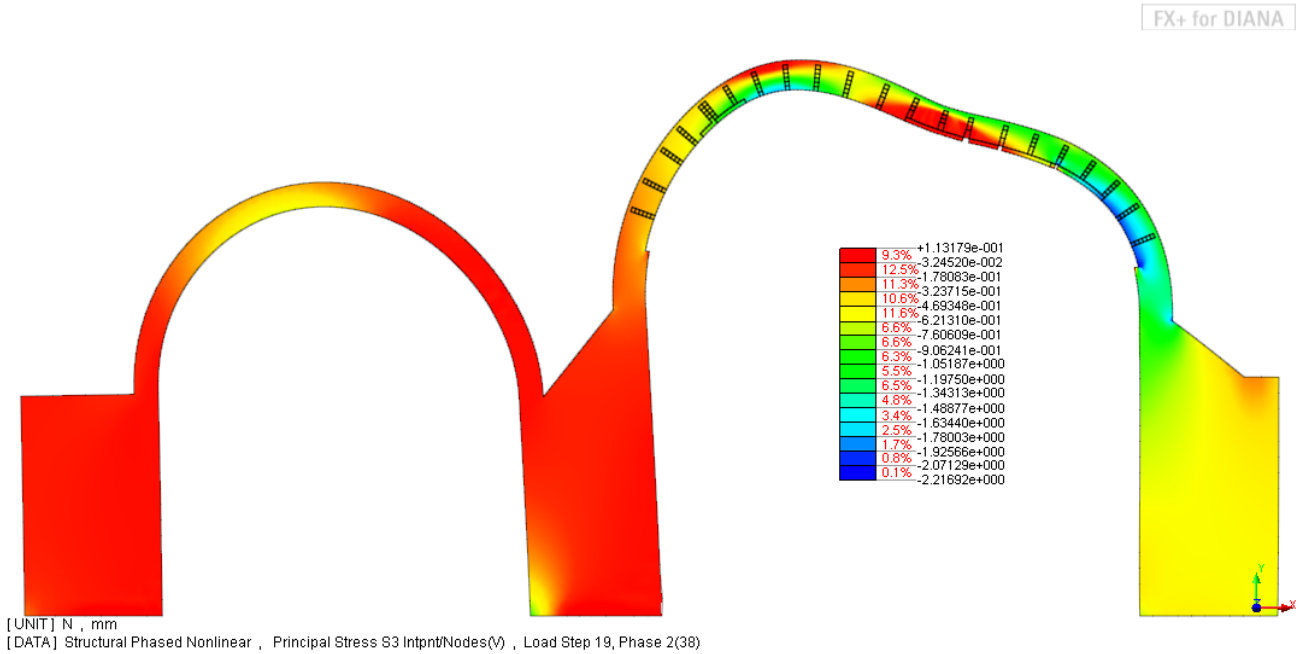

Figure 64. Principal stress S3 for asymmetrical live load Phase 1

5.3.2.2 Phase 2: Removal of second portion of elements currently inexistent

By removing the second section of elements the ultimate factor lowers a total of 33%. The loss of capacity is not as high as compared to the symmetrical scenario in which, by this phase, the structure had already lost half its capacity. Still, a load factor of 36 is obtained, which is still extremely high if compared to reality, where a structure can be considered safe if it can sustain a load factor of 1.5. Figure 65 shows the principal compressive stress S3. It must be noted that the stresses for this scenario are much more concentrated on the joints, where the damage is higher.

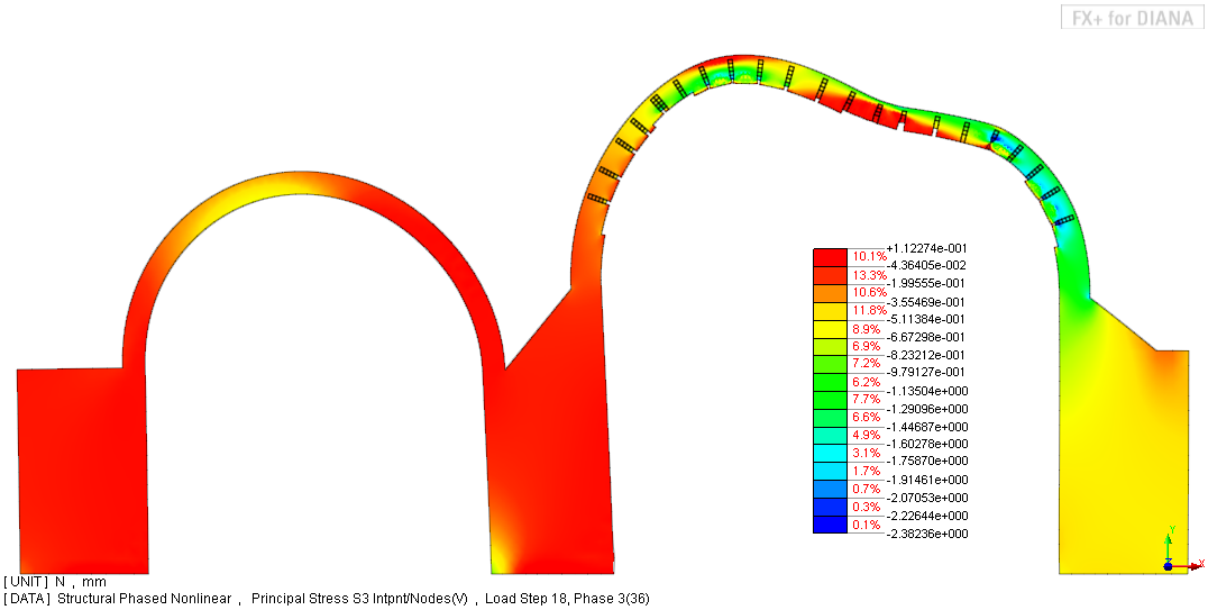

Figure 65. Principal stress S3 for symmetrical live load Phase 2

5.3.2.3 Phase 3: Full removal of elements currently inexistent

For the final scenario that represents the structure's current state, a high compressive zone is clearly formed on the right top of the arch where crushing of the material would most likely occur. The load factor has decreased from 54 to 30, resulting in a decrease of the structure's strength of 44%. Even in this conditions the structure can be considered safe, as the load factor of 30 represents a loading condition of 30 times 5kN/m, which equals to 150kN/m or 15.3tons per meter.

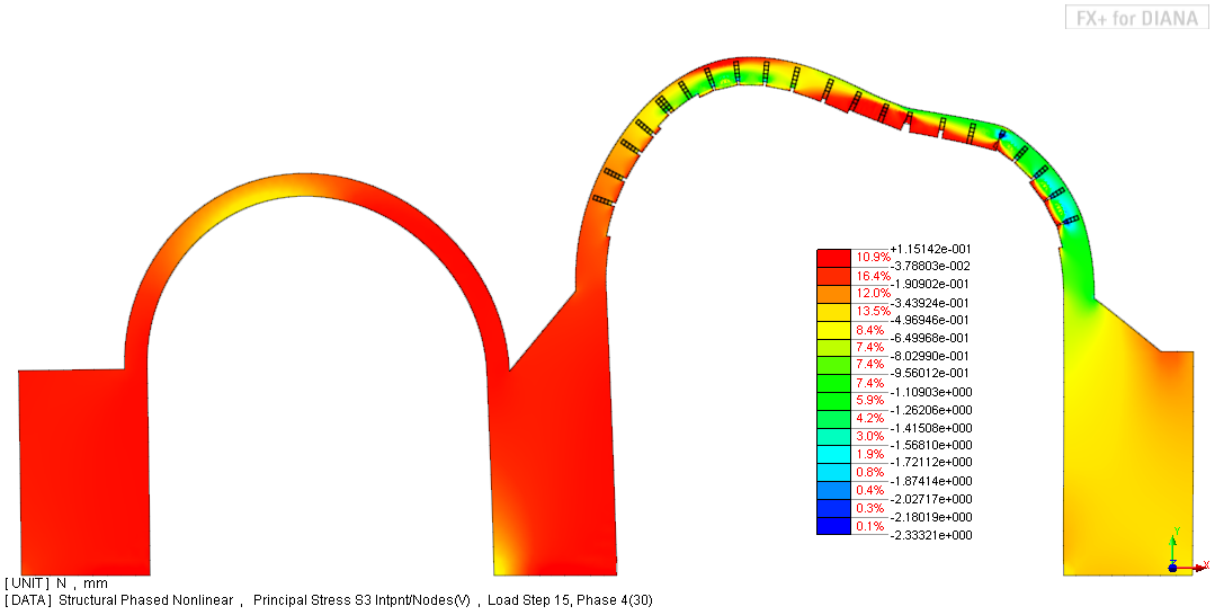

Figure 66. Principal stress S3 for symmetrical live load Phase 3

6 PREDICTIONS OF FUTURE DAMAGE

Previous section studied the evolution of structural properties from zero till the level of current damage. In this section, the objective is to study the behavior of the structure linked to additional damage that could appear in the structure if it is not intervened. There is a really big limitation associated to this new analysis: there is no way to know where the structure will be damaged in the future. It is possible to make predictions that will be logical but it is not possible to have a 100% guarantee that the structure will sustain damage in a certain location. Therefore as a solution to this incognita, five possible damage locations are proposed: Damage in the center of the arch, in the left side, in the right side, in both sides and damage in all positions simultaneously.

Seven out of eight elements of the width of the arch can be removed as to simulate the loss of material. Even when the damage is modeled as to be critical enough to only leave 5cm of width of the arch, results show that the structure can still sustain its self-weight without failure. In order to further comprehend the damage scenarios, a load factor analysis is developed for the live load. The live load will only be applied symmetrically for these analysis.

Five new scenarios will be created and analyzed to represent the five possible hypothesis of damage progression. In each phase, only one element per width was removed at the time in order to smooth the transition of stresses. The final response of the structure after removal of all elements in the location of damage is studied in the following scenarios.

6.1 Scenario 1: Additional damage appear in the center of the arch

In this scenario seven out of eight elements are removed from the joints in the center of the arch. After removal of these elements, the live load is increased till failure, obtaining a load factor of 10.4. The decrease of capacity is equivalent to 55% of the maximum capacity, if compared to the current ultimate factor of the structure: 23, which was studied in the previous chapters. As it can be seen in Figure 67, a crushing zone is developed in the extreme sides of the damaged zones. Figure 68 shows the principal stress S1 and, according to this figure, no tension areas are developed in the arch itself but only in the limit between the continuous frame of the arch and the blocks that come out of it. As a consequence, most of the block of stone is just hanging while only a small part of it is actually compressed which could result in a crack due to incompatibility of stresses as shown in Figure 69.

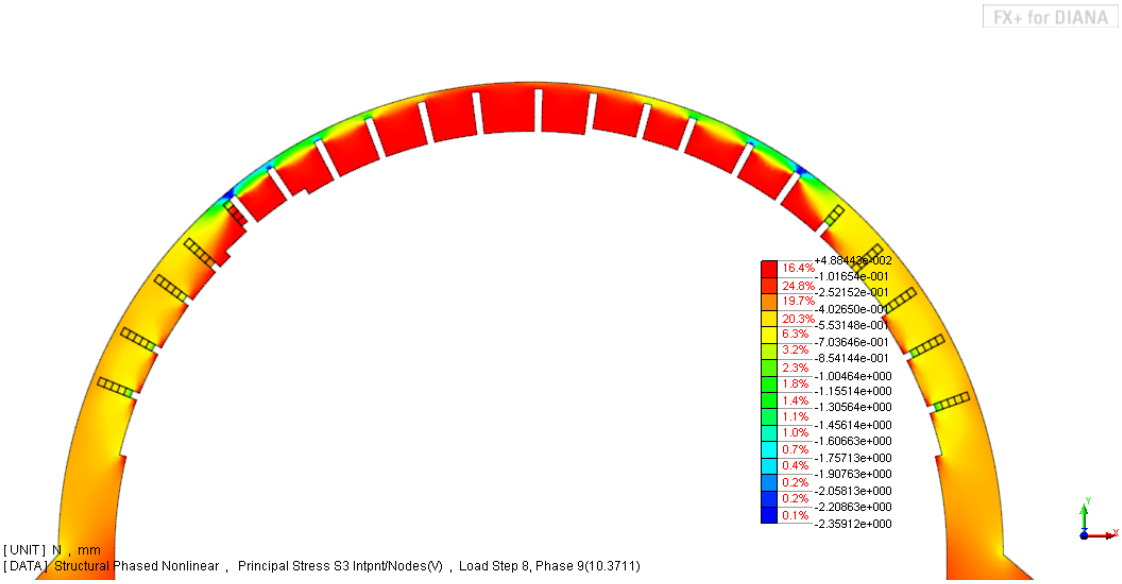

Figure 67. Principal stress S3 for live load and a prediction of damage in the center

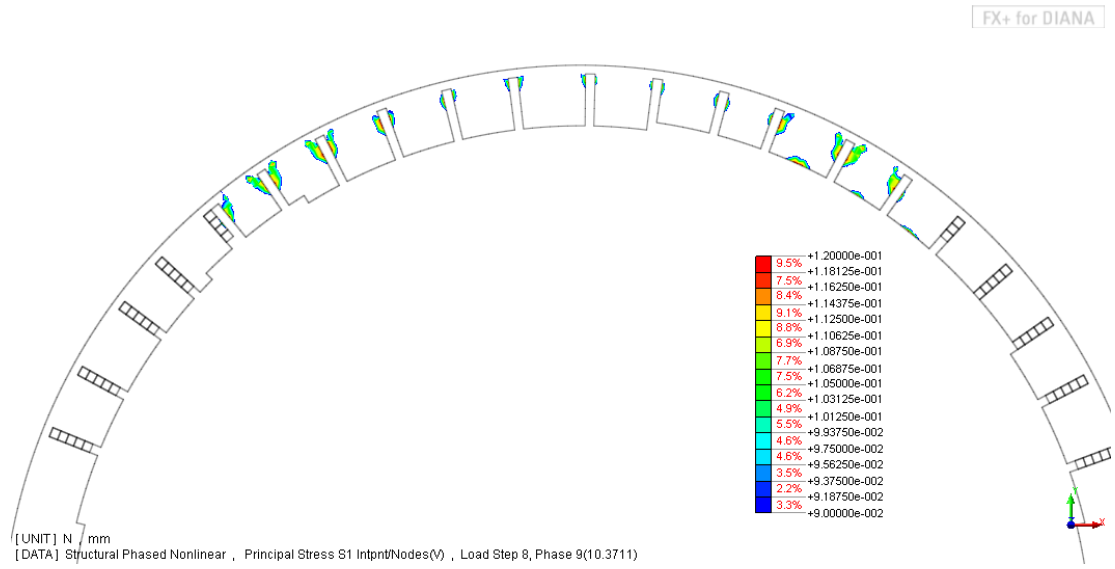

Figure 68. Principal stress S1 for live load and a prediction of damage in the center

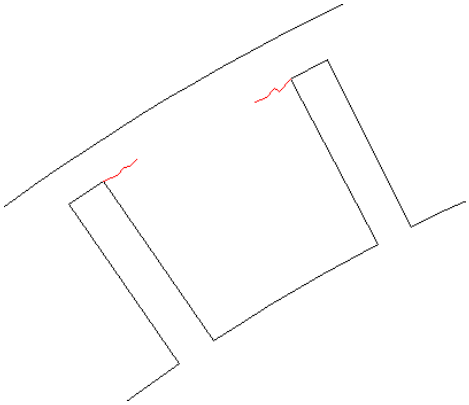

Figure 69. Crack in block due to incompatibility of stresses

6.2 Scenario 2: Additional damage appear in the left of the arch

In this scenario, the elements are removed from the left side of the arch resulting in a decrease of the load factor to 13.8 which is equivalent to a loss of capacity of 40% if compared to the current state scenario studied in the previous chapter. Notice that a compression zone is developed on the right corner of the arch (Figure 70) as it existed in the present state of damage but an additional crushing zone is generated on the left side (blue color) of the arch and is distributed along the whole damaged area.

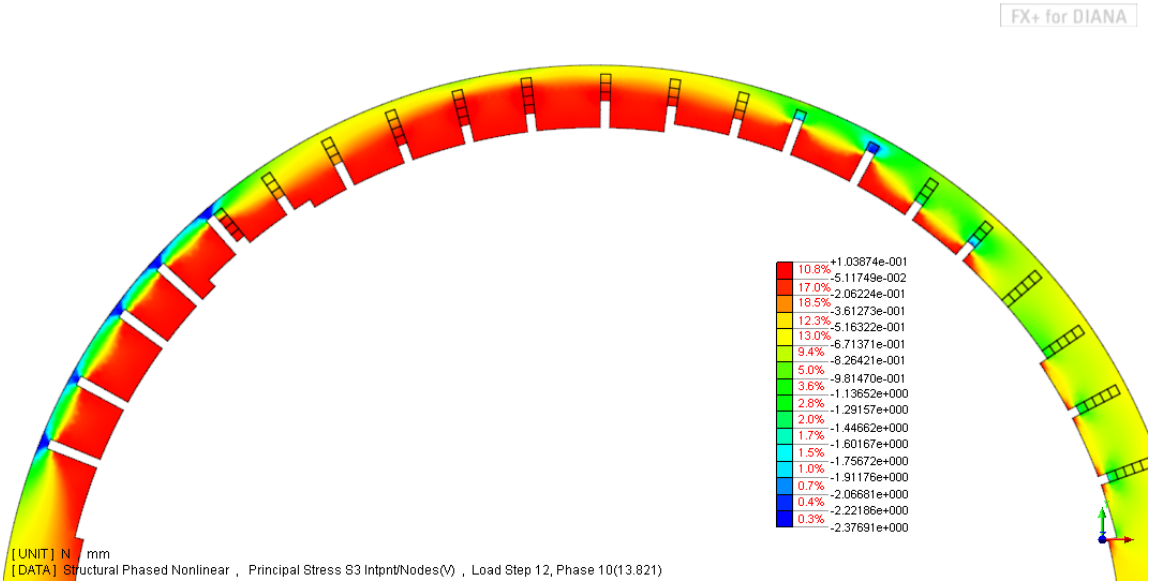

Figure 70. Principal stress S3 for live load and a prediction of damage in the left

Principal stress S1 (Figure 71) shows the formation of a tensile zone on the middle of the arch where cracks would developed as it is proved in the results from crack status in Figure 72. As in the precious case, tensile areas can be seen in the blocks where the joints were carved in the left side of the arch suggesting the possibility of detachment of these blocks.

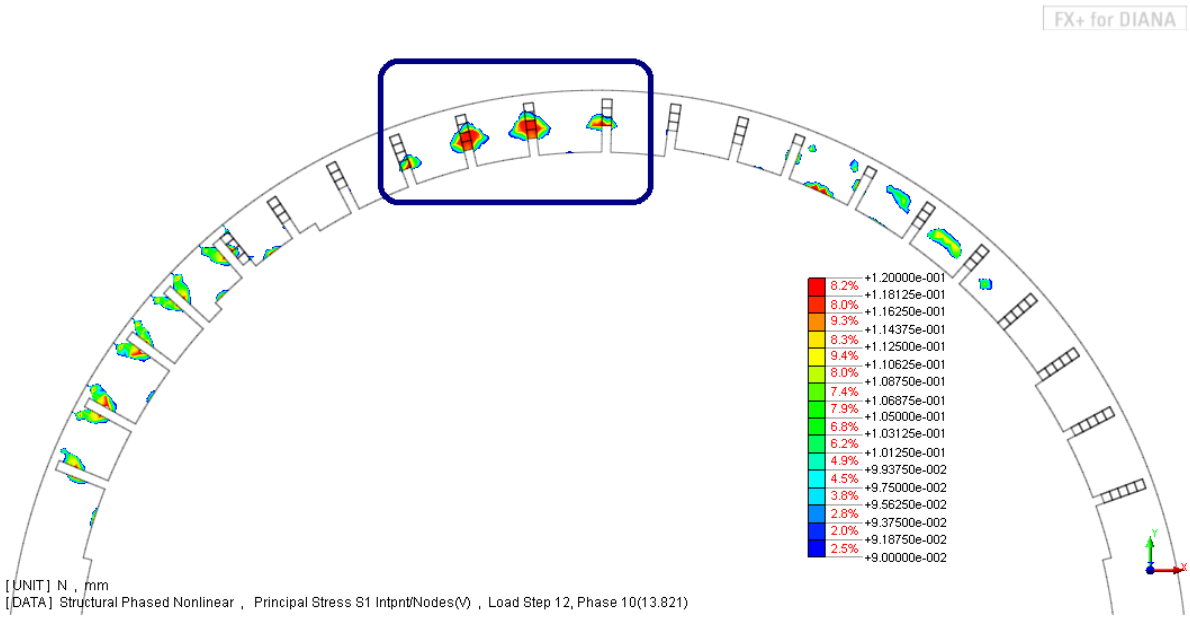

Figure 71. Principal stress S1 for live load and a prediction of damage in the left

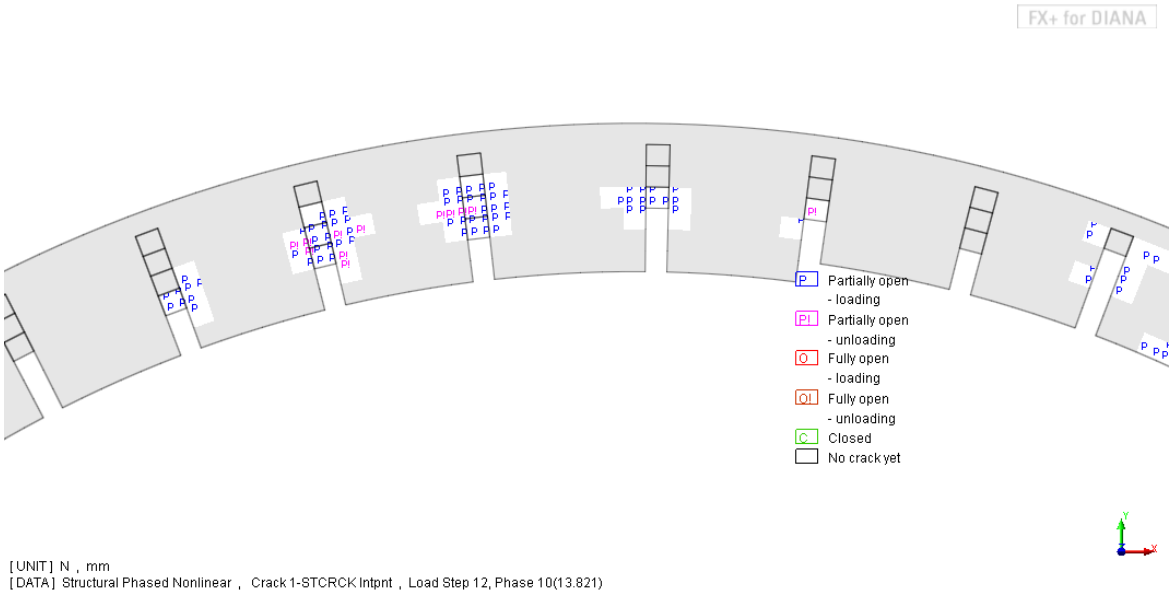

Figure 72. Crack status for live load and a prediction of damage in the left

It is important to mention that even though there has been a great reduction of the ultimate load factor, the structure could still be considered safe for these results.

6.3 Scenario 3: Additional damage appear in the right of the arch

A similar behavior can be seen in this scenario where the formation of a crushing zone appears on the right side (Figure 73). Notice that the compressive concentration that exists in the right corner joint of the actual state of the structure does not exist anymore as compressive stresses have been redistributed along the arch's right side. Load factor has been reduced from 23 to 16.6 for a reduction of capacity of 27.7%. This is the smallest decrease for all five scenarios. According to these results, it is more critically for the structure if damage would be generated in joints that are further away from the current damaged ones. Since the right top joint is the most damaged one in the present, the highest damage response can be obtained by removing materials from joints that are far from the right side. And thus would result in a mechanism of higher deformation.

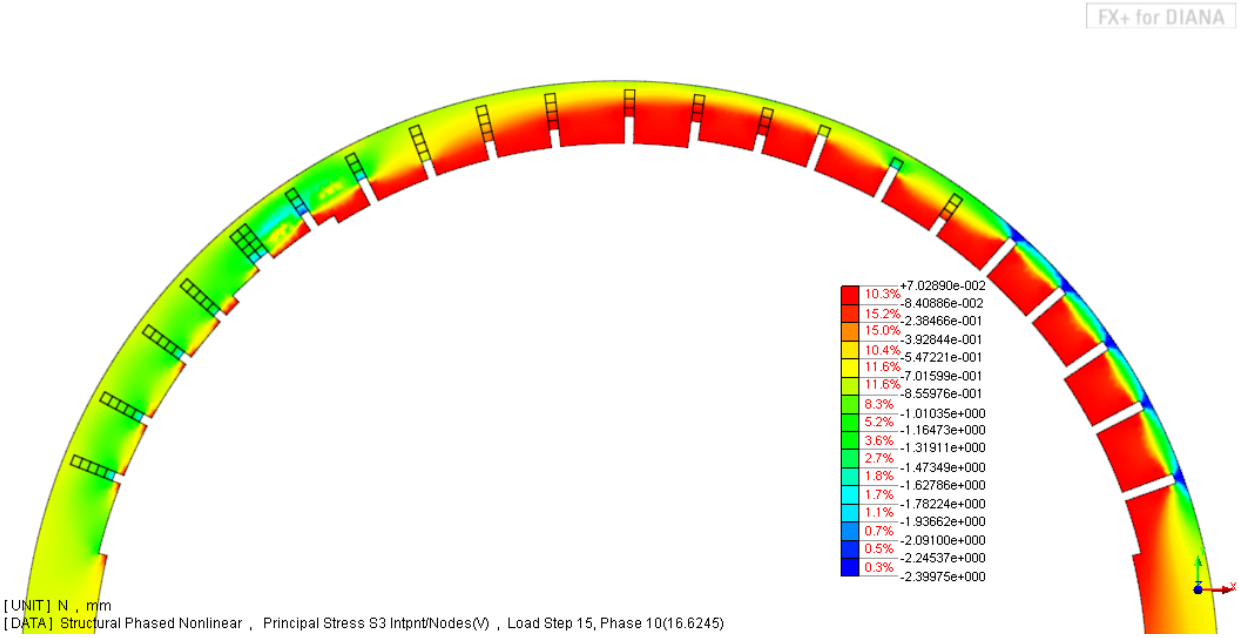

Figure 73. Principal stress S3 for live load and a prediction of damage on the right

Similar to the previous case a tensile stress zone and cracks appear in the middle of the arch (Figure 74 and Figure 75). The difference in the behaviors is that in the case of damage on the left the cracks appear on the middle left while in this scenario the cracks appear in the middle right of the intrados.

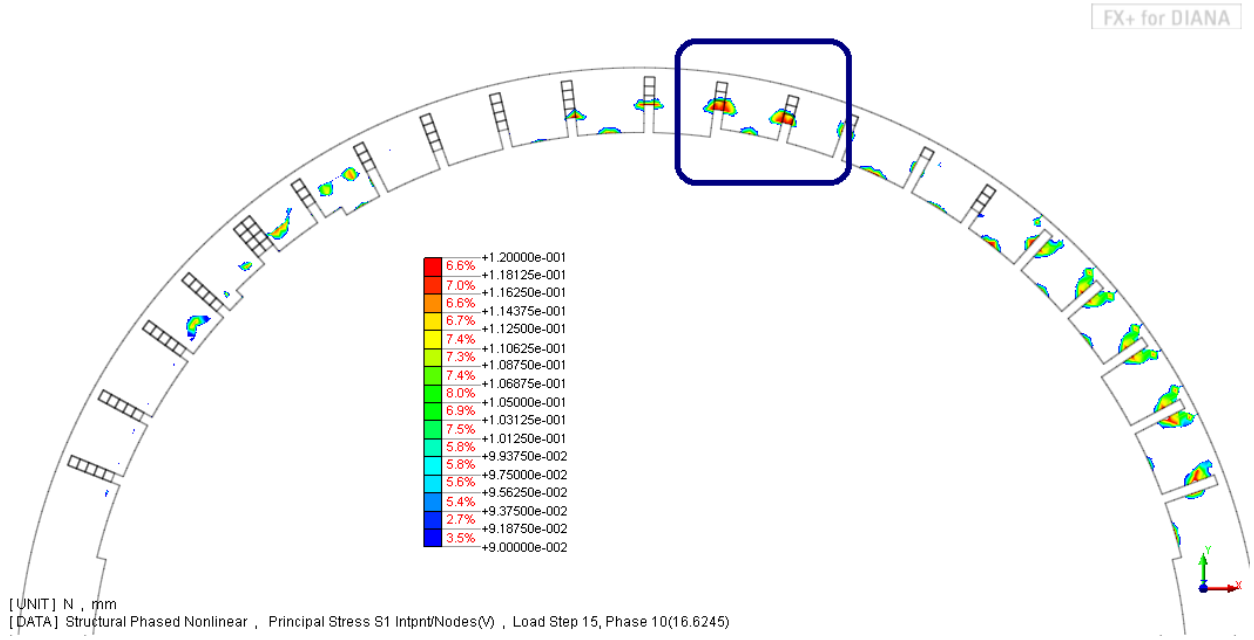

Figure 74. Principal stress S1 for live load and a prediction of damage on the right

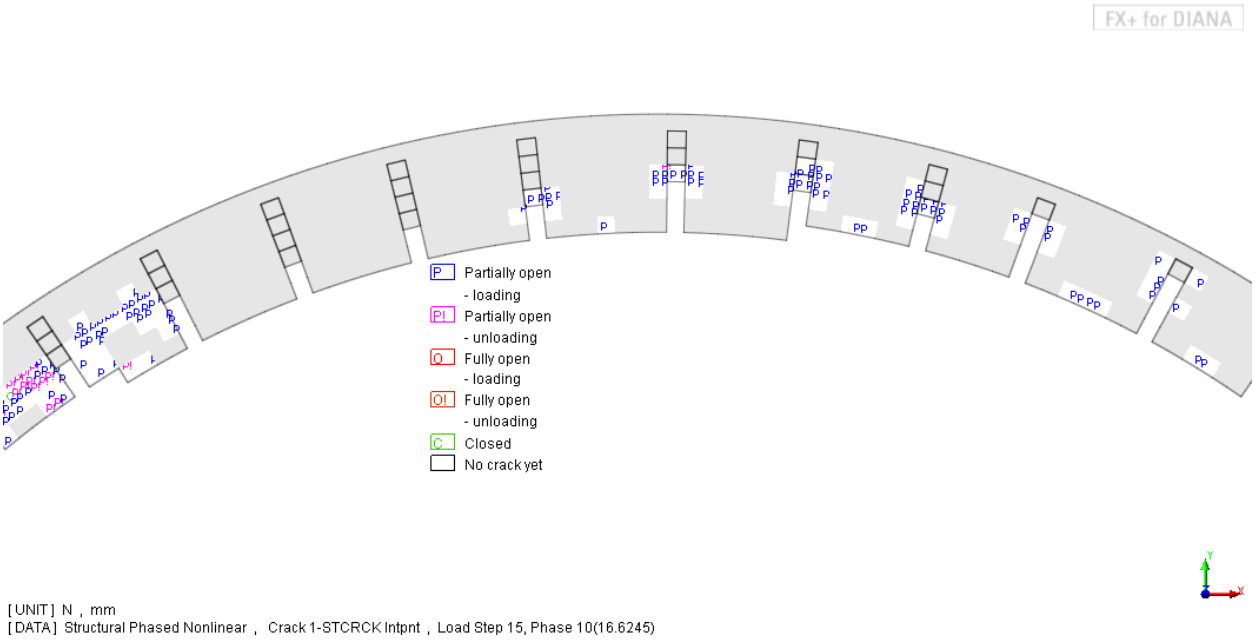

Figure 75. Crack status live load and a prediction of damage on the right

6.4 Scenario 4: Additional damage appear distributed in the whole arch

For this case the damage appears in the whole arch reducing the joints width to only 5cm before loading the structure till failure. Load factor decreases to 13.3 and even though this is the scenario that accounts for damage distributed along the whole structure it does not represent the maximum state of damage since the scenario where the deterioration was concentrated in the center

side had an ultimate load factor of 10.4. A compressive zone is developed in the base of the arch on both sides as shown In Figure 76.

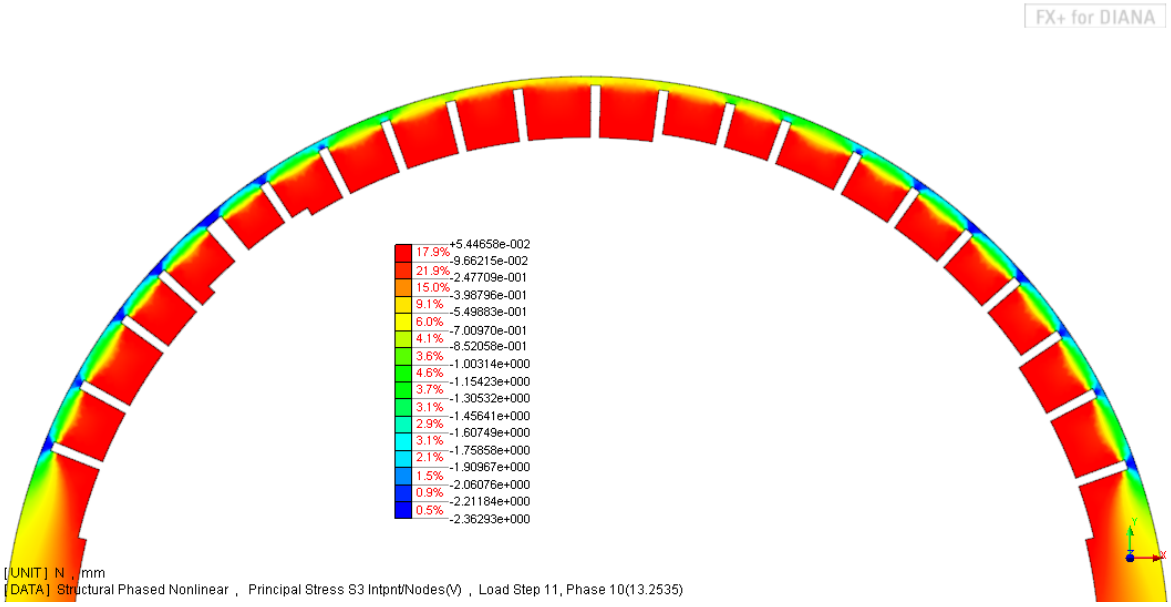

Figure 76. Principal stress S3 for live load and a prediction of damage on distributed along all the arch

As in the case of damage in the middle, no tensile stress is generated in the middle of the arch (Figure 77) probably due to the concentration of compressive stresses as a result of the reduction of the arch's width. The only tensile stress zones develop in the interface between the blocks that seem to come out of the arch and the continuous 5cm that are left.

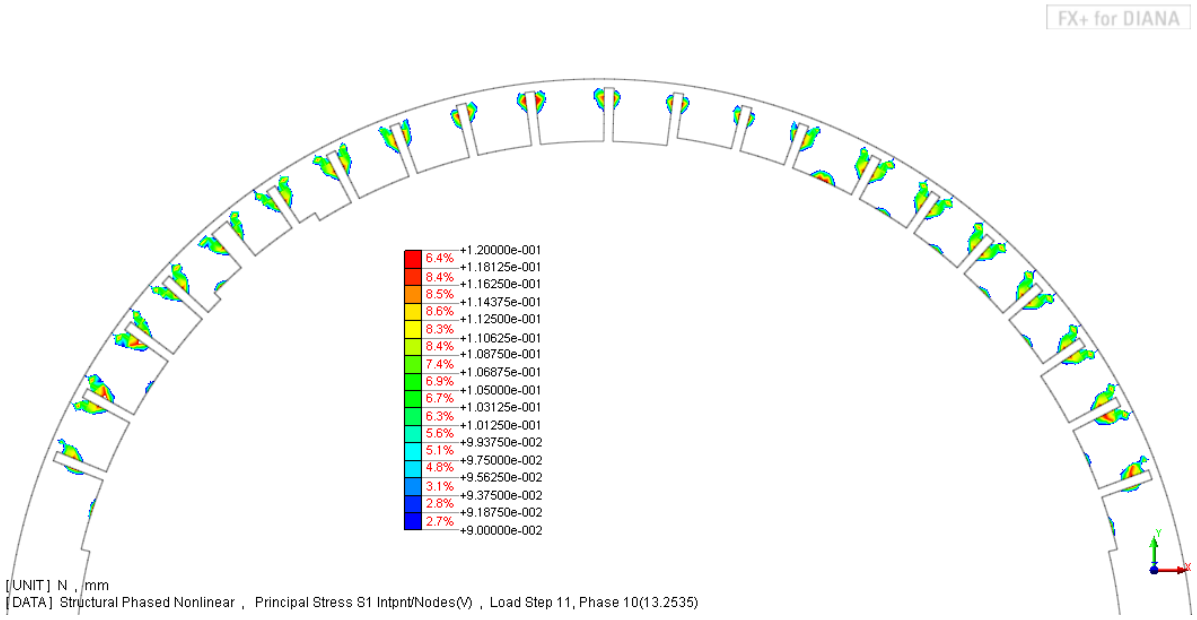

Figure 77. Principal stress S1 for live load and a prediction of damage on distributed along all the arch

6.5 Scenario 5: Additional damage appear in the sides

For this case the joints chosen for further deterioration where the ones located on the sides. Concentration of compressive stresses is then produced as a result in this sections as shown in Figure 78. The material will start to crush when the load factor gets closer to its ultimate value of 12 resulting in the second scenario with highest damage for a loss of capacity of 48%.

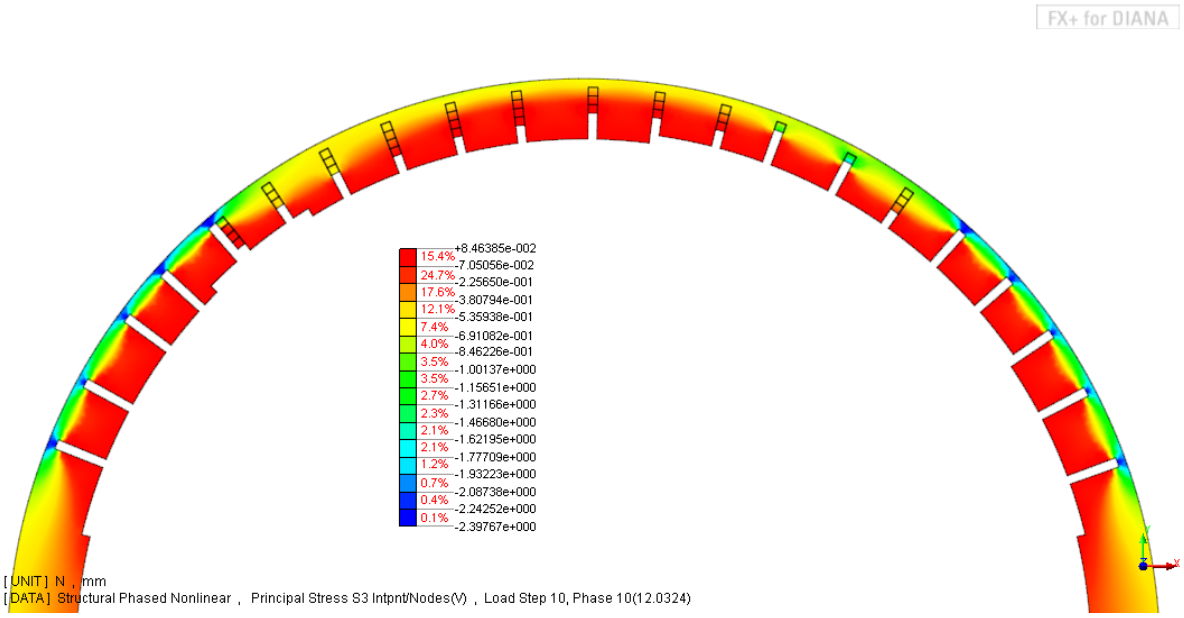

Figure 78. Principal stress S3 for live load and a prediction of damage on the sides

Tensile stresses develop in the top of the structure (Figure 79) where cracks are generated as a result (Figure 80).

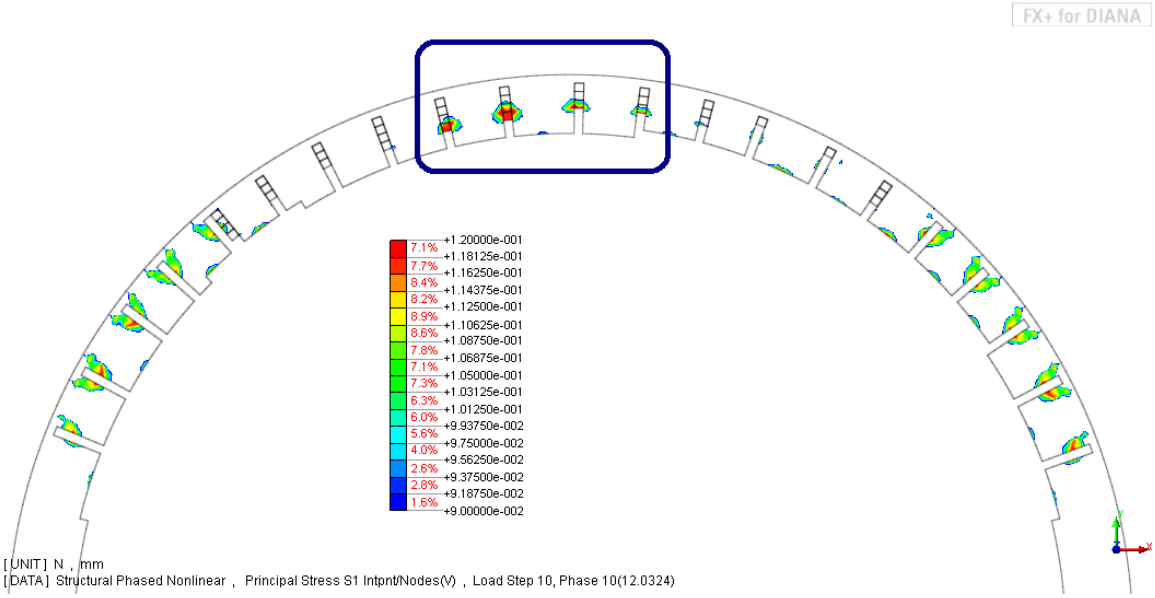

Figure 79. Principal stress S1 for live load and a prediction of damage on the sides

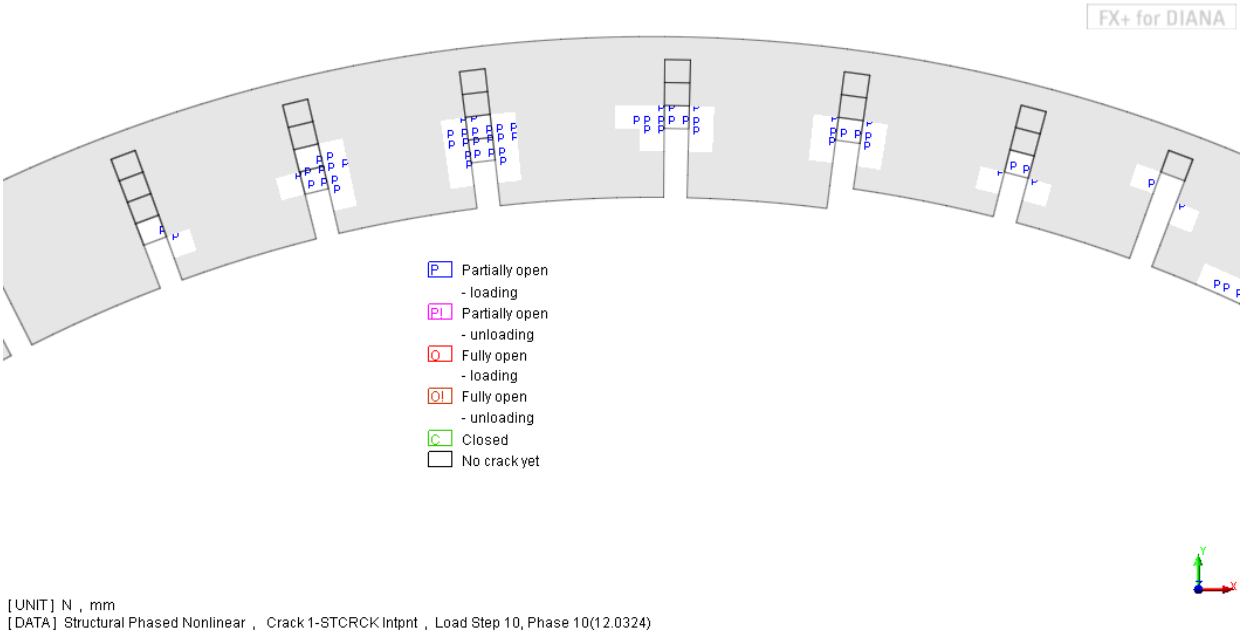

Figure 80. Crack status for live load and a prediction of damage on the sides

In all analysis the highest damaged joint in the top right side of the arch played a fundamental role in the structure's failure. It was seen from the scenario 2 that the critical state would be to generate damage on the left as this additional deterioration would generate a new hinge in this area that combined with the crushed joint that is already present would bring failure of the structure at a more early state.

Table 7 contains a summary of the results obtained in this chapter. It can be seen that the most critical scenarios were in the cases where damage develops further on the left and on both sides.

Table 7. Summary of load factors and maximum displacements for different locations of additional damage

Location of damage	Ultimate load factor	Displacement (mm)	Reduction of capacity (%)
Center	10.37	4.21	54.9
Left	13.8	5.55	40.0
Right	16.62	6.14	27.7
Sides	12.03	5.66	47.7
Wave	13.25	7.6	42.4

7 CONCLUSIONS AND RECOMMENDATIONS

7.1 Conclusions

Analysis for the original geometry shows the Gate of San Francisco had an outstanding ultimate capacity as it was meant for military structures that where designed to resist great impacts.

Sensitivity analysis show that the structure's highest sensibility is due to the compressive strength capacity of masonry. Even though cracks develop in the middle of the arch, it is the crushing of the materials in the base of the arch that brings the structure to failure.

Both analysis using a soil infill or nonlinear total strain crack model infill indicate that the structure is safe.

The safety analysis concludes that even though the structures ultimate capacity has been highly reduced due to damage it continues to be safe.

Live load located on the right side of the structure results in a similar although slightly smaller ultimate load factor for the structure.

The nonlinear behavior shown in the graphs of load versus displacement is mainly a consequence of the crushing of the material. The importance of this parameter was evidenced in the sensitivity analysis.

The study of the state of stress of the structure for no additional load but just gravity in the damage condition show that even though cracks are to be expected in the middle, there is still a good safety factor as the compressive stress does not even reach 25% of the material's maximum compressive capacity.

The variation of the soil properties for the infill have a direct impact on the ultimate load factor. This confirms the necessity for a testing campaign in which the objective would be to define the material properties of the infill material.

The information from the laser scanning had a crucial role in defining the most damaged profiles and allowed to make a general representation of damage for the structure.

Analysis of possible mechanism of deterioration indicate that additional damage on the center would be the most critical situation. Even for this situation a load factor of 10.4 is still required for the collapsing of the structure, meaning the safety of the Gate would still be achieved by a large margin.

7.2 Recommendations

The results show cracks in the top of the side columns. This behavior was unexpected and the hypothesis is a consequence of the lack of an interface between the infill and stone masonry materials. Therefore it is recommended for future studies to make an interface between the two materials. It is recommended that an intervention is prioritized on the top right corner of the arch where the joints already shown a very high level of deterioration and are the most vulnerable in terms of a crushing failure due to compression. Attacking this problem first can largely improve the performance of the structure.

There is a high uncertainty in the properties of the infill material. It is recommended to develop a testing campaign that would obtain the material properties and differentiate whether it acts more like a soil or a mortar. There is no full clarity about the material in between the blocks that form the arch. For this study it was assumed there is no mortar in the joints and that the stones are placed touching faces without any interface in between. It is recommended to do a testing campaign in this section and define whether or not this hypothesis is true.

A limit analysis could be developed in order to verify the arch's capacity from a different perspective. According to the models predicting future damage it should be paid priority to avoid further damage on the center of the structure as further deterioration in this area is which would decrease the ultimate load factor the most. Notice that currently this area is the most damaged and there is a high chance this will continue to be the most damaged section. Intervention to the middle intrados of the arch at the extreme of the tunnel that leads outside of the city should be given priority.

It would be recommended to test different points of the structure when obtaining the infill properties especially close to the entrance where the highest damage occurs.

REFERENCES

Campbell Barraza, J. A. (2012). *Numerical Model for Nonlinear Analysis of Masonry Walls.* Aachen: Rheinisch –Westfälische Technische Hochschule Aachen.

Campos, J. (2009). *Almeida, candidatura das fortificações abaluartadas da Raia Luso-Espanhola a patrimonio mundial – UNESCO.* Guarda, Portugal: Camara Municipal de Almeida.

Cobos, F. (2013). *Almeida/Ciudad Rodrigo: A fortificação da Raia Central.* Salamanca, Spain: Consorcio Transfronterizo de Ciudades Amuralladas.

Garcia Roca, I. (2015). *Safety Evaluation of the Imperfect Chapels from Batalha Monastery.* Braga, Portugal: University of Minho.

Lourenço, P. (1996). *Computational Strategies for Masonry Structures.* Delft, The Netherlands: Delft University Press.

Lourenço, P. B. (2013). Computational strategies for masonry structures: Multi-scale modelling, dynamics engineering applications and other challenges. *Congreso de Métodos Numéricos en Ingeniería.* Bilbao: © SEMNI, 2013.

Núñez García, A. (2015). *Evaluation of structural intervention in the Quartel das Esquadras, Almeida.* University of Minho. Braga, Portugal: University of Minho.

P.B. Lourenco, K.J. Krakowiak, F.M. Fernandes, L.F. Ramos. (2007). Failure analysis of Monastery of Jeronimos, Lisbon: How to learn from sophisticated numerical models. *Engineering Failure Analysis*, 280-300.

Page, A. (1978). Finite element model for masonry. *Journal of the structural division*, S. 1267-1285.

Pedro Lança, Paulo B. Lourenço, Bahman Ghiassi. (n.d.). *Structural assessment of a masonry vault in Portugal.* ISISE, Department of Civil Engineering. Guimarães, Portugal: University of Minho.

Pires, M., & Borg, C. (2016, july 10). *3D Laser Scanning of Architectural Sites*. Retrieved from http://www.science4heritage.org/: http://www.science4heritage.org/COSTG7/booklet/chapters/3D.htm

Ramos, L., & Lourenço, P. (2016). *In situ NDT and MDT for masonry structtures.* Department of Civil Engineering. Braga, Portugal: Universidade do Minho.

Technical comission for the candidacy of Almeida. (2009). *CANDIDACY OF THE BULWARKED FORTIFICATIONS OF THE PORTUGUESE-SPANISH "RAIA" (BORDER LINE) AS WORLD HERITAGE – UNESCO.* Almeida, Guarda, Portugal: Câmara Municipal de Almeida.

TNO DIANA BV. (2014). *DIANA User's Manual Release 9.6.* (J. M. Kikstra, Ed.) Delft, Netherlands: TNO DIANA bv.

URB Atelier, A. e. (2013). *Projecto de Execução de Arquitectura Interior –Quartel das Esquadras, Almeida.*